Joana Fernandes Alberto Wilton Pereira

Licenciada em Bioquímica

Electrochemical characterization of Dps, a DNA-protecting protein

Dissertação para obtenção do Grau de Mestre em Biotecnologia

Orientador: Doutora Cristina Maria Grade Couto da Silva Cordas, Investigadora Auxiliar, DQ-FCT-UNL
Co-orientador: Professor Doutor Pedro António de Brito Tavares, Professor Auxiliar, DQ-FCT-UNL

Júri:

Presidente: Prof. Doutor Pedro Miguel Ribeiro Viana Baptista
Arguente(s): Doutora Alda Maria Baptista do Fundo
Vogal(ais): Doutora Cristina Maria Grade Couto da Silva Cordas

FACULDADE DE CIÊNCIAS E TECNOLOGIA
UNIVERSIDADE NOVA DE LISBOA

Setembro 2011

Joana Fernandes Alberto Wilton Pereira

Licenciada em Bioquímica

Electrochemical characterization of Dps, a DNA-protecting protein

Dissertação para obtenção do Grau de Mestre em

Biotecnologia

Orientador: Doutora Cristina Maria Grade Couto da Silva Cordas, Investigadora Auxiliar, DQ-FCT-UNL

Co-orientador: Pedro António de Brito Tavares, Professor Auxiliar, DQ-FCT-UNL

“Copyright”

Electrochemical characterization of Dps, a DNA-protecting protein

Joana Fernandes Alberto Wilton Pereira

Faculdade de Ciências e Tecnologia / Universidade Nova de Lisboa

Universidade Nova de Lisboa

Dedicatória e agradecimentos

Em primeiro lugar, gostaria de agradecer aos meus orientadores, Doutora Cristina Cordas e Professor Doutor Pedro Tavares, por todo o seu trabalho na orientação da minha dissertação de Mestrado em Biotecnologia.

À Doutora Cristina Cordas, ficarei sempre grata pela oportunidade, pela orientação sempre no sentido de me tornar independente e pela relação que criámos ao longo do ano. Mais do que uma orientadora, foi uma mentora durante todos estes meses, incentivando-me sempre para trabalhar cada vez melhor, como a minha maior crítica, apoiante e encorajadora q.b., desde a fase de planeamento do trabalho aos toques finais deste documento.

Ao Professor Pedro Tavares, o meu muito e muito obrigada pelas conversas esclarecedoras e intensivas acerca do mecanismo da Dps e pelo incentivo em melhorar noutras áreas que não a ciência.

À Professora Doutora Alice Pereira, à Doutora Cristina Timóteo e ao Doutor Filipe Folgosa, muito obrigada pelo apoio imprescindível durante a purificação da proteína. À Professora Alice Pereira, agradeço também a ajuda atenta e disponível durante todo o ano. Ao Doutor Filipe Folgosa, muito e muito obrigada pelas críticas e elogios sempre sinceros, que me fizeram aprender e tornar mais humilde à medida que os meses passavam e me apercebia cada vez mais do esforço a dispender para traçar o meu próprio caminho na ciência.

Gostaria também de agradecer aos meus colegas estudantes e/ou bolseiros que trabalharam no laboratório 425 e em muito contribuíram para o ambiente laboratorial agradável: Daniela Silva, Magda Reis (obrigada pela ajuda nas traduções!), Inês Graça, Tânia Cardoso, Sérgio Portovedo, Madalena Lourenço e João Froes. De igual forma, gostaria de agradecer aos restantes colegas - Doutores Rui Almeida e Susana Ramos, Leonor Morgado, Ana Pina, Sara Santana, Inês Camacho, Renato Santos.

Não posso esquecer também os meus amigos toda a paciência para me aturar quando me esquecia que estava fora do laboratório e toda a conversa acabava em trabalho, especialmente nos últimos tempos. Filipa, obrigada pelas conversas e perguntas difíceis e acutilantes; Ana, muito e muito obrigada pela empatia e cafés semestrais; João e Mariana, muito me alegrei em fazer com que futuros Engenheiros Civis percebam mais sobre as biocoisas desta vida.

Por último, e não menos importante, o meu agradecimento vitalício à minha família. Obrigada aos meus pais pelo incentivo e amor que sempre me fez sentir capaz de fazer tudo ao qual me dedicasse com trabalho e empenho - esta tese é tão vossa quanto minha. Desculpem a minha falta de tempo e distracção crónicas. Obrigada ao meu irmão, por me obrigar a continuar a ser criança e a fazer disparates de vez em quando. Aos meus avós, pelo amor incondicional e perguntas sempre interessadas e atentas sobre o trabalho e a vida. Perdoem-me não estar com vocês tantas vezes quanto gostaria. Aos meus tios P., B. e R.A. e aos meus primos. Ao Luís, por ser o meu confidente, me apoiar e ralhar nas alturas certas sem me deixar abater nos dias mais difíceis.

Resumo

Os objectivos do presente trabalho foram a purificação e caracterização electroquímica da proteína Dps e o estudo do seu mecanismo de armazenamento de ferro na presença de H_2O_2.

Uma miniferritina bacteriana (Dps) proveniente de *Pseudomonas* (*Ps.*) *nautica 617* foi expressa em células de *E. coli* BL21(DE3) transformadas com o vector plasmídico pET21c(+)-1dps. A sobreexpressão da proteína pelas células transformadas foi realizada em meio rico (LB) contendo 100 µg/mL de ampicilina. A Dps recombinante foi purificada através de dois passos: cromatografia de permuta iónica fraca (resina DEAE Sepharose Fast Flow XK 26/40) e cromatografia de permuta iónica forte (resina Q Resource). A concentração da proteína foi determinada por espectroscopia UV/Visível.

O estudo electroquímico foi realizado por voltametria cíclica, de onda quadrada e cronoamperometria, com a proteína solubilizada ou adsorvida ao eléctrodo de trabalho. Utilizou-se como electrólito suporte o tampão 200 mM MOPS/ 200 mM NaCl, pH 7.1. Os ensaios foram realizados em ambiente aeróbio e anaeróbio e na presença de Dps, iões Fe(II) e H_2O_2, ambos co-substratos da proteína. Para diferentes ensaios, foram utilizados eléctrodos de ouro, carbono vítreo e grafite, com diferentes resultados e conclusões. Foi estudada a incorporação deste no centro ferroxidático e a ocorrência de formação de core mineral, tendo sido possível obter resultados por transferência electrónica directa. De salientar, entre os resultados obtidos, a observação da oxidação do ferro durante a incubação na proteína e a prova da produção de oxigénio durante o mecanismo catalítico. Do ponto de vista da protecção ao DNA, não foi possível obter resultados conclusivos, embora haja indícios de protecção pela Dps à oxidação electroquímica.

Palavras-Chave
Bioelectroquímica; Dps; *Pseudomonas nautica 617*; DNA; fase estacionária

Abstract

The objectives of the present work were the purification and electrochemical characterization of Dps and study its iron incorporation mechanism in the presence of hydrogen peroxide.

A bacterial miniferritin (Dps) from *Pseudomonas* (*Ps.*) *nautica 617* was expressed in BL21(DE3) *E. coli* cells transformed with pET21c(+)-1dps plasmid vector. Protein overexpression was performed in nutritionally rich LB medium containing 100 µg/mL ampicillin. Recombinant Dps was purified through a two-step process: weak ionic exchange chromatography (DEAE Sepharose Fast Flow XK 26/40 resin) and strong ionic exchange chromatography (Q Resource resin). Protein concentration was determined through UV/Visible spectroscopy.

The electrochemical study was performed through cyclic voltammetry, square wave voltammetry and chronoamperometry; Dps was either in solution or adsorbed to the working electrode. The chosen supporting electrolyte was 200 mM MOPS pH 7.1 buffer with 200 mM NaCl. Electrochemical assays were performed in aerobic and anaerobic environment and in the presence of Dps and Fe(II) and H_2O_2, both of Dps co-substrates. For the different assays, working electrodes made of gold, glassy carbon and graphite were used with different results and conclusions. The iron incorporation in the ferroxidase centers and mineral core formation were studied. Assay results were obtained through direct electron transfer. Among the observed results, iron oxidation during protein incubation and oxygen production during the catalytic mechanism were observed. DNA-Dps interaction results were inconclusive, although some unconfirmed evidence exists of DNA protection by Dps from electrochemical oxidation.

Keywords

Bioelectrochemistry; Dps; *Pseudomonas nautica 617*; stationary phase

Table of Contents

Figure Index

Table Index

Symbols and Abbreviations

Symbols

Abs_x – Absorbance (x nm)

c – concentration (M)

ε - molar extinction coefficient (M^{-1} cm^{-1})

E – redox potential (V)

E_{OCP} – open circuit potential (V)

E_p – peak potential (V)

E_{pa} – anodic peak potential (V)

E_{pc} – cathodic peak potential (V)

$E^{0'}$ – formal reduction potential (V)

ΔE – potential difference (V)

I – electrical current (A)

I_{cat} – catalytic electrical current (A)

I_p – maximum electrical peak current (A)

I_{pa} – maximum anodic electrical peak current (A)

I_{pc} - maximum cathodic electrical peak current (A)

MW – molecular weight

n – number of electrons

rpm – rotations per minute

T – temperature (K)

ν - scan rate (mV/s)

V – volume (L)

Abbreviations

AES – Atomic Emission Spectroscopy

Amp – Ampicillin

apoDps – Dps apoprotein

bp – (DNA) base pairs

CE – counter electrode

CV – cyclic voltammetry

DNA – deoxyribonucleic acid

Dps – DNA-binding protein from starved cells

ds – double stranded

E. coli – *Escherichia coli*

ICP – Inductively Coupled Plasma

IPTG – Isopropyl-ß-D-1-thiogalactopyranoside

LB – Lysogeny Broth (aka Luria Broth / Luria Bertani)

mUA – milliunits of absorbance

M. aquaeolei – *Marinobacter aquaeolei*

MOPS – 3-(N-morpholino)propanesulfonic acid

MWCO – molecular weight cut-off

OD_x – optical density (x nm)

PDB – Protein Data Bank

ppm – parts per million

PSA – Ammonium persulfate

Ps. nautica 617– *Pseudomonas nautica* 617

RE – Reference Electrode

ROS – Reactive Oxygen Species

SCE –Saturated Calomel Electrode

SDS – Sodium Dodecyl Sulfate

SDS-PAGE – Sodium Dodecyl Sulfate Polyacrylamide Gel Electrophoresis

ss – single stranded

SHE – Standard Hydrogen Electrode

TEMED – N,N,N',N'-tetramethylethylenodiamine

UV – ultraviolet radiation

Vis – Visible radiation

WE – working electrode

Chapter I – Introduction

I.1 Iron – an essential element

As the second most abundant metal on Earth[1], iron has been broadly available throughout evolution as a versatile cell component, for protein incorporation and as an electron carrier or a cell cofactor for several cell mechanisms – photosynthesis, respiration, nitrogen fixation or DNA (deoxyribonucleic acid) synthesis. Since it can adopt different oxidation states, spin states and redox potentials, depending on the surrounding ligand environment, it has long been considered as the ideal choice for protein incorporation dating back to early life and is now almost ubiquitous in all lifeforms[2].

Iron chemical properties show its versatility as a protein cofactor transversally present in the three domains of life[1]. The cellular oxidant environment displaces the iron redox equilibrium favoring the formation of ferric iron. At physiological pH, iron is mostly present in two redox states, Fe(II) - relatively soluble ferrous iron (typically 10^{-8} M free cellular iron, s = 0.1 M) – and Fe(III) - insoluble ferric iron (s = 10^{-18} M cellular iron)[3,4]. Fe(II) is thermodynamically more stable than Fe(III), due to its standard redox potential (0.77 V *vs.* Standard Hydrogen Electrode, SHE [5]).

Fe(III) reacts with several key cell anions (e.g. hydroxide anion, OH^- [6]), forming insoluble complexes in equilibrium with free iron, which lowers its bioavailability and thus hinders cell growth, rendering iron a limiting nutrient since the optimal iron concentration for bacterial growth is ~10^-7 M. This situation interferes with normal cellular functions even in the short-term; thus, cells have ferritin-like iron storage proteins for cellular iron complexation[3,6].

However, living organisms have to achieve efficient iron homeostasis, scavenging it to maintain adequate cellular supplies without reaching toxic concentrations. Iron storage as an inorganic mineral solubilized inside a protein core is one possible solution to maintain iron available inside the cell in an inherently non-toxic, easily accessible form[6].

Another important cellular consequence in iron metabolism is its potential toxicity, due to formation of iron oxides and, further along, reactive oxygen species (ROS) according to the following reactions:

$$Fe^{2+} + O_2 \rightarrow Fe^{3+} + O_2^{\cdot} \quad (\mathbf{1.1})$$

$$2O_2^- + 2H^+ \rightarrow H_2O_2 + O_2 \quad (\mathbf{1.2})$$

$$H_2O_2 + Fe^{2+} \rightarrow OH^{\cdot} + OH^- + Fe^{3+} \quad (\mathbf{1.3}, \text{Fenton reaction})$$

Addition of molecular oxygen to Fe(II) triggers iron oxidation and formation of ROS, mainly superoxide (O_2^-), hydroxy (OH^-), hydroxyl radical ($OH^{\cdot}$), water (H_2O) and hydrogen peroxide (H_2O_2).

The Fenton reaction rate increases in the presence of bound iron[7], from 76 M^{-1} Fe(II) s^{-1} to 2000-6000 M^{-1} s^{-1}, upon binding of iron to DNA or nucleotides[8]. Consequently, even low H_2O_2 cellular levels have a physiologically significant effect on DNA damage[7].

While $OH^{\cdot}$ and H_2O_2 are very reactive towards biological systems, participating in rapid biomolecular degradation such as lipid peroxidation and DNA destruction[9], H_2O_2 is inevitably formed during aerobic respiration[10,11], reacting rapidly with Fe(II) as is demonstrated on reaction 1.3. Hydrogen peroxide diffuses across cell membranes and is lethal to *E. coli* cells in both low (1-2 mM) and high (>20 mM) concentrations [12]. At low H_2O_2 concentrations, cell death is considered to occur through DNA damage mediated by H_2O_2-Fe(II) interaction[9,13]. Fe(III) can be reduced to Fe(II) through the Haber-Weiss catalytic cycle[14], involving several cytoplasmic reductants, among which $^{\cdot}O_2^-$:

$O_2^- + Fe^{3+} \rightarrow Fe^{2+} + O_2$ (iron reduction, inverse **1.1**)

$H_2O_2 + Fe^{2+} \rightarrow OH^{\cdot} + OH^- + Fe^{3+}$ (**1.3**)

$O_2^- + H_2O_2 \xrightarrow{Fe\ catalysis} OH^{\cdot} + OH^- + O_2$ (**1.4**, Haber-Weiss reaction)

The iron-catalyzed Haber-Weiss reaction, which uses Fenton chemistry to obtain hydroxyl radical, is considered to be the main mechanism through which this radical is induced in biological systems[14]. In some cases, either $^{\cdot}O_2^-$ or H_2O_2 can be directly implicated in cell damage or indirectly leading to formation of increasingly oxidant species $OH^{\cdot}$ [7], as is presented in Figure 1.1.

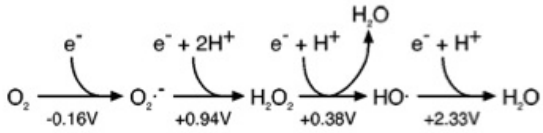

Figure 1.1 – Reduction potentials of various oxygen species, assuming 1 M starting O_2 concentration (adapted from [7]).

$OH^{\cdot}$ is the main species mediating cell injury, targeting proteins, DNA and lipids. However, since $OH^{\cdot}$ action is limited by diffusion, once formed it is unlikely to travel before oxidizing an available substrate. Consequently, $OH^{\cdot}$ generation will mediate cell injury directly when near a vital cell[7,9,15].

ROS as a whole have a direct effect on DNA damage, increasing its general propensity for genetic mutations and transcription disregulation. DNA damage is caused by direct interaction (base or nucleotide damage), interference on DNA repair mechanisms, affecting cell division through carcinogen activation promotion.

According to Andrews *et al.* [2], bacteria use several different strategies to ensure intracellular iron management:

1. Scavenging iron after high-affinity transport from the outside environment.
2. Deposition of intracellular iron as an additional iron source to be used when external supplies are limited.
3. Launch redox stress resistance systems inside the cell (repair of stress-induced damage and degradation of iron-induced ROS)
4. Control of iron cellular levels through down-regulating expression of iron-containing proteins under iron-restricted conditions.
5. Iron-sensitive regulatory system that coordinates expression of the aforementioned iron homeostatic machinery according to intracellular iron availability.

These strategies are differentially employed according to cell phylogeny, surrounding environment and ecological niche. However, ferritins protein are mainly responsible for iron storage (strategy 2) and a subset of them is also responsible for iron-induced cell repair (strategy 3). Namely, two types of iron storage ferritin proteins are currently recognized in eubacteria: maxiferritins and miniferritins, formed respectively by 24 and 12 homo-oligomers, which will be discussed below on section I.2.

I.2 Ferritin family proteins

Ferritins are ubiquitous iron storage proteins responsible for the control of iron phase transition between solid and solution, through effective utilization of oxygen to concentrate iron for protein biosynthesis. They are involved in several crucial cellular processes, such as respiration, nitrogen fixation, photosynthesis or DNA synthesis, precisely the same processes that need high levels of iron[16].

Ferritins scavenge Fe(II) inside the cell and deposit it in the hollow central cavity in the oxidized ferric form. Namely, fast ferritins within which Dps are included have an iron incorporation mechanism that includes a ferroxidation step catalyzed in the ferroxidase centers located within the protein shell. The amino acid residues forming this site are highly conserved throughout both groups and interact with Fe(II), binding it on the first step of the iron uptake process, which will be discussed below.

Although both maxi- and miniferritins are organized in evolutionary distinct families, they are related to each other. Ferritins have retained many structural and functional similarities throughout evolution, the most recognizable of which their distinctive molecular architecture that enables them to store iron effectively. Both groups are composed of *n* identical subunits folded into a four α-helix bundle,

joining together to form a nearly spherical shell surrounding a central hollow cavity that stores iron. *n* varies between the subfamilies but not inside them. Thus, ferritins control the intracellular microenvironment, determining the mineral phase formed – if the protein is present, ferrihydrite is the iron precipitate formed; if no ferritin is present, the prevalent hydrous iron oxide is lepdocrocite or goethite[17].

Maxiferritins (ferritin and bacterioferritin proteins) are composed of 24 identical subunits with one central ferroxidase center per monomer. They can accommodate a minimum of 2000-3000 iron atoms, while miniferritins (Dps) are composed of 12 identical subunits and can hold until ~500 iron atoms. Dps proteins have 2 ferroxidase centers per dimer, located at the two-fold interface between each two subunits[18]. In conclusion, maxi- and miniferritins have similar iron deposition properties, despite having different iron ferroxidation processes.

Ferritins are used as supramolecular templates for synthesis of nanoparticles inside the protein shell[19] for several technological applications, because of their intrinsic mineralization capability and robustness at inhospitable conditions. Highlighting applications include construction platforms for antigen and vaccine development, cancer therapy, drug delivery and molecular imaging[20]. Future prospects for these proteins include study of iron core formation and mechanism of iron release in different cellular conditions and the elucidation of the DNA-binding mechanism, where applicable.

1.2.1 Dps proteins

In the last two decades, it has been recognized that a protein subfamily other than maxiferritins possesses both iron storage and detoxification capacity in bacterial cells. The Dps family (DNA-binding proteins from starved cells) is highly conserved throughout *Bacteria* (shown on Appendix G.1), which make 97% or the family [20-23] or contain similarities with other ferritin proteins[24]; some related proteins have also been found in *Archaea*[25,26]. Dps proteins were named after the discovery of the prototype originating from *Escherichia coli*, expressed under starvation or oxidative stress[22] and were found to be crucial for long-term stationary-phase viability under starvation conditions[27].

Originally, Dps proteins were found to protect DNA from oxidative damage through extremely stable complexation without sequence specificity[28], size or topology both *in vitro* and *in vivo*. Cells lacking Dps alter their protein expression pattern dramatically during starvation and do not develop starvation-induced resistance to H_2O_2 [22]. Dps synthesis is induced upon the late stationary growth phase, continuing on after several days of starvation until it becomes the most abundant cellular protein[29], or is alternatively induced constitutively by the organism to effectively control iron toxicity in the presence of hydrogen peroxide[30]. Almirón *et al.* [22] also found Dps to play a global regulatory role in gene expression during prolonged starvation, along with its protective role. Dps is not only a

cage in which iron is transiently stored or made available to cells, but also a trap for oxidant molecules and free electrons that are otherwise generated[31].

More recent findings recognized that Dps proteins have ferritin-like properties such as detoxification mechanisms upon exposure to both iron and H_2O_2. Several Dps proteins have been identified over the last decades[21,23,30,32-42], not all of which bind DNA[30,43-45]. Furthermore, Dps proteins have been found to protect DNA from pH stress[27,46] and ionizing and ultraviolet radiation[27,33]. Other possible functions of Dps proteins include managing copper homeostasis[27,47], zinc removal[48] increased survival of virulent bacteria[35], a negative role in regulation of antibiotic resistance[49], *in vitro* and *in vivo* neurotoxin[50], temperature resistance[27] and virulence[51,52].

With 23-point-group symmetry, the Dps protein is a homododecamer with a ~40 Å central cavity that can store up to 500 irons. The ~20 kDa monomers spontaneously fold to 4-helix (A–D) bundles and then to the quaternary structure (as four trimers at tetrahedron vertices) which resembles a hollow sphere with 8-9 Å external and 4-5 Å internal diameter (Figures 1.2 and 1.3).

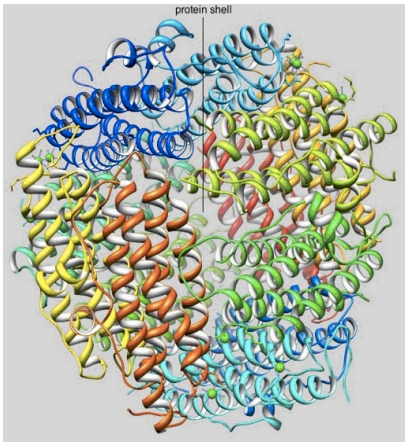

Figure 1.2 – Dps homododecamer from *E. coli* (PDB source file: 1dps), drawn on Chimera[53].

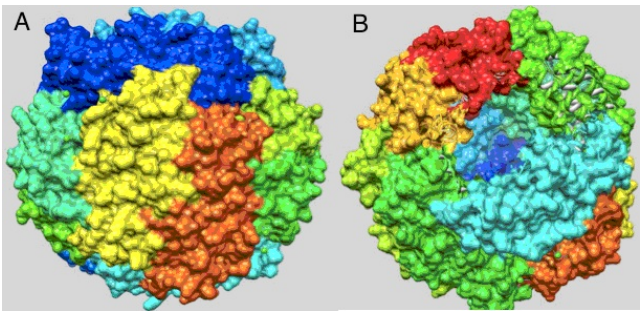

Figure 1.3 – A) Dps homododecamer (12 chains); B) Incomplete Dps homodecamer (excluding one monomer), both drawn on Chimera[53] (PDB source file: 1dps).

Dps monomers differ from ferritins because of the presence of a small extra helix, located between the B and C helices, as can be seen on Figure 1.5. The Dps surface shows negatively charged areas and spots with positive and neutral charge, not presenting areas with preferred surface charge. Electrostatic surface is shown below on figure 1.4:

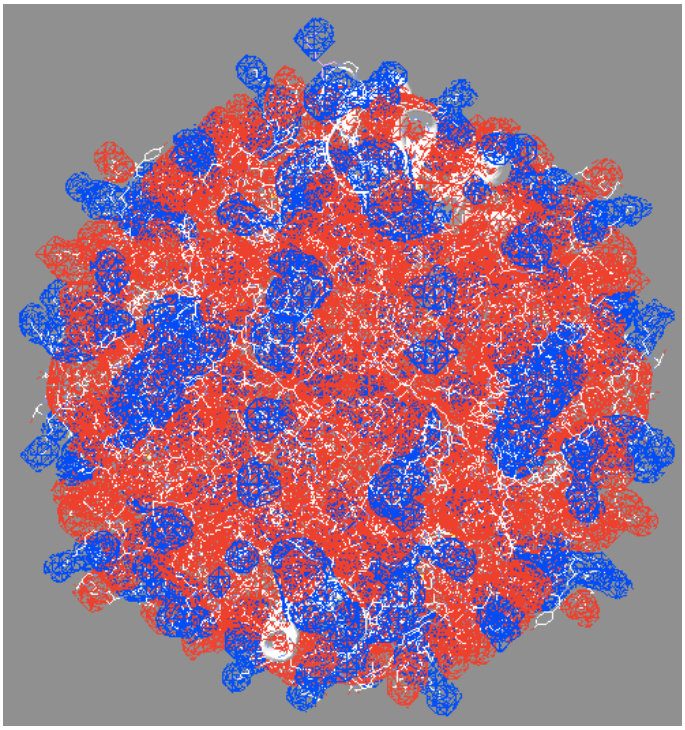

Figure 1.4 – *E. coli* Dps surface electrostatic charge (PDB source file: 1dps). The homododecamer is shown in 3D with positive residues shown in blue, neutral residues in white and negative residues in red. This figure was drawn on Swiss Pdb Viewer[54], using Poisson-Boltzmann computation method, 0.4 M ionic strength and default dielectric constants (4 for Dps and 80.1 for solvent).

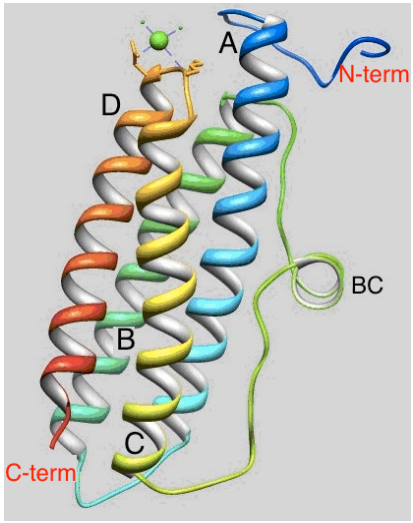

Figure 1.5 –Dps monomer from *E. coli* (PDB source file: 1dps) showing 4 antiparallel helices and the ferroxidase center (green sphere). This figure was drawn on Chimera [53].

Dps iron sites can be divided in 3 types: ferroxidase and nucleation centers and entry/exit pores[20]. As can be seen by Figure 1.5, Dps monomers feature a very flexible N-terminus protruding out of the folded dodecamer, responsible for DNA binding and stabilization of the dodecamer[20,55]. The C-terminus has been suggested to be an iron exit or alternate entry route or to bind DNA as well, since it has appropriate charge and motility characteristics [20,33,36,56].

No mineral core formation has been detected in the protein assembly process – Fe(II) is scavenged to form the mineral after the first incorporation step (ferroxidation). The ferroxidation sites are located at the subunit dimer interface opposite the mineralization cavity. Each ferroxidation site is formed by amino acid residues from the 2 adjacent subunits and is highly conserved throughout eubacteria[20,57]. The molecule symmetry means that two different channel types are present along the three-fold axes, one of which is hydrophilic and is proposed to be the one through which Fe(II) accesses the central Dps cavity[6,58].

Several studies have been conducted to understand the consequences of DNA binding to Dps, and it has been found that in *E. coli*, Dps is induced in two situations:

- during cell growth, OxyR, a redox-sensitive transcriptional activator present in gamma-Proteobacteria[59,60] acts as a metabolic feedback for the cell and the community through H_2O_2 level regulation[61];
- at stationary phase, σ^S is a transcription initiation factor which directs RNA polymerase core enzyme to activate mainly stress-related promoters, while IHF histone-like protein controls some Dps dependent expression[20,62].

Dps is also regulated by growth-phase dependent degradation upon the action of ClpXP and ClpAP proteases[63]. As a regulatory protein, it is also one of the main participants of DNA structure regulation during environmental stress, promoting transition from unpacked to condensed nucleoid, which is critical for DNA-Dps crystallization[64-66]. On the other hand, Dps levels are also controlled by proteolysis during carbon-abundant conditions[20,63].

While the results obtained by Zhao *et al*. pointed to a dual protective action being done by Dps, through physical association with DNA and nullification of the toxic combination of Fe(II) and H_2O_2[67], Dps function was found until recently to be mutually exclusive[20]. To achieve cell viability in the stationary growth phase, iron incorporation leads to H_2O_2 elimination and avoidance of Fenton chemistry, storing Fe(III) oxides in the Dps core. This process will be discussed in the next section.

I.2.1.1 Iron incorporation

The iron oxidation reaction path has been determined in both *Listeria innocua* and *E. coli* Dps[45,67] and involves five consecutive phases schematized in Figure 1.6:

1. iron entry inside the protein;
2. iron binding to one of the ferroxidase centers;
3. iron oxidation at the ferroxidase center;
4. nucleation
5. mineralization (mainly as ferrihydrite)

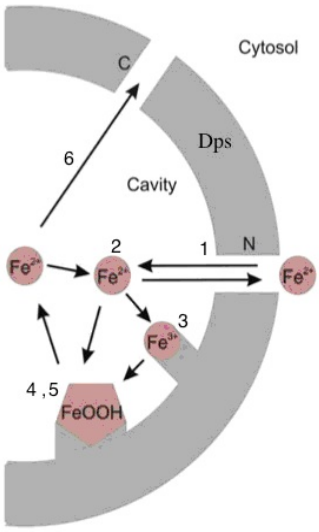

Figure 1.6 – Possible iron paths in Dps. Fe(II) enters the dodecamer through N-terminal pores (1),binds to the ferroxidase center (2) oxidizes to Fe(III) (3) and mineralizes in ferrihydrite form from a nucleation/core center. Fe(III) can reduce back to Fe(II) and leave the Dps shell through C-terminal pores (adapted from [20]).

The ferroxidation reaction with H_2O_2 as an oxidant occurs as follows:

$$2Fe^{2+} + P^Z \rightarrow \left[Fe_2 - P\right]^{z+2} + 2H^+ \quad (\mathbf{1.5})$$

$$\left[Fe_2 - P\right]^{Z+2} + H_2O_2 + H_2O \rightarrow \left[Fe_2O_2\left(OH\right) - P\right]^Z + 3H^+ \quad (\mathbf{1.6} \text{ - iron oxidation})$$

$$2Fe^{2+} + H_2O_2 + 2H_2O \rightarrow 2Fe^{3+}OOH_{core} + 4H^+ \quad (\mathbf{1.7}\text{- iron core mineralization})^{20,67}$$

P^Z represents the Dps apoprotein and $[Fe2\text{-}P]^{Z+2}$ the bimetallic iron complexed to the ferroxidase center. In reaction 1.6, Fe(II) oxidizes to Fe(III) as $[Fe_2O_2(OH)\text{-}P]^Z$, an oxidized iron complex in the ferroxidase center. Afterwards, iron suffers mineralization as hydrous Fe(III) oxide (FeOOH). In Dps proteins, the ferric core formation happens faster than the ferroxidation reaction[45,67] and enables Dps to obtain up to 500 Fe (III) per dodecamer. Several Dps structures have been presented with either one or two bound irons or two H_2O molecules, indicating influence of the second metal coordination shell[55]. Dps water ligands, in particular, are highly conserved and may be involved in protein stability, flexibility and continuing subunit association[68]. Iron in ferritin biominerals occurs differently *in vitro* and *in vivo*, albeit always in an acidic formation surface[16].

Dps can also utilize O_2 as an oxidant, albeit with 1000-fold lower intensity[45,67]. This reaction path is shown below:

$$2Fe^{2+} + P^Z \rightarrow \left[Fe_2 - P\right]^{z+2} + 2H^+ (\mathbf{1.5})$$

$$\left[Fe_2 - P\right]^{Z+2} + \tfrac{1}{2}O_2 + H_2O \rightarrow \left[Fe_2(OH)_2 - P\right]^Z + 2H^+ (\mathbf{1.8})$$

$$2Fe^{2+} + O_2 + 2H_2O \rightarrow 2FeOOH + 2H^+ (\mathbf{1.9})$$

Each binding site of the 12 bimetallic ferroxidase centers in the Dps antiparallel dimer is composed of four highly conserved amino acid residues from both symmetry-related subunits as is shown below on Figure 1.7 – two histidines (His), one aspartic acid (Asp) and one glutamic acid (Glu) – as well as two conserved residues: one tryptophan (Trp) ~3Å away from site A, present on 99% of reported Dps sequences and a nearby tyrosine (Tyr), that form short-lived intraprotein species that act as radical traps[31,55].

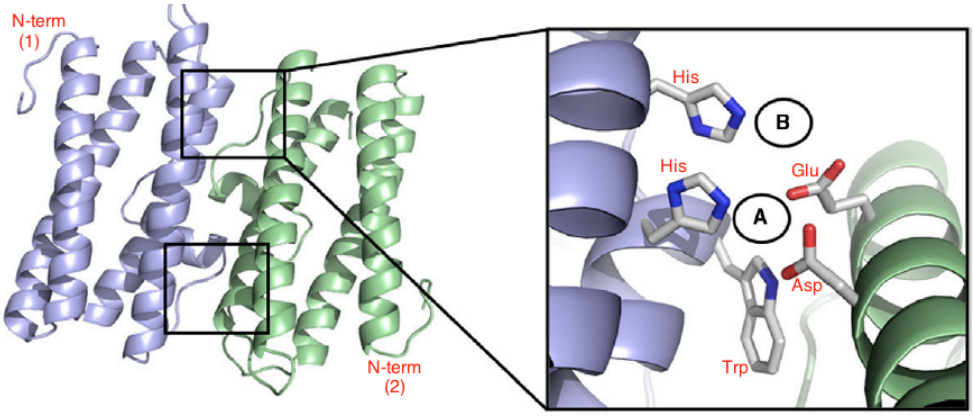

Figure 1.7 - Dps ferroxidase centers from *E. coli*, showing the high affinity A site (coordinated by histidine and carboxylate residues) and the low affinity B site (coordinated by carboxylate residues). One Dps monomer provides both histidine residues, while the remaining monomer provides two carboxylate residues (adapted from [55]).

Dps proteins have 23 symmetry points; hence, the dodecameric structure has a total of eight trimeric interfaces, formed at the N- or C-terminus ends. Hydrophilic pores formed at the N-terminus are 10 Å long, negatively charged and between 9-17 Å (external diameter) and 7-11 Å (internal) wide, based on distances between C^{α}; their cationic transport function is characteristic of both Dps and ferritins: negatively charged pores attract positive metallic ions through an electrostatic gradient, from the outside environment to the ferroxidase center and onwards to the Dps core; the same pores are also thought to be useful as an iron exit route. Hydrophobic, less conserved pores formed at the C-terminus are 7-21 Å long, between 6-14 Å (external diameter) and 8-10 Å (internal) wide, based on distances between C^{α}. Because of these properties, C-terminus pores have been considered to be either a iron exit route or an auxiliary cation passage route after protein rearrangements, since their hydrophobicity makes them an unlikely target for main cation passage[20,33].

According to Zhao *et al.* [67], this mineralization reaction, as well as the ferroxidation reaction, occurs with rapid and complete ferrous ion oxidation with 2Fe(II) : H_2O_2 stoichiometry. Hydrogen peroxide is, consequently, a more efficient oxidant for Dps than O_2. It has also been discovered that the mineralization reaction is faster in Dps proteins than in maxiferritins with H_2O_2 as an oxidant[67].

Although the ferritin studies began to provide answers to some ferritin-related questions, such as the exploitation of the ferritin cage-like structure for novel (nano)materials and drug-delivery systems[20], some questions concerning ferritin proteins remain grossly unanswered, such as understanding protein nanocage and cavity assembly and information about the physiological electron and proton donors to the iron mineral.

According to Bellapadrona *et al.* [31], conserved amino acid residues in Dps trap oxidants inside the protein shell. Furthermore, free cytoplasmatic Fe(II) levels are very low under stationary-phase conditions, which makes the earlier accepted mechanism unlikely to occur[45] and further validates the model proposed by Bellapadrona, in which odd numbers of electrons and consequently of intraprotein radicals trapped in the protein shell are of greatest coherence to the protective role of Dps. The aforementioned Trp adopts a radical form on iron oxidation by addition of H_2O_2, preventings ROS diffusion into the cellular environment and consequent DNA damage[31].

Nucleation sites at the Dps core manage early stages of oxidized iron mineralization as ferrihydrite. Dps nucleation site residues include non-conserved amino acid residues common to L-chain ferritin (at the twofold symmetry axis), aided by several negatively charged amino acids surrounding the ferroxidase center that can direct nucleation. As the nucleated ferric mineral grows, Fe(II) ions flowing into the core can oxidize at the surface of the growing mineral, as has been observed in ferritins[20].

Greater cellular iron bioavailability in the cell is largely due to Dps, as it has been proposed that a small amount of iron is cyclically released from and re-deposited into the Dps core[20]. The two different types of iron core in Dps have been extensively studied by a variety of techniques including Mössbauer, X-ray absorption and polarized single-crystal absorption spectroscopies. The native core is present in purified Dps without further iron additions, as well as an *in vitro* loaded Dps core, formed after iron addition. This core normally contains iron atoms with different phosphate ratios[32], although other metals can also be present – Zn, Cu, Cr, Mn, Co, Ni and Mo[69]. The *in vitro* core contains up to 500 iron atoms and is structurally irregular, possibly existing as a mixture of octahedrally and tetrahedrally coordinated ferrihydrite[32]. This core is consistent with cellular iron distribution needs, making iron more readily available than the crystalline state of the native core.

I.2.1.2 Cell defense mechanisms: oxidative stress

Fenton chemistry avoidance by Dps appears to only be fully achieved if Fe(II) and H_2O_2 are added in the correct order and appropriate ratio, although ROS production always decreased in the sole presence of Dps[67].

Excess amounts of iron and superoxide radicals were found to be responsible for $OH^{\cdot}$ generation and consequent formation of DNA lesions and hypermutability[70]. Consersely, it has been discovered that Dps knockout organisms have extreme sensitivity to H_2O_2 even at low concentrations (0.5 mM), with 96% decline in survival[71].

I.2.1.3 Cell defense mechanisms: DNA interaction

DNA structure was discovered in 1953 by Watson and Crick, from X-ray diffraction data obtained by Wilkins and Franklin. DNA is more frequently found double-stranded (ds), formed by 2 antiparallel nucleotide chains, each in the 5'-3' direction and connected through chemical interactions shown below in Figure 1.8 in the most frequently found B-form DNA. Nucleotides are composed of pentose rings connected to a phosphate group and a nucleobase (adenine (A), cytosine (C), guanine (G) and thymine (T)). Less stable single stranded DNA (ssDNA) is also found inside cells.

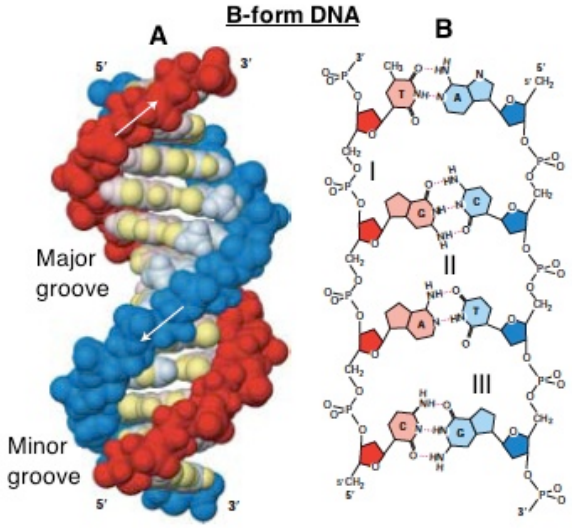

Figure 1.8 – A. 3D scheme B-form DNA, showing differently colored antiparallel strands with major and minor grooves; B. 2D molecular DNA scheme showing 3 types of chemical interaction: I – phosphodiester bond between a phosphate group and 2 pentoses (5-carbon rings); II – hydrogen bonds between 2 nucleobases (2 for AT, 3 for CG); III – weak hydrophobic interactions between adjacent nucleobases in the same nucleotide chain (adapted from [72]).

DNA electrochemistry is a fast-growing subject worldwide. At acidic pH, DNA electrooxidation occurs in purines (G and A) since pyrimidines are inactive in acidic environment, at approximately 0.77 and 1.1 V vs. SCE on gold electrodes[73]. Furthermore, it has been established that ssDNA has higher anodic currents than dsDNA, since the detectable purines are in direct contact with the working electrode. In dsDNA, by contrast, hybridization greatly diminishes or even dispels the nucleobases electrochemical signal due to greater stability – free electrons in ssDNA participate in hydrogen bridges shown above on Figure 1.8 B.II[72].

Nucleic acids suffer spontaneous decomposition in solution, releasing free base residues (guanine and adenine) as a function of pH, temperature, ionic strength and secondary structure. *In vivo*, B-DNA present in metabolically active cells is expected to undergo depurination at similar rates to that in solution[74]. A 1972 study estimated the depurination rate of *Bacillus subtilis* DNA[75] as 0.5 purine bases lost on the bacterial genome per generation.

A study by Frienkel-Krispin *et al.* [76] has shown that bacterial cytoplasm has hierarchical spatial organization, both with non-random protein and genomic DNA localization. This is only possible through permanent energy consumption, to obtain a non-uniform organization and polarized exchanges. However, during stationary growth phase, bacteria become increasingly ineffective at managing energy, switching from a dynamic order to a stepwise structure assembly consisting of DNA-Dps co-crystals that physically sequester DNA molecules. According to this study, during starvation DNA lies between a lipid layer and hexagonally packed Dps[76].

Ferritin regulation in bacteria has only one genetic target – DNA – responding to several different environmental signals during growth or stationary state, whether it is through iron levels or other stationary state levels, or nutrient and ROS levels during active growth[77].

When Dps was discovered in *E. coli* with non-sequence specific binding and DNA co-crystallization was found to be resistant to detergents, solvents and temperature up to 100ºC [22], consistent with a generic defense strategy for efficient protection against environmental stress. Dps induction in *E. coli* allows for continuous cell growth, revealing that Dps evolution rendered it capable of two different activities under different cell environments; during cell growth, iron sequestration appears to be sufficient to protect DNA from ROS during log growth phase; in contrast, the predominant Dps function during the stationary growth phase is DNA protection[11].

The direct, physical protection of Dps is ensured through efficient DNA complexation, also known as stress-induced biocrystallization[21,64], which provides generalized wide-range DNA protection crucial for prokaryote survival, as a growth-phase-dependent mechanism. Doubly charged cations are crucial to DNA-Dps co-crystallization, acting as ion bridges to the negatively charged Dps dodecamer during the late stationary phase. Specifically, when Mg^{2+} levels are lower than 5 mM, crystal formation and consequent DNA protection are possible[21].

Dps prevents DNA strand breaks and mutagenic events introduced by H_2O_2 *in vivo*, independently of addition order of Fe(II) and H_2O_2 and focusing particularly on guanine protection[62]. However, Dps overexpression during log growth phase does not cause co-crystallization due to high nutrient availability for bacterial multiplication[21].

According to a study by Ceci *et al.* [78], DNA condensation and Dps-DNA co-crystallization is largely controlled by the Dps lysine-rich N-terminus, since it has been suggested that DNA binding only

seems to require a flexible N-terminal domain[79], while self-aggregation and DNA condensation need at least one lysine residue. When protonated, the last 3 N-terminus Lys residues interact with unprotonated surface carboxyl groups from adjoining Dps molecules[78]. Non-DNA binding Dps, either contain shorter or less flexible N-terminal regions[18,43], also protect DNA from stress conditions[42].

The indirect, chemical *in vitro* DNA protection by Dps does not require DNA-Dps complexation, but rather Dps ability to scavenge iron from the cell compartment and limit ROS formation under starvation conditions[34,43]. According to Martinez and Kolter[62], complete *in vitro* DNA-Dps binding elicits maximum protection against oxidative stress in a 1.4 bp DNA : Dps ratio, given that Dps binds both major and minor grooves in DNA.

Electron microscopy studies show that the Dps-DNA complex is highly ordered; since both Dps and DNA are negatively charged, binding has been suggested to be indirectly involve positively charged N-terminus residues (lysines) and the divalent cations, in the correct concentration, that form multiple bridges between Dps and DNA ions. However, the binding mechanism is not fully understood[20].

Chapter II – Instrumental Methods

II.1 Electrochemical fundamentals: Bioelectrochemistry as a tool for studying biological systems

Electrochemistry is primarily concerned with the connection between the chemical and electrical effects on substances. Since the invention of the electrochemical cell in 1800 by Volta, several electrochemical techniques have been developed to perform quantitative, qualitative and monitoring biochemical analysis for many purposes[80].

The main principle of electrochemistry is the occurrence of redox reactions, which involve simultaneous gain (reduction) and loss (oxidation) of electrons by two different chemical species, monitored by an electrode in a controlled environment:

$$Red \rightarrow Ox + ne^- \quad (\mathbf{2.1}),$$

where Red and Ox are respectively the reduced and oxidized species and *n* is the number of electrons. The resulting current is proportional to the electrode reaction rate, and depends on the rates of the processes listed below:

1. Mass transfer (e.g., transport of Red or Ox to the electrode surface)
2. Electron transfer at the electrode surface
3. Chemical reactions occuring at or before the electron transfer
4. Physical reactions at the electrode surface (adsorption, desorption, crystallization).

Two main types of techniques can be distinguished in analytical electrochemistry[81]:

- Potentiometry determines the potential (E) of electrochemical cells at approximately zero current, where E is proportional to the activity of the species under study, in relation to a standard reference electrode (e.g., the ubiquitous pH meter);

- Amperometry is significantly more versatile, since it is based on passing current (I) whose intensity is proportional to the electrolyte concentration, through a polarizable electrode. It can be further divided into several other techniques, among which voltammetry and chronoamperometry, which have been used on this thesis.

Thus, bioelectrochemistry is the study of chemical interactions between biological molecules through the application of electricity. Electrochemical techniques are especially adequate to verify protein interference, namely in oxidorreductases, given its low detection limit and high signal/noise ratio.

This thesis will be following IUPAC conventions when current signs are concerned; therefore, reductive current will be considered negative.

II. 2 Electrochemical techniques

The observed potentials at which any redox reaction occur on the electrochemical assays will always be shown with respect to their reference potentials (Saturated Calomel Electrode (SCE) or silver/silver chloride (Ag/AgCl peek – polyether ketone)). As such, Table II.I below shows each reference electrode potential with respect to the Standard Hydrogen Electrode (SHE), whose potential has been conventionally decided as zero.

Table II.I – Correspondence table between reference electrode potentials used in this project *vs.* Standard Hydrogen Electrode (SHE).

Reference electrode	Electrode potential (*vs.* SHE), at T=25ºC
SCE	0.2412 V
Ag/AgCl	0.236 V

II.2.1 Cyclic voltammetry

Cyclic voltammetry is efficient for rapid observations of redox behavior throughout a broad range of potential. It is also a good methodology for quantitative determination and mechanism elucidation, since I_p (current peak) is proportional to the analyte concentration.

During a voltammetry assay, electrode potential is linearly swept and the resulting current is monitored as a result of working electrode polarization (driving the potential away from equilibrium or open-circuit conditions, as a function of time). In this 3 electrode technique, electrochemical behavior is monitored at the working electrode (WE), immersed in an electrolyte solution containing ions which allow conductivity passage; a reference electrode (RE) with a fixed, known potential is used to measure a potential difference between the WE and the RE. The absolute voltage value can then be calculated through the standard hydrogen electrode (SHE) corresponding Table II.I above. The remaining electrode is the counter electrode (CE), used to favor current passage at the WE. Therefore, while WE potential is measured with respect to the RE which is itself at equilibrium, WE current is observed with respect to the CE; it should be noted that the WE and the CE should have approximate surface areas.

Peak current has two components: capacitive current is the initial adjustment of superficial analyte concentration to its equilibrium constant through double layer unloading (given by the Nernst equation); whereas faradaic current is controlled by diffusion. The capacitive component decays rapidly as the diffusion layer extends progressively farther away from the WE surface.

Regarding cyclic voltammetry, the electrode potential is varied from the equilibrium value (E_{OCP}, at the open circuit potential) to a vertex potential, where the potential scan direction is reversed, according to

$$\begin{matrix}\left(0 < t \le \lambda\right), E = E_i - \nu t \\ \left(t > \lambda\right), E = E_i - 2\nu\lambda + \upsilon t\end{matrix} \quad (\mathbf{2.2}, \mathbf{2.3})$$

Figure 2.1 summarizes the technique. The electrochemical sign reads as a triangular potential *vs.* time wave between vertex potentials; measured current is plotted against potential resulting in a cyclic voltammogram.

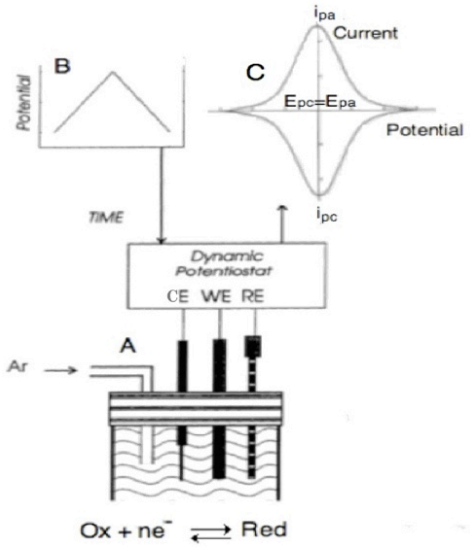

Figure 2.1 – Scheme of a cyclic voltammetry assay, including electrochemical cell (A), potential scan over time plot (B) and a voltammogram showing current variation as a function of applied potential (C). Legend: $i_{pc/a}$=cathodic/anodic peak current; $E_{pc/a}$=cathodic/anodic peak potential[82].

The cyclic voltammogram above shows two redox peaks ($E_{pc/a}$=cathodic/anodic peak potential), belonging to the forward and reverse sides of the plot, of similar shape and identical intensity. Thus, these peaks are indicative of an electrochemically reversible reaction or system. If the mass transport is controlled by diffusion, molecule movement in solution will obey Fick's Law:

$$J = -D\frac{\delta\phi}{\partial x} \quad (\mathbf{2.4}),$$

which asserts that molecular diffusion flux (J) moves from high concentration to low concentration areas (concentration ϕ) in a finite compartment of length x, depending on the diffusion coefficient D.

Reversible systems/reactions obey five rules:

1. $I_{pc} = I_{pa}$ (**2.5**, equal current intensity in both redox peaks)
2. E_{pc} and E_{pa} independent of scan rate (v)
3. $E^{0'} = \frac{E_{pc} + E_{pa}}{2}$ (**2.6**)
4. $I_p \alpha v^{1/2}$
5. $E_{pc} - E_{pa} = \frac{0.059V}{n}$ (**2.7**, T=298 K)

Mass transport can also be controlled by convection and adsorption. While the first will not be covered in this work, the diffusive transport control system will obey the Randles-Sevcik equation:

$$i_p = (2.69X10^5)n^{3/2}ACD^{1/2}v^{1/2} \quad \textbf{(2.8)}$$

This equation asserts that redox peak current is proportional to scan rate (v), n transferred electrons at a given concentration (C, mol/L) of the electrochemically active protein (n) and D.

The non-diffusive transport control system will obey equation 2.9,

$$ip = \frac{n^2F^2}{4RT}\upsilon A\Gamma^*_0 \quad \textbf{(2.9)}$$

Peak current is proportional to scan rate (v) and the active adsorbed electrochemical species (Γ^*_0) on adsorption assays.

In this work, the Langmuir isotherm was applied to the electrochemical system, which predicts a flat electrode surface, adsorption saturation at high solute/protein levels and no interaction between adsorbed molecules. From that system, it is observed that the surface coverage (θ) is proportional to electroactive surface concentration, until a threshold limit (equation 2.9). The adoption of Langmuir isotherm was chosen since it is predicted that the adsorbed amount and tri-dimensional constraints will avoid interprotein interactions and thus validate the equation below:

$$\frac{\theta}{1-\theta} = \beta_i a_{i,\infty} \quad \textbf{(2.10)}$$

In metallic electrodes, specific adsorption is more efficient if the electroacive species is negatively charged, since in that situation, electrode metals can be seen as a cationic net around and through which electrons circulate freely. This situation is advantageous to the system in study, since Dps surface charge is partially negative, as can be seen in Figure 1.4.

II.2.2 Square wave voltammetry

In this technique, the stationary WE is submitted to a potential waveform and the resulting current is measured in pairs. Square wave voltammetry (SWV) is a differential method, thus more accurate and appropriate for assaying DNA protection by Dps. In addition, SWV has comparably lower detection limits, background suppression, wider spectrum of time scales and increased scan rates due to low capacitive current[80]. However, since SWV is very susceptible to species adsorption to the electrode, which is one of the premises of the assay, peak area should be the measure taken, instead of peak height[81]. A typical square wave voltammogram for this technique is shown on Figure 2.2 below.

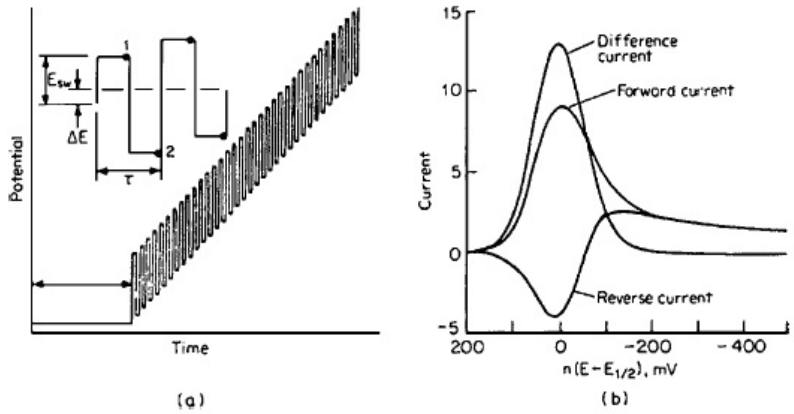

Figure 2.2 – A typical result for a square wave voltammetry assay, showing a staircase evolution of potential through time (excitation signal) and the resulting currents (forward, reverse and difference) through potential evolution[83].

Result interpretation through SWV is done by viewing the obtained waveform as a staircase scan in which each step is superimposed with a symmetrical double pulse (one going forward, one backward) on the waveform in relation to the mean applied potential. Throughout sufficient cycles, the waveform is transfigured to a bipolar square superimposed on the potential staircase.

II.2.3 Chronoamperometry

During a chronoamperometry assay, current is recorded as a function of time and results from a monitored time-constant applied potential at which the analyzed species is electroactive[80].

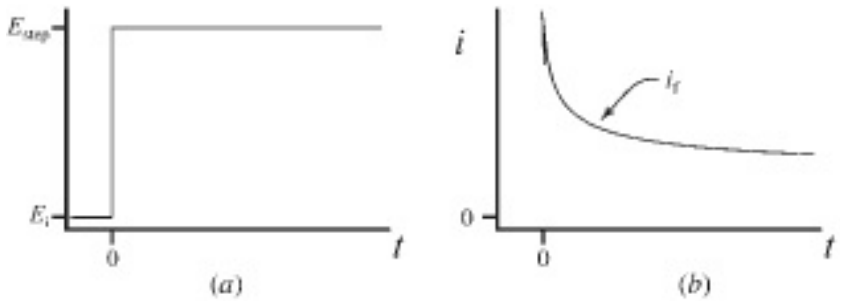

Figure 2.3 – A typical result for a chronoamperometry assay, showing electrode polarization at a given potential, constantly after t=0. The resulting current varies through time in a logarithmic curve if the system is left unperturbed (adapted from [84]).

II.3 Dps electrochemical studies

II.3.1 Electrochemical set-up

Electrochemical assays were done at the µAutolab type III potentiostat. With the exception of the anaerobic assays performed inside the gloved chamber, all assays took place inside a Faraday box, aiming to minimize electromagnetic interferences that would otherwise have been detected through voltammogram noise, as can be seen in Figure 2.4.

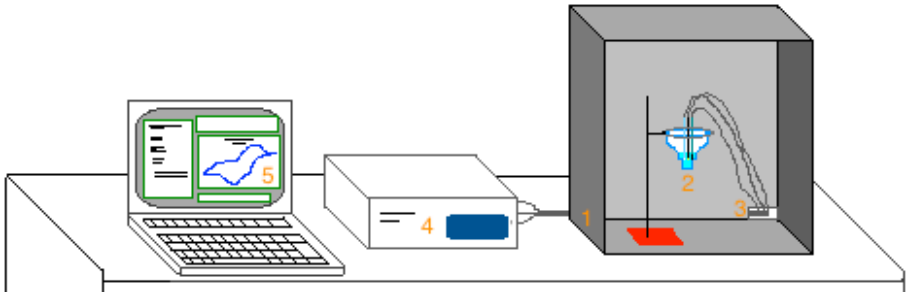

Figure 2.4 – Aerobic electrochemical set-up, consisting of a Faraday box (**1**), electrochemical cell equipped with assay solution and electrodes (**2**) each specifically connected to their respective wires (**3**) and to the potentiostat (**4**). Signal modulation and transfer to digital medium in the computer (**5**).

Iron-incubated Dps (in the presence of 0; 6; 12; 24; 36; 48 and 96 iron atoms per Dps molecule), was studied through cyclic voltammetry; Dps-DNA interaction assays were done through cyclic voltammetry and square wave voltammetry; lastly, chronoamperometry was used to study the effect of hydrogen peroxide or oxygen addition to Dps (specifically, to quantify O_2 production and presence at the Clark electrode surface).

Oxygen interference minimization on the aerobic assays were performed through gaseous argon ventilation (*Alfagaz* Ar(1) B50); anaerobic assays were also performed inside the *UniLab* gloved chamber (*MBraun*) with a controlled atmosphere to minimize oxygen interference (oxygen partial pressure, $pO_2 \approx 0.1$ parts per million (ppm)), shown on Figure 2.5.

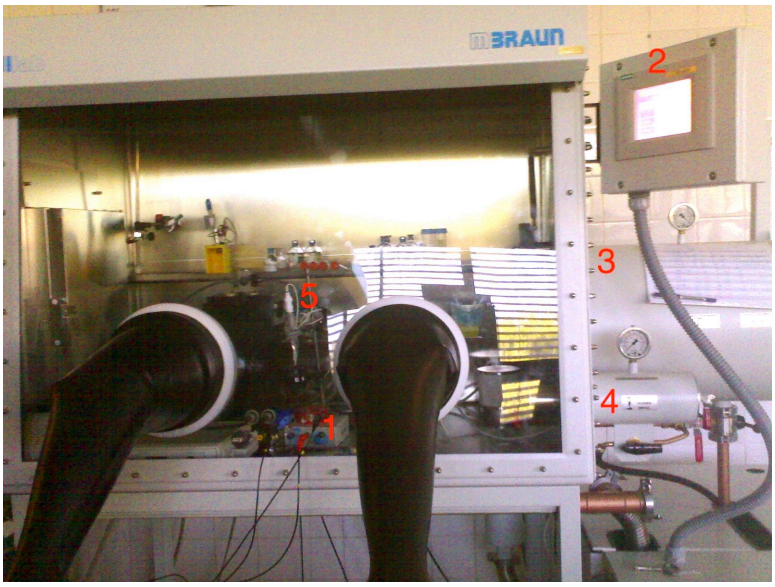

Figure 2.5 – Gloved chamber (*UniLab*) with controlled atmosphere ($pO_2 \approx 0.1$ ppm). Number **1** shows the electrochemical interface between the potentiostat and the inside environment; **2** is a user control interface showing oxygen and pressure levels; **3** and **4** respectively show the large and small antechambers; **5** is the inside chamber environment, specifically the ideal, reachable place for the electrochemical reaction to occur. As in Figure 2.4, the electrochemical cell is connected to the potentiostat and the electrical signal is then modulated to digital in a computer.

Assays inside the anaerobic chamber have special requirements for ideal electrochemical set-up: solutions are deaerated before entry, excluding hydrogen peroxide. All equipment enters the gloved chamber through one of two available antechambers (shown above) and deaerated through 3 vacuum/argon cycles – 3 to 7 minutes each for the small antechamber and 20 to 30 minutes each for the large antechamber, depending on material composition.

Different experimental conditions were used for each assay, whether the protein was directly adsorbed to the electrode (non-diffusive regime) or solubilized in the supporting electrolyte (diffusive regime). A single-compartment electrochemical cell on a 3-electrode configuration was used (individual electrodes are named below, for each assay type); before each assay, the working electrode was polished in Alpha Micropolish alumina powder (particle diameter: 5; 1 and 0.3 µm; *Buehler*) and ultrasonically cleaned for 90 seconds in MilliQ water; finally, all 3 electrodes were thoroughly washed in MilliQ water before beginning the assay.

The chosen supporting electrolyte was 200 mM MOPS pH 7.1 / 200 mM NaCl, freshly diluted from 1M parent solutions. $FeCl_2$ and H_2O_2 solutions were prepared after quantification (present in Appendixes C.4 and C.5) and were added to the electrochemical system concurring with preferred H_2O_2 : Fe : Dps ratios (hydrogen peroxide was 15 times greater than any given Fe : Dps ratio, excepting cases where other quantity is specifically stated). H_2O_2 excess was chosen based on unpublished previous lab research: since Dps is a dodecamer with 12 ferroxidase centers, an excess of 15x for H_2O_2 concentration in relation to iron is sufficient to prevent substrate limitation even in

diffusive systems or if dismutation occurs; consequently, Dps addition ensures sufficient entry of hydrogen peroxide inside the Dps core and its detection on electrochemical assays.

Dps assays using the prototype electrode as a working electrode (WE) were performed in a 1 mL electrochemical cell, platinum wire counter electrode (CE) and silver/silver chloride (Ag/AgCl) or SCE as the reference electrode (RE). 500 µL supporting electrolyte were deaerated for 10 minutes, or, for anaerobic assays, the electrochemical set-up was built at the anaerobic gloved chamber shown on page 21.

Dps assays using commercial graphite as the WE were performed in a single-compartment, narrow end electrochemical cell, platinum wire CE and Ag/AgCl or SCE as the RE. 20 mL supporting electrolyte were deaerated for 45 minutes before starting the assay.

Dps assays using glassy carbon as the WE were performed in a single-compartment, narrow end electrochemical cell, platinum wire CE and peek Ag/AgCl or SCE as the RE.

II.3.2 Dps immobilization procedure

Dps was adsorbed at the commercial graphite or glassy carbon electrode through solvent casting; in commercial graphite, 5 µL Dps solubilized in supporting electrolyte were pipetted onto the electrode surface and incubated for 30 minutes, after which the electrode was immersed in the already prepared electrochemical cell and deaerated for 45 minutes. Electrode diameter was 1.5 mm for prototype pyrolytic graphite, 2.5 mm for commercial graphite and 3 mm for glassy carbon.

II.4 DNA-Dps interaction

II.4.1 Electrochemical set-up

For DNA-Dps interaction assays on a 2 mm gold electrode, a single-compartment, narrow end electrochemical cell, platinum wire CE and SCE RE were used. 20 mL supporting electrolyte were deaerated for 20 minutes.

II.4.2 DNA immobilization procedure

Single-stranded DNA oligonucleotides were purchased as lyophilized powder at STABVIDA, Lda., with the following sequences:

Forward primer – 5’ gat gaa att gcc ggt c gc gtt ctc acc ctg ggc 3’ (modified at 3’ with propanethiol)

Reverse primer – 5’ gcc cag ggt gag aac gcg acc ggc aat ttc atc 3’

DNA complementary oligomer sequences were designed for optimal hybridization and stability (e.g., a high GC content), making it possible to analyze purine bases, whose electrochemical signal is most frequently detectable. DNA adsorption protocol was adapted from [85].

Single stranded DNA assays: 5 µL propanethiol-truncated forward DNA primer were immobilized on the gold electrode surface for 20 hours, after which it was cleaned through water immersion and put in the already prepared electrochemical cell including 20 mL supporting electrolyte and the remaining electrodes, deaerating for 20 minutes before initiating scans. During the assay, 5 µL Dps, iron (in 24 and 120 per protein ratios) and excess hydrogen peroxide were sequentially added through pipetting.

Double stranded DNA assays: 5 µL propanethiol-truncated forward DNA primer were immobilized on the gold WE for 20 h, after which it was cleaned through water immersion. 5 µL reverse DNA primer were added through the same protocol and hybridized for 2 h. The gold electrode was put in the already prepared electrochemical cell including 20 mL supporting electrolyte and the remaining electrodes, deaerating for 20 minutes before initiating scans. During the assay, 5 µL Dps, iron (in 24 and 120 per protein ratios) and excess hydrogen peroxide were sequentially added through pipetting.

Double stranded DNA assays with added propanethiol before hybridization: 5 µL propanethiol-truncated forward DNA primer were immobilized on the gold WE for 20 h, after which it was cleaned through water immersion; 5 µL propanethiol 10 µM were added to the electrode and incubated for 20 h, after which 5 µL reverse DNA primer were added through the same protocol and hybridized for 2 h. The gold electrode was put in the already prepared electrochemical cell including 20 mL supporting electrolyte and the remaining electrodes, deaerating for 20 minutes before initiating scans. During the assay, 5 µL Dps, iron (24 and 120 Fe per protein molecule) and excess hydrogen peroxide were sequentially added through pipetting.

DNA bases have remarkably different adsorption behaviors to inorganic solids such as graphite and crystalline gold, described by the series G>A>T>C[86]. Consequently, a successful DNA primer sequence for adsorption in gold would not only have to contain thiols for optimal electrode interaction, but also equal amounts of all DNA bases to allow for adsorption only on one end instead of the whole sequence being adsorbed, which would then not allow for hybridization.

Chapter III – Recombinant Dps from *Pseudomonas nautica* 617

III.1 Recombinant production of Dps from *P. nautica 617* in *E. coli*

This chapter aims to present the biochemical and spectroscopic characterization of *Ps. nautica* 617 Dps, through heterologous overproduction in *E. coli*.

The earlier lab protocol (developed by Márcia Guilherme[87] during her doctorate thesis) was followed.

> Two separate purification series were performed, but only the latter is shown in the main text. In this series, a higher yield was achieved at the expense of lower purification grade, but consultation of Appendix D provides the results of lower yield, high purification grade.

Recombinant production of Dps from *Ps. nautica 617* in *E. coli*

Transformation of competent BL21 (DE3) *E. coli* cells was performed according to the manufacturer protocol (Appendix B.3). Cells were transformed with a pET-21c (+) plasmid vector, containing the coding gene for wild type Dps, pET21c(+)-1dps.

The primer coding sequence for Dps was obtained from *M. aquaeolei,* invariant to *Ps. nautica 617* and is presented below:

5'ATGGGTAAGAACTTTATAGGTCTCGACACAGACAAACCCAGAAGCTGGCAGACGACTG
AACGAACTGCTCTCTAACTACCAGATTTTCTACATGAATGTGCGTGGCTATCACTGGAAC
ATAAGGGTGACAATTTCTTTGAGCTGCACGCCAAATTTGAAGAACTCTACGATGACCTGC
TGCTCAAGATTGATGAAATTGCCGAGCGCGTTCTCACCCTGGGCCATCGTCCTGCGCACG
CCTACAGTCCTACATTGAAAAGTCCGAAGTGCCGGAGCGCAAGGACGTATCTGATGGCA
AAGAAGCGGTGGGTAACATCGTTGAGAGTTTCGGTAAGCTCATCGCCAAGCAGCGTGGC
CTGCTGAACCTGGCCGGTGAAGCAGAAGATGAAGGTACCGTGGCACTGATGAGTGACTA
CATCTCTCAGCAGAAAAAACGGTATGGATGTACCGGAGCTACCTGGGCCAGTAA 3'

The protein sequence coding for the Dps monomer was then deduced from the nucleotide sequence through the genetic code:

MGKNFIGLDT DKTQKLADAL NELLSNYQIF YMNVRGYHWN IKGDNFFELH
AKFEELYDDL LLKIDEIAER VLTLGHRPAH AYSTYIEKSE VPERKDVSDG
KEAVGNIVES FGKLIAKQRG LLNLAGEAED EGTVALMSDY ISQQEKTVWM
YRSYLGQ

Since the aforementioned plasmid vector contains an ampicillin resistance gene, ampicillin was added to every culture medium, to only select the transformed bacteria containing the pET-21c(+)vector. The ampicillin concentration was 100 µg/mL, diluted from a 100 mg/mL stock solution (Appendix A.2).

After transformation, cells were distributed in sterile Petri dishes containing solid LB culture medium with ampicillin (LB/agar/Amp) and incubated overnight at 37ºC, which promoted colony growth. The aforementioned colonies were then picked and incubated in liquid medium until $OD_{600\ nm}$=0.5, at which point they were induced with 0.5 mM IPTG and incubated for 3 h. Finally, cells were collected in a single tube through centrifugation at 4000 rpm in a Swinging Bucket rotor.

The overexpression conditions are summarized and schematized in figure 3.1. An average of 3.7 g cells/ liter culture medium (wet weight) were obtained.

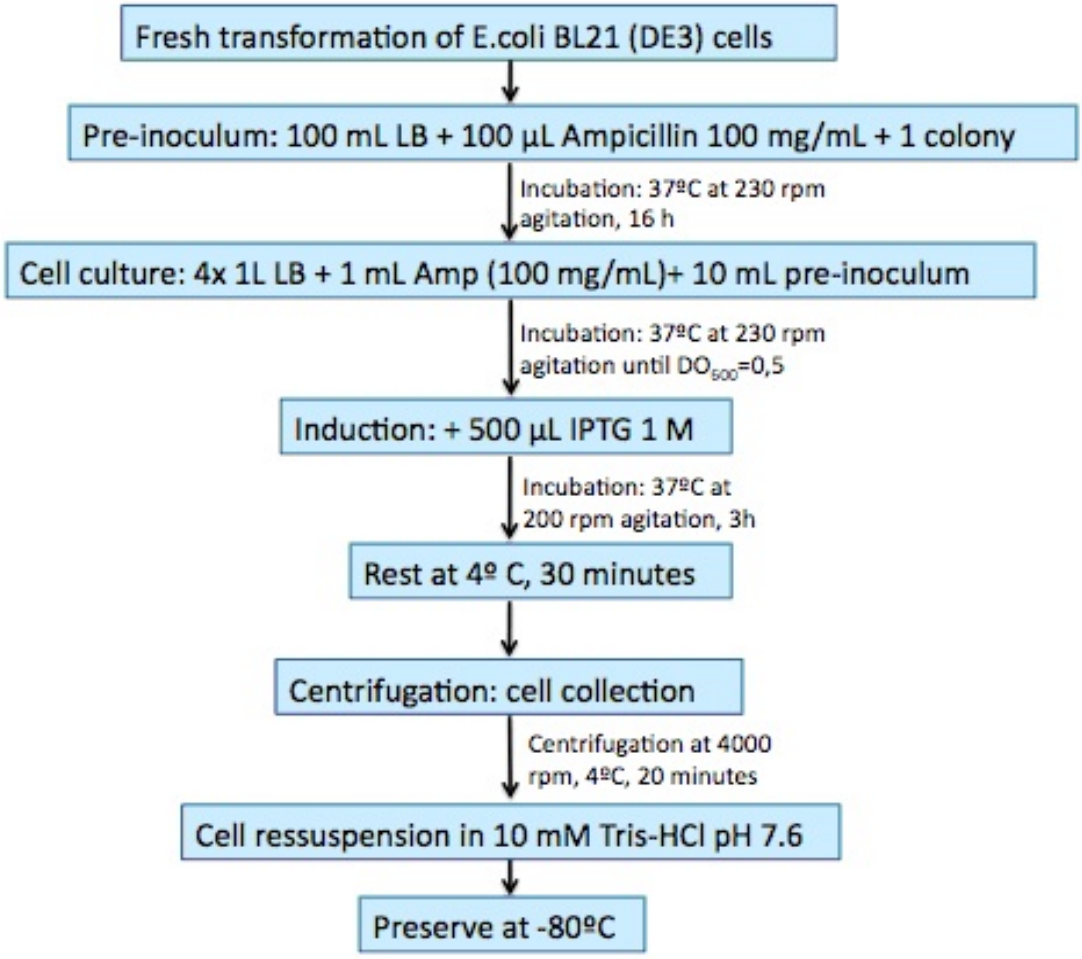

Figure 3.1 – Schematization representing the heterologous overexpression of Dps in *E. coli*.

Dps overproduction in *E. coli* was assessed through SDS-PAGE (Figure 3.2). The first step in assessment was normalization of cellular samples for SDS-PAGE injection through the equation

$$V_{medium}(mL) = \frac{1.2}{DO_{600\,nm}} \quad \text{or} \quad \frac{1}{DO_{600\,nm}} \quad (\mathbf{3.1})$$

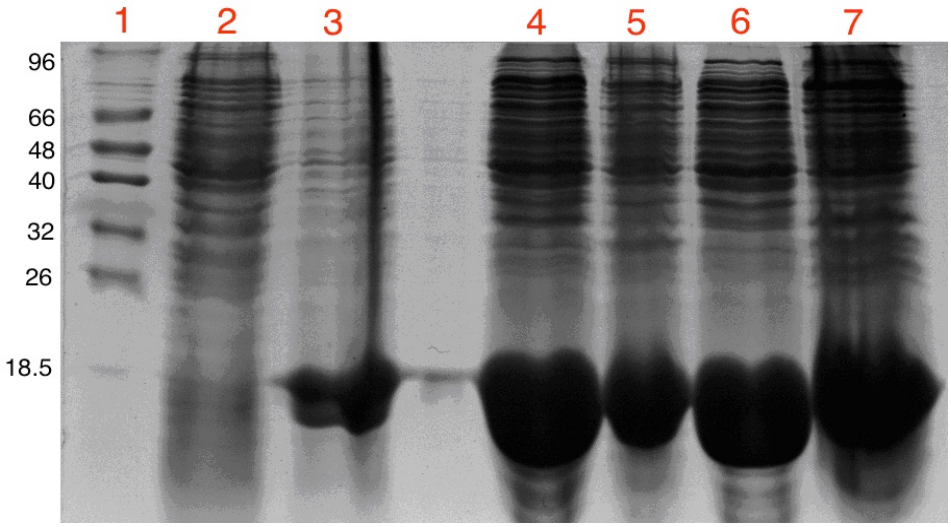

Figure 3.2 – SDS-PAGE (12.5% acrylamide) assessing the overexpression of Dps in *E. coli*. Lanes: **1.** Molecular Weight Marker (LMW-SDS Marker, *nzytech*; molecular weights in kDa); **2.** Total protein content before induction; **3.** Total protein content after induction with 0.5 mM IPTG; **4.** Supernatant after French Press and centrifugation steps; **5.** Pellet after French Press and centrifugation steps; **6.** Supernatant after ultracentrifugation; **7.** Pellet after ultracentrifugation.

III.2 Dps purification

After Dps overexpression, the protein was isolated from the remaining cellular components, before proceeding with its purification. Therefore, the extraction protocol included firstly cell disintegration through rapid liquid nitrogen freezing/thawing cycles in the presence of DNase, followed by passing the remaining extract through a *French Press* at 16,000 Psi (the complete protocol is in Appendix B). After obtaining the cellular suspension, it was centrifuged at 10,000 rpm for 15 minutes and the supernatant was ultracentrifuged at 40,000 rpm for 2h at 4º C, aiming to separate the membrane and the soluble fractions. Our protein was part of the soluble fraction, also known as cellular extract. The results of the aforementioned steps are presented above in figure 3.2.

From observation of Figure 3.2, the ultracentrifugation step had lower separation efficiency of Dps from remaining proteins than was expected; an estimated half of the overexpressed Dps has been transferred to the pellet instead of staying in the supernatant. This can have been caused by a malfunctioning ultracentrifuge, since the protocol standard time for this step had to be doubled to achieve sufficient separation. However, the Dps amount in the pellet was deemed sufficient to follow the remaining purification protocol and the remaining fractions 4, 5 and 7 of Figure 3.2 were preserved at -80º C for safekeeping.

After obtaining the cellular extract, the Dps purification phase was initiated, through dialysis with 10 mM Tris-HCl pH 7.6 (buffer A) and injection in an ionic exchange chromatography column with *DEAE-Sepharose Fast Flow* resin as a chromatographic holder in a glass column (2.6 x 25.4 cm) buffered with 10 mM Tris-HCl pH 7.6 (buffer A) at 5 mL/min.

After injecting and washing the cellular extract with buffer A, the adsorbed proteins were eluted with a discontinuous linear gradient of 10 mM Tris-HCl pH 7.6 / 500 mM NaCl (buffer B). Dps is eluted between 218 and 260 mM NaCl. Figure 3.3 represents the elution profile of this purification step.

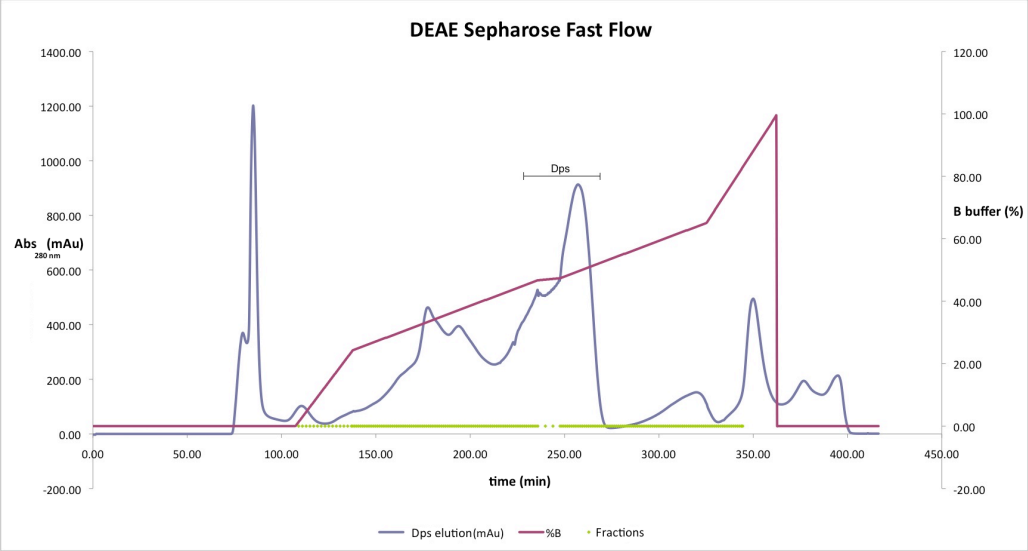

Figure 3.3 – Elution profile of *DEAE Sepharose Fast Flow* chromatographic column (2.6 x 30 cm) used for Dps purification. After equilibrating the column in buffer A (10 mM Tris-HCl pH 7.6), a discontinuous linear 5mL/min gradient of buffer B (10 mM Tris-HCl pH 7.6/ 500 mM NaCl) was applied.

From observation of Figure 3.3, it is concluded that most protein contaminants were eliminated at the first ion exchange chromatography step, showing that chosen experimental conditions were successful. Dps fraction purity was assessed through SDS-PAGE (not shown) and it was decided to recover fractions from 215 to 257 mM NaCl (from 43% to 51.5 % buffer B gradient) and continue with concentration, dialysis to buffer A and vacuum filtration with a 0.45 µm pore filter, proceeding with a more powerful, second ion exchange chromatography step using strongly charged anionic resins.

Dps was injected in a *Q-Resource* (*GE Healthcare*) column. A continuous linear 2 mL/min buffer B gradient was applied. Dps was eluted between 225 and 285 mM NaCl. The elution profile of this purification step is presented in figure 3.4.

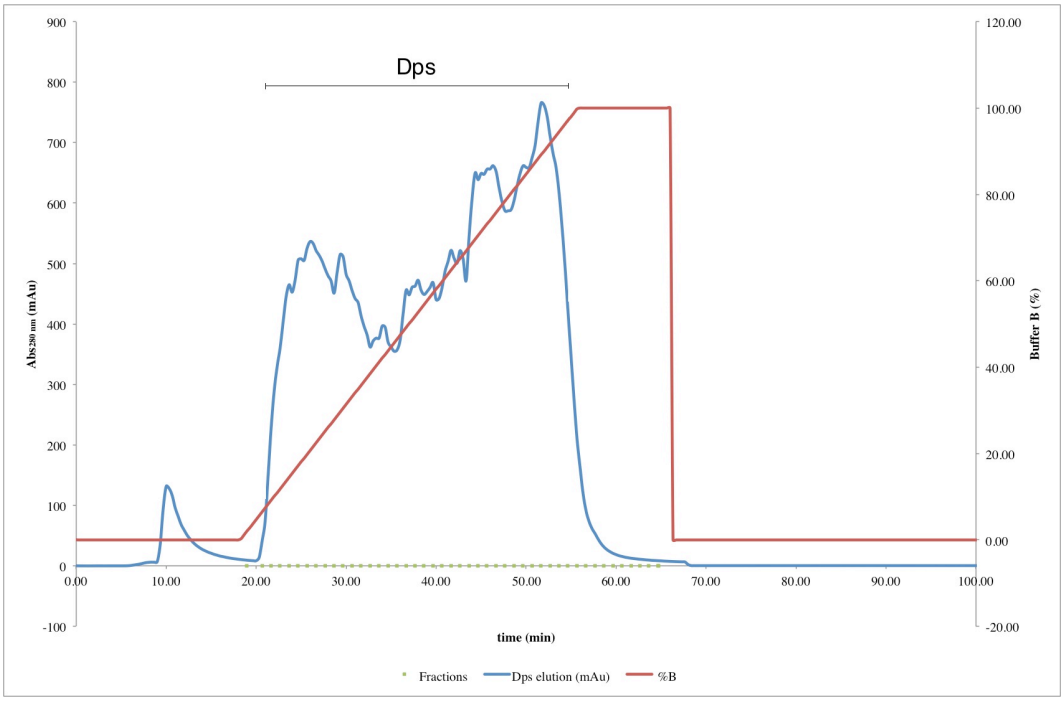

Figure 3.4 – Elution profile of *Q Resource* chromatographic column used in Dps purification. After equilibrating the column in buffer A (10 mM Tris-HCl pH 7.6), a discontinuous linear 5mL/min gradient of buffer B (10 mM Tris-HCl pH 7.6/ 500 mM NaCl) was applied.

From observation of Figure 3.4 above, it can be concluded that the protein separation through ionic exchange was lower than expected, in comparison with the same purification step in the first series (Figure D.3 in Appendix D), however, this result may have been caused by pressure excess inside the ionic exchange column.

After obtaining the pure fraction of Dps through recovery of fractions from 28 to 454.5 mM NaCl (5.6% to 90.9% NaCl gradient), the sample was tested for catalase; this enzyme is an extremely common contaminant in purification protocols and catalyzes the reaction

$$2H_2O_2 \rightarrow O_2 + 2H_2O \quad \textbf{(3.2)}$$

Our protein tested negative for catalase, since no O_2 formation was detected upon hydrogen peroxide addition, which would have been detected through bubble formation.

Figure 3.5 shows the complete purification assessment through SDS-PAGE from overexpression to pure Dps. The purification yield of Dps is an average of 2 mg protein per liter of initial culture.

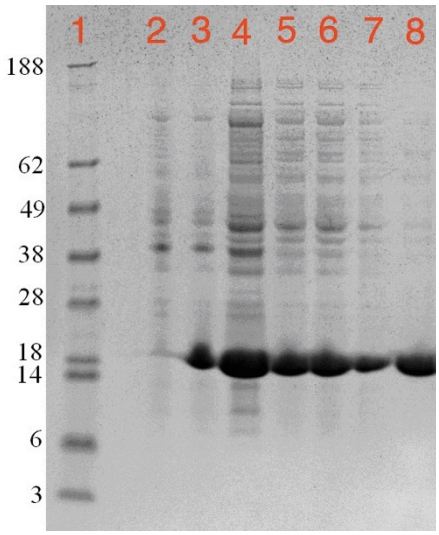

Figure 3.5 – SDS-PAGE (Gradient 3-12% acrylamide) assessing the whole Dps purification protocol. Lanes: **1.** Molecular Weight Marker (See Blue Prestained, Invitrogen; molecular weights in kDa); **2.** Total protein content before induction; **3.** Total protein content after induction with 0.5 mM IPTG; **4.** Supernatant after French Press and centrifugation steps; **5.** Supernatant after ultracentrifugation; **6.** Supernatant after dialysis; **7.** Purest Dps fraction after ionic exchange chromatography using DEAE Sepharose Fast Flow column; **8.** Purest Dps fraction after ionic exchange chromatography using Q-Resource column, concentration and buffer permutation, in 200 mM Mops pH 7.1/200 mM NaCl (1.5 µL + 10 µL sample buffer on 4-8 lanes).

III.3 Inductively Coupled Plasma (ICP) results

After Dps purification, assessing iron levels was important to ensure that Dps was in the apo form for electrochemical assays. Consequently, the Atomic Emission Spectroscopic Service (AES) at DQ-FCT-UNL was responsible for performing Inductively Coupled Plasma (ICP) analyses of Dps and several iron controls. Dps was found to be iron-free above the detection limit (1 ppm).

Chapter IV – Results and Discussion

IV.1 Dps iron incorporation assays in the presence of H_2O_2 (Cyclic voltammetry)

This section aims to analyze Fe(II) catalytic oxidation mechanism on Dps and study its contributive function in DNA protection and ROS avoidance.

Electrochemical techniques are useful to characterize protein mechanisms under diffusive, non-diffusive and convective control systems. In the present case, Dps was studied for the influence of iron ions and hydrogen peroxide presence, as the protein co-substrates. Cyclic voltammetry was the main technique used to characterize Dps electrochemical behavior in adsorption and solution assays with modest contribution from chronoamperometry for oxygen consumption calculation in a Clark electrode, while square wave voltammetry was used for DNA-Dps interaction studies. All techniques are summarized in Chapter II and selected references from the bibliography are also recommended for further clarification.

According to previous results[88-90], Dps has a discernible electrochemical signal in the presence of Fe and H_2O_2, mimetizing its physiological activity. Therefore, the electrochemical assays were performed to confirm the previous results using several experimental conditions: different substrate proportions (iron and hydrogen peroxide), electrode materials and mass transfer control systems (diffusion or adsorption).

Electrode materials used included graphite (built prototype and commercial conventional disk), gold and glassy carbon conventional disks, to obtain the best system for observation of Dps behavior as apoprotein and holoprotein, in the presence of iron and hydrogen peroxide.

Dps expected behavior can be predicted according to our previously obtained knowledge, either in apoprotein form or after adding several iron ratios: apoDps is not expected to be electrochemically active since it lacks both co-substrates (iron and hydrogen peroxide); consequently, all processes observed in the sole presence of Dps will also be expected in control assays in the sole presence of supporting electrolyte, given the WE material properties.

Addition of 6 Fe atoms per Dps (6Fe:Dps ratio) fills ¼ of the ferroxidase centers and will likely produce little to no current, since residual oxygen from solvent, buffer and impurities would not be enough to provoke the less-efficient ferroxidation reaction with such low iron content.

When 12 Fe:Dps is added, semifilling the ferroxidase center, iron entry in Dps would be detected from this ratio and beyond; iron incorporation in Dps would be detected through Fe(II) / Fe(III) oxidation (anodic wave),

Hydrogen peroxide addition to an assay already containing Dps and iron should result in hydrogen peroxide reduction to oxygen at ~ -0.2 V and oxygen reduction to water at a prolonged wave from

-0.4 to -0.7 V. This process is indicative of Dps catalysis and is not present in control assays.

Beyond 24Fe:Dps ratio (including 36; 48; 96 Fe : Dps), iron entry occurs progressively which can possibly include core formation, since iron moves to the protein cavity after oxidation if the second co-substrate (hydrogen peroxide) is added.

Addition of 120 Fe : Dps was exclusively performed for the Dps-DNA interaction assays, since this iron ratio is approximately ¼ of the total Dps iron incorporation capacity. This ratio forces the ferroxidase reaction through abrupt increase on iron levels in contact with Dps and the electrode.

Control of open circuit potential

Except for chronoamperometry assays, scans were initiated at the open circuit potential of each assay.

IV.1.1 Sample graphite electrode

The Dps electrochemical system was firstly studied with a pyrolytic graphite WE, adequate for adsorption due to its high conductivity, anisotropy and irregular structure.

Electrochemical assays under non-diffusive control were attempted with a smaller, custom-built to scale, self-designed graphite electrode to minimize the reaction volume. Briefly, a pyrolytic graphite disk was connected to copper wire with silver glue and perpendicularly enclosed within a glass cylinder. Epoxy glue was then applied to isolate the inside connection from the outside environment as Figure 4.1F shows.

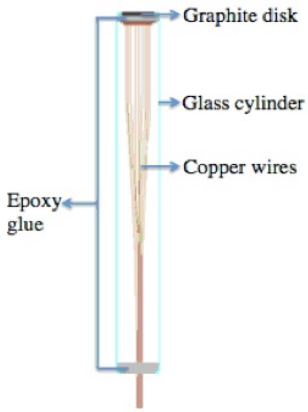

Figure 4.1 – Prototype electrode viewed transversally. A graphite disk (1 mm radius) was connected to copper wires and inserted into a 7 cm glass cylinder. Both extremities were protected with epoxy glue.

In the electrochemical study of Dps from *Pseudomonas nautica 617*, several potential ranges aiming to obtain the appropriate stability window for the supporting electrolyte (200 mM MOPS pH 7.1 / 200 mM NaCl in MilliQ water).

However, the control assay showed interferences, seen below on Figure 4.2:

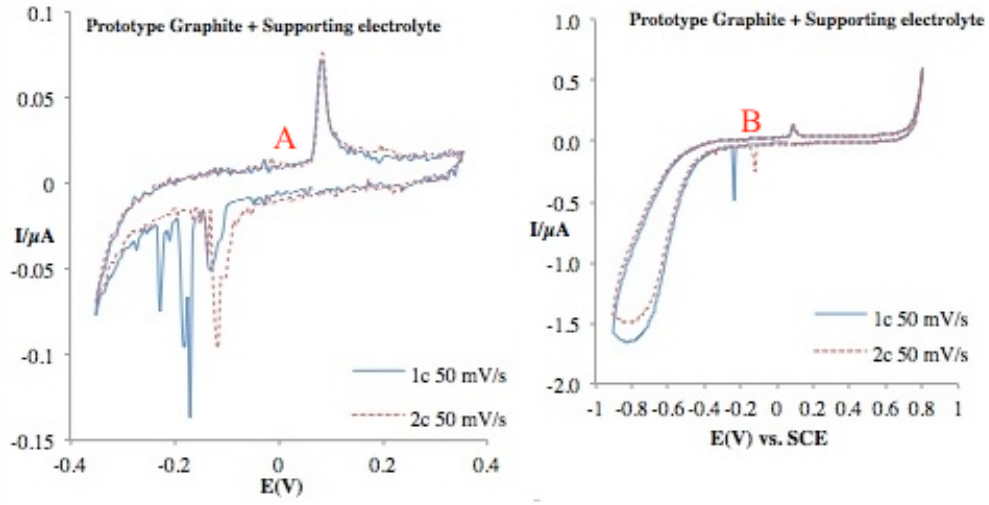

Figure 4.2 – Voltammograms for first and second cycles of the control assay (supporting electrolyte) at 50 mV/s scan rate on pyrolytic graphite, moving from E_{OCP} in the reductive direction. A – between -0.4 and 0.4 V; B – from -0.9 to 0.9 V.

Table 4.I – Control assay cycle 2 peak potentials. Standard potential for the redox peak was calculated as an average of cathodic and anodic potentials.

	E_{pc} (V)	E_{pa} (V)	$E^{0'}$ (V)
Cycle 2	-0.1156	0.0796	-0.018

After observing all assays performed with this electrode, including Figure 4.2 above, it was concluded that, despite interferences, the supporting electrolyte was stable between -0.6 and 0.8 V at 50 mV/s, showing oxygen reduction at negative potentials. Therefore, electrochemical assays performed with graphite as the WE were based on this interval, allowing for adjustments inside the maximum interval not interfering with electrode stability.

After the aforementioned assay, a leak was observed at the electrode that allowed solvent entry and therefore could cause the above voltammogram interferences.

Considering the cycle at which the redox pair is better defined, a formal standard potential of -0.018 V *vs*. SCE is obtained. Converting the value according to the correspondence table at page 16 – 0.2232 V *vs*. SHE – and knowing the prototype electrode composition, it can be suggested that the interference is due to the silver/silver chloride glue whose standard potential – 0.2223 V *vs*. SHE[5] – coincides with the calculated value above.

Adsorption assays were performed at the prototype graphite electrode built at the lab, through solvent casting for 30 minutes. Iron and hydrogen peroxide ratios were added (0; 12; 24; 48 and 96 Fe : Dps. H_2O_2 was added in an excess of 15x as has been explained on page 21). However, the interference mentioned above is present at higher current intensity than the Dps signal; beyond that, resulting

voltammograms had a high noise : protein signal ratio, the reason for which the prototype was rebuilt to repeat the assays. However, the interference occurred again in the same potentials (results not shown) due to material and assembly fragility, which made it unable to resist assay protocol repetition (polishing, sonication and potential scanning); interference was also present in anaerobic assays.

IV.1.2 Commercial graphite – Adsorption assays

The first electrochemical assays performed for this work were under non-diffusive control; Dps was adsorbed in commercial graphite through the same solvent casting protocol explained above for the prototype graphite electrode; assays were performed for 12; 24; 48 and 96 Fe:Dps ratios, adding proportional excess hydrogen peroxide and scanning the electrode potential up to -0.9 to 1.1 V, from 2.5 to 100 mV/s. All control assays were adequately performed with supporting electrolyte and both co-substrates, individually and grouped.

Comparing the electrochemical behavior of apoDps with the supporting electrolyte below on Figure 4.3, it can be concluded that the apoprotein does not have characteristic redox peaks other than the ones already present in the supporting electrolyte:

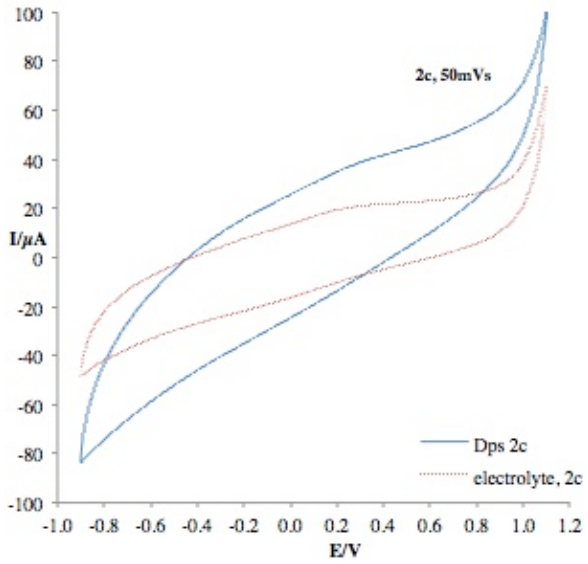

Figure 4.3 – Voltammograms from cycle 2 of apoDps (blue line) and supporting electrolyte (200 mM MOPS pH 7.1 / 200 mM NaCl; dashed red line) at 50 mV/s from -0.9 to 1.1 V, moving from E_{OCP} in the oxidative direction.

From observation of Figure 4.3 above, potential redox peaks are detected at -0.2 and 0.2 V (approximately) in both curves, which can be characteristic of the electrode material (graphite); higher current intensities shown close to the anodic inversion potentials on both curves are consistent with oxide formation (positive potentials). Both these electrochemical phenomena vary in intensity and potential with pH and electrode material. Considering that the untreated graphite surface is irregular and prone to oxygen adsorption as oxides, higher current intensity shown above are frequent in adsorption assays, given that adsorbed Dps partially occupies the large graphite surface; thus, a

considerable surface area is available for the remaining compounds, including oxygen, to interact with the electrode. The enhanced voltammogram slope for the Dps assay indicates greater resistivity, possibly due to insufficient deaeration, oxide or gas formation.

After all apoDps assays were performed, precise Fe ratios were added to Dps through 2 different protocols: 1. Fe addition upon Dps adsorption to the WE; 2. Fe incubation with Dps for 30 minutes. Using both addition types allows us to discern the difference between the results. Figure 4.4 below shows the comparison between supporting electrolyte and Dps incubated with 24 Fe per protein that match filling Dps ferroxidase centers.

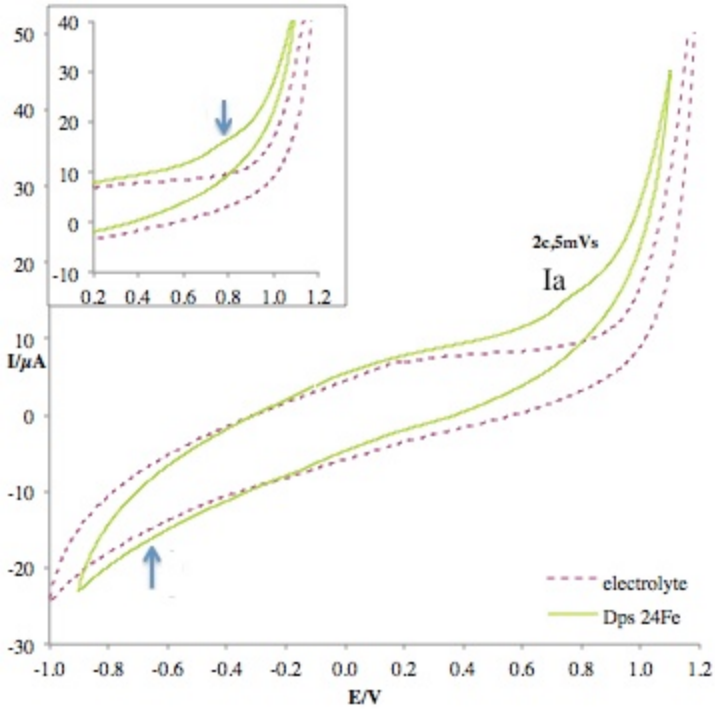

Figure 4.4 – Voltammograms from cycle 2 of Dps with 24Fe ratio added at adsorption (green line) and supporting electrolyte (dashed red line) at 5 mV/s from -0.9 to 1.1 V (Dps) and -1 V to 1.2 V (electrolyte) moving from E_{OCP} in the oxidative direction.

Table 4.II – Possible occurring electrochemical processes in the above iron-loaded Dps voltammogram.

Possible electrochemical process	**Potential (V)**
Iron oxidation	0.759 (Ia)
Core formation?	0.900
Iron reduction?	-0.600

Since adsorption voltammograms were performed in the oxidative direction, it is expected that an anodic wave or peak occurs indicating iron oxidation Fe(II) / Fe(III), whose absolute current intensity will diminish as the reaction occurs and ferrous iron is spent, (Fe(II) could stay undetected if it is

already inside Dps at the beggining of the electrochemical assay); in the presence of Dps, iron oxidation could be consistent with the ferroxidation reaction if an available and adequate oxidant is available in the electrochemical cell; after passing the inversion potential to the reductive direction, several cathodic peaks or waves can be expected, depending on the specific assay: iron reduction, hydrogen peroxide conversion to oxygen and subsequently to water.

On Figure 4.4 above, at 5 mV/s and in the presence of 24Fe : Dps ratio, a significant anodic peak is observed at 0.759 V (peak I_a) that might indicate iron oxidation. As scan rates increase, redox reactions are progressively more irreversible, resulting in a less well-defined anodic peak at 50 and 100 mV/s at 0.761 V. At 100 mV/s, characteristic graphite peaks are less visible, which can indicate electrochemical species adsorption at the electrode surface. The anodic peak is still well defined but its current intensity is lower than other scan rates, since higher scan rates promote irreversibility on electrochemical reactions. Intensity of oxidation peaks nearing the inversion potentials increase proportionally with scan rate (from 5 to 100 mV/s), which can be due to iron or graphite oxide formation at the electrode surface. For better space organization, higher scan rates are shown on Appendix H at page 98.

Anodic current intensity increase is also discernible on the above voltammogram at 0.9 V and can be indicative of core formation initiated at the lower potential, which would be expected since all the ferroxidase centers are occupied at this iron ratio. A small cathodic wave at -0.6 V is also present at higher scan rates and can thus be indicative of ferrous oxide reduction at the electrode surface.

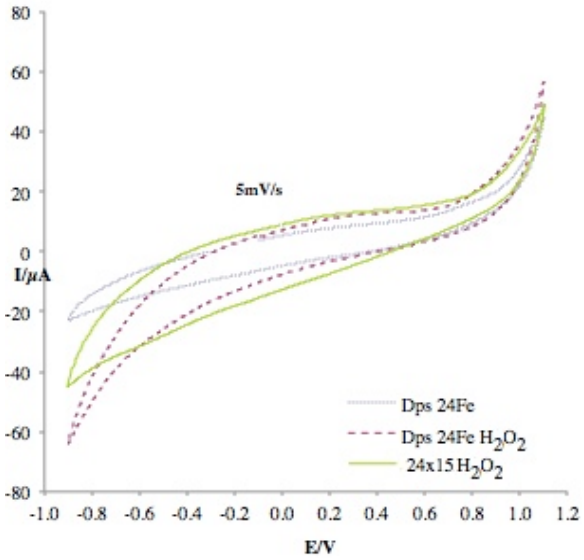

Figure 4.5 – Voltammograms from cycle 2 of Dps : 24 Fe ratio added at adsorption in the presence (dashed red line) and absence (thin blue dashed line) of H_2O_2, comparing with control and electrolyte (200 mM MOPS pH 7.1 / 200 mM NaCl) at 50 mV/s from -0.9 to 1.1 V, moving from E_{OCP} in the oxidative direction.

Observing Figure 4.5 above, at 5 mV/s, both anodic current at positive potentials and cathodic current at negative potentials are higher in Dps containing both substrates, as should be expected upon H_2O_2

addition. At stoichiometric conditions, at 5 mV/s the peak mentioned above at 0.759 V is absent in iron-incubated Dps (results not shown); presence of O_2 from H_2O_2 reduction can possibly be causing it; at negative potentials, a generalized cathodic current increase from 0.1 to -0.9 V could also be due to the presence of O_2 and H_2O_2. Hydrogen peroxide addition increases cathodic and anodic currents nearing the potential inversions as has been explained above, whose intensity can possible be masking ferroxidation reaction and iron incorporation, both processes occurring in Dps with stoichiometric iron amounts per protein molecule. Assays at 50 and 100 mV/s are shown on Appendix H on page 98, for reading ease.

At the above assay, with 24 Fe : Dps ratio and proportional hydrogen peroxide excess, it is expected that the iron would have entered and been incorporated as ferrihydrite inside the Dps core. However, since the electrochemical process is controlled by adsorption, not all of the ferroxidase centers are available for iron entry due to tri-dimensional constraints, since the spherical protein must connect with the electrode and thus lose some of its interaction with substrates.

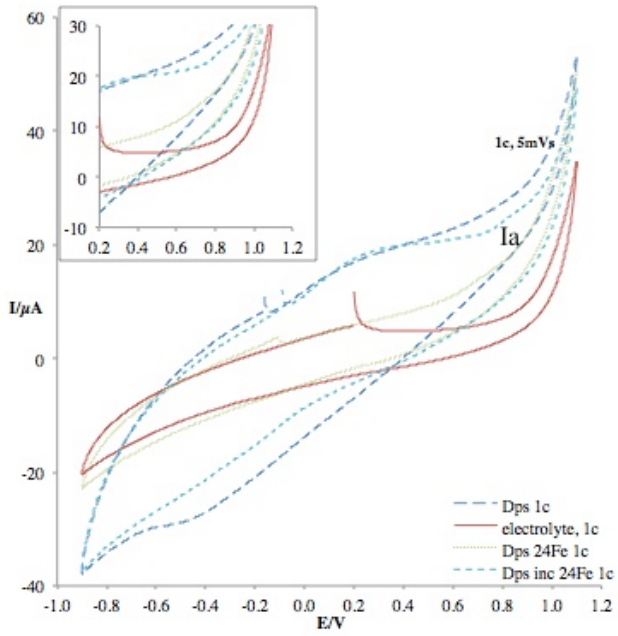

Figure 4.6 – Voltammograms from cycle 1 of apoDps (dashed blue line), electrolyte (continuous red line), Dps with 24 Fe added at adsorption (dashed thin green line) and Dps incubated with 24 Fe (light blue dashed line) at 5 mV/s from -0.9 to 1.1 V, moving from E_{OCP} in the oxidative direction.

Figure 4.6 above suggests that iron-incubated Dps has characteristic electrochemical processes that are more distinctive than apoDps and non-incubated Dps upon iron addition; iron incubation in Dps before adsorption increases the probability of iron successfully entering the ferroxidase center in a somewhat constrained environment.

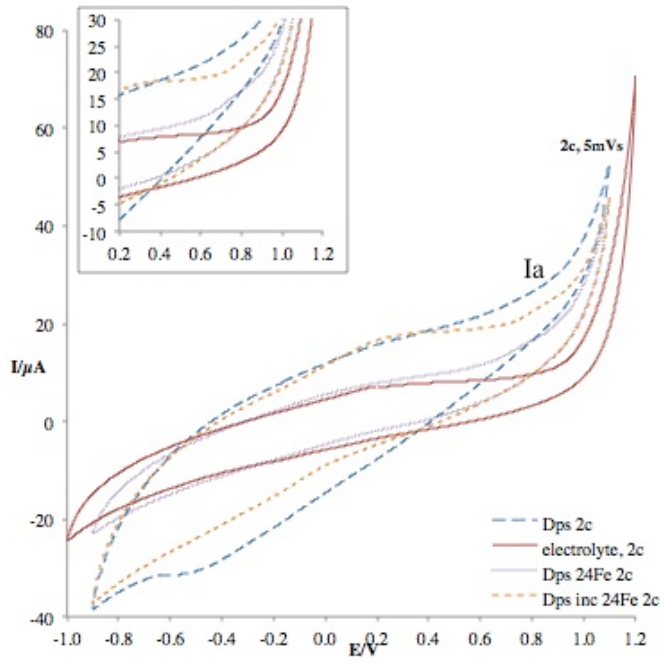

Figure 4.7 – Voltammograms from cycle 2 of apoDps (dashed blue line), electrolyte (continuous red line), Dps with 24 Fe added at adsorption (dashed thin green line) and Dps incubated with 24 Fe (light blue dashed line) at 5 mV/s from -0.9 to 1.1 V, moving from E_{OCP} in the oxidative direction.

Since no hydrogen peroxide was present, assays containing Dps are not catalytic. Furthermore, the same redox processes are observed on the first and second cycles on Figures 4.6 and 4.7 above. The generalized increase on cathodic current on apoDps and Dps incubated with iron, around -0.5 V in apoDps where a small peak can be discerned, which can have been caused by atmospheric oxygen due to insufficient deaeration after the adsorption protocol was performed aerobically inside a Faraday box.

Out of several scan rates studied, processes occurring at 50 and 100 mV/s show expected electrochemical reaction irreversibility increase along with scan rate increase and can be found on Appendix H, page 98.

Addition of suprastoichiometric iron ratios allows for semicontinuous iron entry and Dps catalysis, including nucleation at the Dps core, which could be detected in the voltammogram as small, slightly undefined cathodic and anodic waves. Beyond 48 Fe : Dps (specifically, 96 Fe : Dps), no difference was detected in the adsorption electrochemical assays. Figure 4.8 below shows similar electrochemical behavior to the previously shown 24 Fe : Dps ratio, although the I_a anodic peak is not shown.

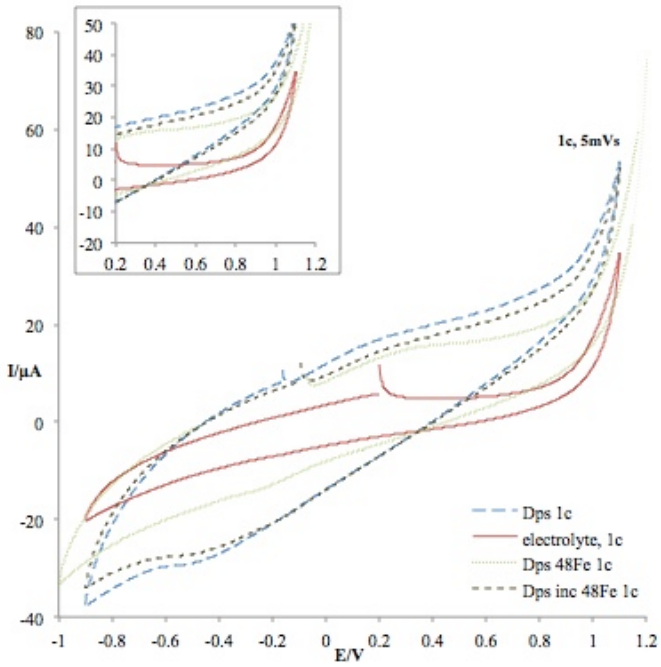

Figure 4.8 – Voltammograms from cycle 1 of apoDps (dashed blue line), electrolyte (continuous red line), Dps with 48 Fe added at adsorption (dashed green line) and Dps incubated with 48 Fe (black dashed line) at 5 mV/s from -0.9 to 1.1 V, moving from E_{OCP} in the oxidative direction.

As Figure 4.8 above shows, differences attributed to incubation are lessened in 48 Fe : Dps ratio, which could be expected since a greater amount of iron incorporation would have originated greater current intensity. The cathodic shoulder at approximately -0.5 V also suggests insufficient deaeration since no hydrogen peroxide is available for reduction and reaction rate of Dps with O_2 is much lower than with H_2O_2.

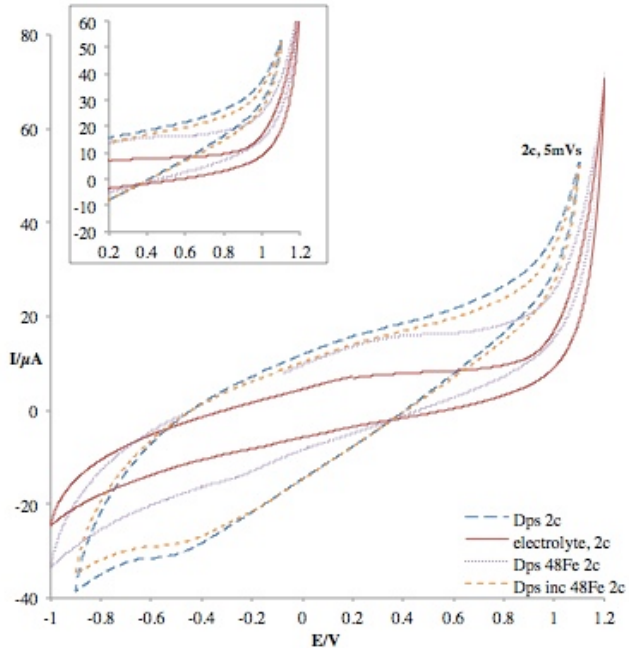

Figure 4.9 – Voltammograms from cycle 2 of apoDps (dashed blue line), electrolyte (continuous red line), Dps with 48 Fe added at adsorption (dashed purple line) and Dps incubated with 48 Fe (dashed orange line) at 5 mV/s from -0.9 to 1.1 V, moving from E_{OCP} in the oxidative direction.

In conclusion, given the inherent disadvantages of non-diffusive control and aerobic system, the results presented above are unexpected; adsorbed Dps in both apo and iron-incubated forms have limited electrochemical response. Adsorption results could have been improved using other electrode materials or surface modifiers, both of which could improve Dps interaction with the electrode resulting in greater electrochemical response.

Adsorption assays were also attempted with neomycin sulphate as an electrochemical promoter, on glassy carbon, pyrolytic and untreated graphite electrodes. The adsorption protocol varied proportionally with the electrode diameter, allowing proportional protein and promoter interference and adsorption with the electrode. Briefly, 1-5 µL 2 mM neomycin sulphate were adsorbed until solvent casting on the respective electrode; 3-10 µL Dps 126 µM were adsorbed for 30 minutes, put onto the electrochemical cell (SCE RE, Pt CE in 2 mL SE (200 mM MOPS pH 7.1 / 200 mM NaCl)) and deaerated for 10 minutes. Cyclic voltammetry scans were performed sequentially 0.2 and 0.6 V away from E_{OCP} in both directions in the reductive direction at 10 to 100 mV/s. Results were not reproducible and the approach was abandoned in favour of solution assays.

IV.1.3 Solution assays with glassy carbon WE

After performing electrochemical assays through non-diffusive control, whose results had oxygen interference and limited characteristic Dps electrochemical response, it was decided to alter the electrochemical system design: placing Dps in solution and allowing for interaction with the WE through diffusion control. Therefore, there was a need for system miniaturization to increase assay yield while using low protein amounts per assay. Miniaturization also included the use of peek Ag/AgCl as the Reference Electrode, reducing reaction volume to 2-3 mL and increasing Dps volume from 5 µL (adsorption assays) to 20 µL, ensuring constant diffusion of electroactive species in contact with the electrode (including Dps).

Solution assays were also performed with pyrolytic graphite with a similar protocol. However, given the aforementioned silver interferences, obtained results (not shown) lacked reproducibility and the characteristic Dps electrochemical response was not detected. Consequently, these assays were successfully performed on glassy carbon electrode.

Cyclic voltammetry assays were performed inside the anaerobic chamber (Figure 2.5 at page 21) to minimize atmospheric oxygen interference and force the catalytic reaction exclusively in the presence of hydrogen peroxide. Consequently, any oxygen reduction detected in the voltammograms comes solely from H_2O_2 reduction. Dps was incubated with several iron ratios (6; 12; 24; 36; 48 and 96 Fe : Dps) for 30 minutes inside an eppendorf tube/flask to allow iron entry inside the dodecamer cavity; the protein was then transferred to a single compartment narrow-end electrochemical cell. Potential scanning was performed sequentially from 50; 100 and 20 mV/s, between E_{OCP} and the potential interval [-0.75 V;0.75 V] moving in the reductive direction.

Two assay types were attempted. Direct assays involved hydrogen peroxide addition immediately before any potential scan, whereas phased assays had two potential scan sets: the first potential scan only monitorizes iron-incubated Dps; after H_2O_2 addition, the potential is scanned again. The whole process is schematized on Figure 4.10 on the next page.

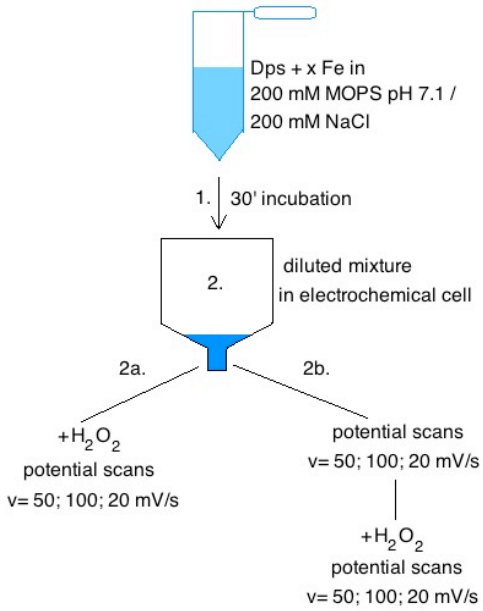

Figure 4.10 – Schematization of both solution assay protocols. Apoprotein Dps (apoDps) is incubated with the appropriate iron ratio for 30 minutes (**1.**), after which it is diluted in the electrochemical cell (**2.**). Two routes are possible from this set-up: direct assays (**2a.**) involve hydrogen peroxide addition before scanning potential; phased assays (**2b.**) scan potential before and after hydrogen peroxide addition.

The decision to perform two different assay sets was made to verify the differences between Dps electrochemical behavior in the presence of one or both co-substrates, since the existing literature suggests that Dps incorporates iron independently of H_2O_2, but the incorporation of hydrogen peroxide is dependent upon iron, as per reactions 1.5-1.7 on Chapter I).

On the other hand, control assays were made to successfully validate results, including apoDps and several substrate and buffer combinations without any protein, to observe the individual and combined behavior of reagents. In the case of apoprotein assays, the main goals were to observe its electrochemical behavior and to verify the vestigial presence of contaminant iron from purification, as well as the presence of other proteins.

Out of the several control assays, the first shown below on Figure 4.11 is a comparison of apoDps and supporting electrolyte.

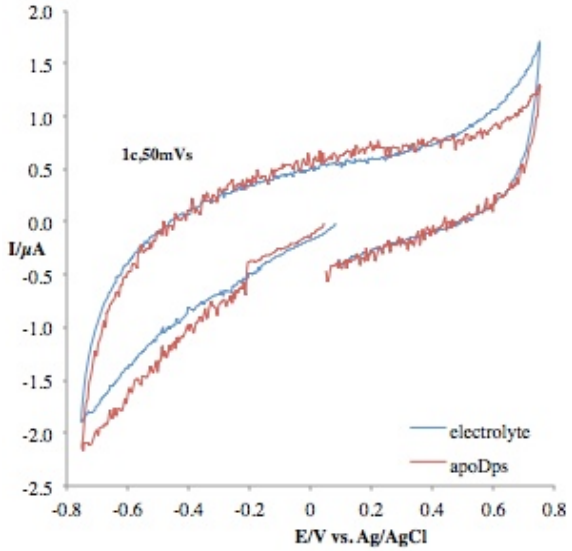

Figure 4.11 – Voltammograms from cycle 1 of supporting electrolyte (blue line) and apoDps (red line) at 50 mV/s from -0.75 to 0.75 V, moving from E_{OCP} in the reductive direction, on glassy carbon WE.

Comparing both assays above, apoDps has no characteristic redox process in the absence of substrates, with the exception of the generalized slight cathodic current increase between –0.2 and -0.75 V that indicates insufficient deaeration of the Dps solution. Also of note was the similar noise from E_{OCP} until approx. -0.2 V, due to initial resistance that is ultimately resolved.

Dps direct assays

The initial goal was to perceive the electrochemical behavior of the direct assays, whose scan rate was performed after sequential addition of iron-incubated Dps, Fe and H_2O_2 ratios. Control assays included, as was explained above, scans made only with iron (6-96Fe) or hydrogen peroxide (6x15-96x15H_2O_2), and both co-substrates (6 to 96 Fe : Dps ratio and proportional excess H_2O_2). Figure 4.12 compares and contrasts the control assays (with the equivalent amount of 6Fe : Dps and 6x15 H_2O_2 : Dps used in the experimental assays) with the Dps assay in the same condition and with both co-substrates.

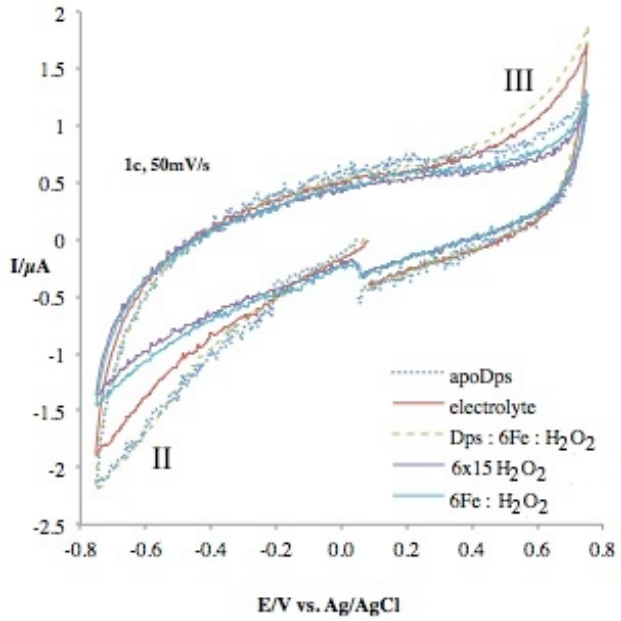

Figure 4.12 – Voltammograms from cycle 1 of apoDps (dashed blue line), supporting electrolyte (red line), direct assay Dps : 6Fe : 6x15 H_2O_2 (dashed green line), 6x15 H_2O_2 (purple line) and 6Fe: 6x15 H_2O_2 (Light blue line) at 50 mV/s from -0.75 to 0.75 V, moving from E_{OCP} in the reductive direction.

Observing Figure 4.12 above, at Dps : 6Fe : 6x15 H_2O_2 direct assay, oxygen production is much more visible at –0.5 V (wave II) at the below scan rate at 20 mV/s than the initial scan at 50 mV/s, which can indicate that the iron incorporation that ultimately leads to oxygen production needs 1,5 minutes to form and reach the electrode (sum of assay timeframes at 50 and 100 mV/s). The cathodic wave has higher current intensity than in Dps; the wave format in the above iron-incubated assay from -0.4 V onwards can be due to O_2 produced either by H_2O_2 dismutation or by Dps. Assuming that O_2 concentration from dismutation is invariable from the H_2O_2 quantification on Appendix C.5 and that H_2O_2 concentration is constant in direct 6Fe:Dps and 6x15 H_2O_2 assay, the difference in current between the direct assay and apoDps indicates O_2 production via Dps.

When the minimum iron amount is added to Dps (6Fe:Dps) filling ¼ of the ferroxidase centres, the oxygen reduction catalysis shown above (wave II) can also be due to H_2O_2 retention inside the Dps core.

Considering the initial scans in each assay, at 50 mV/s, in the presence of Dps, Fe and H_2O_2, the observed redox peaks are only comparable to the assay with apoDps. Redox processes can therefore be related to the electrode material (glassy carbon), since they are also present in Dps; still, the amount of Fe can be insufficient for detection or, alternatively, Fe (II) oxidation could have occurred during the incubation time. If it is the case, the amount of iron detected by the electrode can be lower than the real one, since it has travelled to the ferroxidase centres of the dodecamer and inside the core in ferrihydrite form, or the total amount is diluted in the voltammogram and its detection and signal are not significantly greater than the noise characteristic of the anaerobic chamber, which does not

have the electromagnetic wave minimization ability of a Faraday box. Therefore, the electrode can only have sensitivity to Fe ions in each protein and not individually.

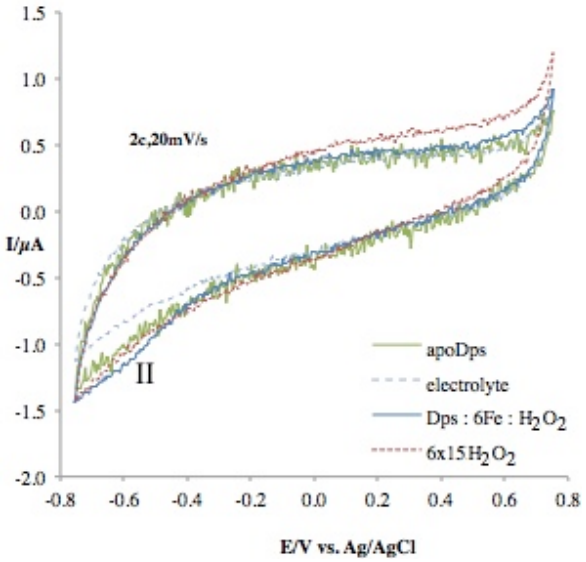

Figure 4.13 – Voltammograms from cycle 2 of apoDps (green line), supporting electrolyte (dashed blue line), direct assay Dps : 6Fe : 6x15 H_2O_2 (blue line) and 6x15 H_2O_2 (dashed red line) at 20 mV/s from -0.75 to 0.75 V, moving from E_{OCP} in the reductive direction.

The last voltammogram of each assay on Figure 4.13 above (second cycle at 20 mV/s) shows the electrochemical behavior evolution of the species after 6 potential scans at different rates. Therefore, O_2 production is first observed at the first cycle at 20 mV/s, albeit lower than in the second cycle. At 50 mV/s, Dps response is not visible in the first cycle; since Dps response to iron is somewhat slow in this iron ratio, the lower scan rate is more adequate, since electron transfer to the electrode is compatible with the protein response in almost real-time.

Other Fe : Dps ratios will be needed to conclude successfully about Dps iron incorporation mechanism, starting with 12 Fe : Dps direct assay below on Figures 4.14 and 4.15.

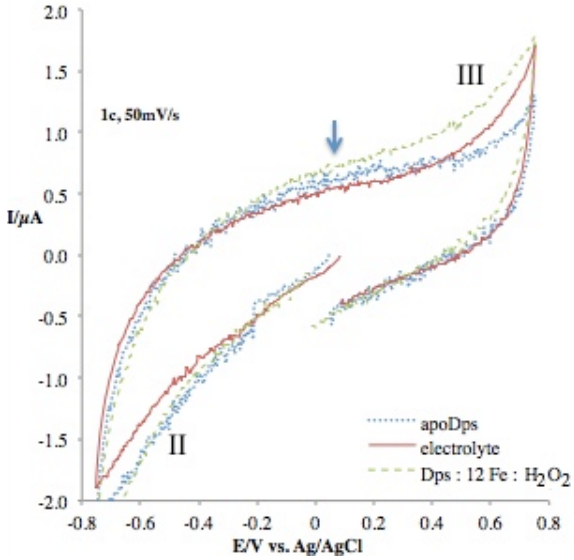

Figure 4.14 – Voltammograms from cycle 1 of apoDps (dashed blue line), supporting electrolyte (red line) and direct assay Dps : 12 Fe : 12x15 H_2O_2 (dashed green line) at 50 mV/s from -0.75 to 0.75 V, moving from E_{OCP} in the reductive direction.

Observation of the first scans at 50 mV/s of 12 Fe:Dps direct assay above on Figure 4.14 suggests that semifilling ferroxidase centers is not detected through cyclic voltammetry, except for greater current intensity at both extreme potentials (waves II and III) and a small anodic shoulder at 0.1 V that can indicate Fe(II) / Fe(III) oxidation.

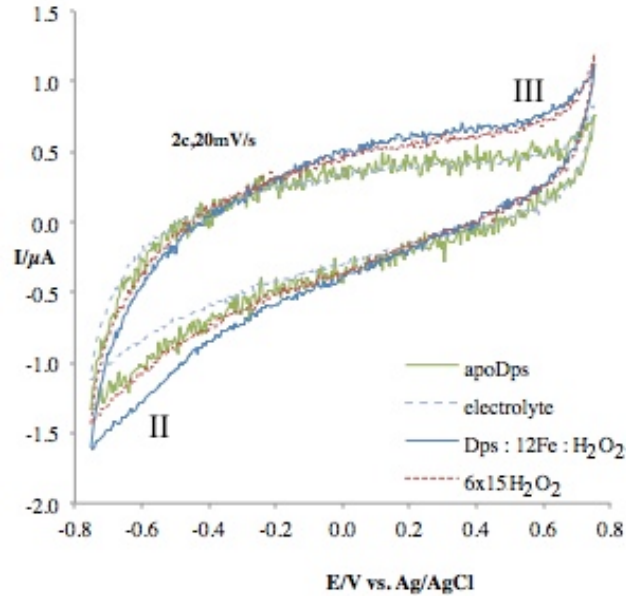

Figure 4.15 – Voltammograms from cycle 2 of apoDps (green line), supporting electrolyte (dashed blue line), direct assay Dps : 12Fe : 12x15 H_2O_2 (blue line) and 6x15 H_2O_2 (dashed red line) at 20 mV/s from -0.75 to 0.75 V, moving from the E_{OCP} in the reductive direction.

At the final 20 mV/s scan shown above on Figure 4.15, the cathodic shoulder of 12Fe:Dps assay is more intense than apoDps particularly at approximately -0.5 V (part of wave II), suggesting that oxygen reduction has continued throughout the scans. A small cathodic wave detected at approximately -0.1 V suggests Fe(III) / Fe(II) reduction. In combination with the anodic shoulder

suggesting iron oxidation is proportionally lowered at 20 mV/s, there may have been iron incorporation into the ferroxidase centers of Dps at this iron ratio.

Continuing on with increasing Fe : Dps ratios, from 24 Fe onwards the electrochemical behavior is markedly different than substoichiometric iron ratios added earlier. The first scans of each iron ratio are especially interesting for this work and are shown below. The latter scans at 20 mV/s all show the same pattern, which will be discussed below and are present at Appendix H, page 98.

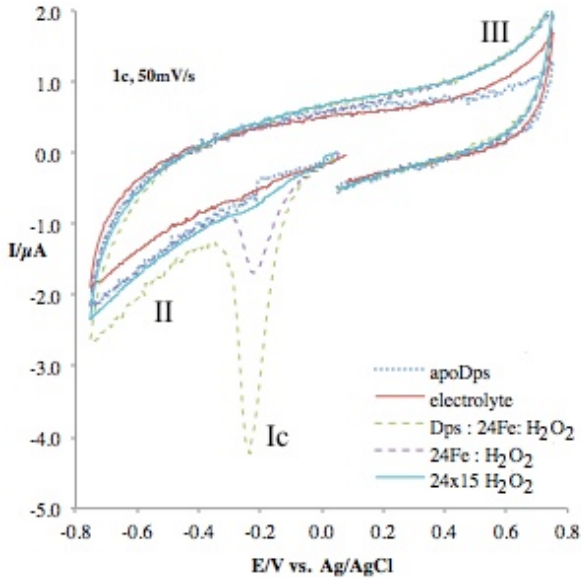

Figure 4.16 – Voltammograms from cycle 1 of apoDps (dashed light blue line), supporting electrolyte (red line), direct assay Dps : 24Fe : 24x15 H_2O_2 (dashed green line), 24 Fe : 24x15 H_2O_2 (dashed purple line) and 24x15 H_2O_2 (blue line) at 50 mV/s from -0.75 to 0.75 V, moving from E_{OCP} in the reductive direction.

At 24 Fe : Dps ratio shown above on Figure 4.16, ferroxidase centers can be fully filled (stoichiometric iron ratio). In comparison to the assay containing both co-substrates (24Fe : H_2O_2), the direct 24 Fe : Dps assay shows greater cathodic current intensity at -0.2 V (peak I_c) which has been previously considered to be characteristic of Fe reduction showing iron incorporation. It can therefore be suggested that iron is in contact with the electrode, either free or inside the Dps molecule, and the difference between both current intensities of the direct assay and the one containing both co-substrates can be due to Dps action since it is the only variable of both assays. As scans increase, iron entry is progressively smaller, shown by disappearing cathodic peak at approximately -0.2 V, while the anodic shoulder considered to be iron oxidation stays the same. Also of note is the increasing generalized cathodic current increase from -0.4 V onwards (wave II); these phenomena can indicate that H_2O_2 is reacting with iron inside Dps resulting in O_2 formation and subsequent reduction while iron is entering into Dps until this process ends when the limiting iron levels deplete.

The 36Fe : Dps direct assay on Figure 4.17 below shows similar behaviour to the 24Fe : Dps assay above, with the maximum current intensity of all direct assays.

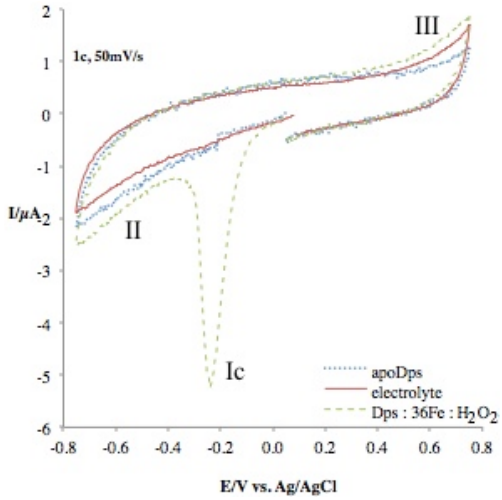

Figure 4.17 – Voltammograms from cycle 1 of apoDps (dashed light blue line), supporting electrolyte (red line) and direct assay Dps : 36Fe : 36x15 H_2O_2 (dashed green line) at 50 mV/s from -0.75 to 0.75 V, moving from E_{OCP} in the reductive direction.

Assays with 48 and 96Fe:Dps on Figures 4.18 and 4.19 below show a second current intensity increase at the supposed iron reduction peak after the maximum at the Dps : 36 Fe : H_2O_2 assay. As scans progress, current intensity at the peak continues to lower (peak I_c decreases and disappears) while the cathodic generalized decrease (wave II) is markedly higher on the Dps : 48 Fe : H_2O_2 assay at 20 mV/s than the Dps : 96 Fe : H_2O_2 assay (shown on Appendix H); however, since iron and hydrogen peroxide ratios on assays containing 96Fe : Dps are double of Dps : 48 Fe : H_2O_2 assay , it might be that maximum reaction rate was not reached at the time of the scan at 20 mV/s. Increasing assay repetition would have been useful to guarantee reproducibility and fortify the aforementioned conclusions about reaction mechanisms in Dps.

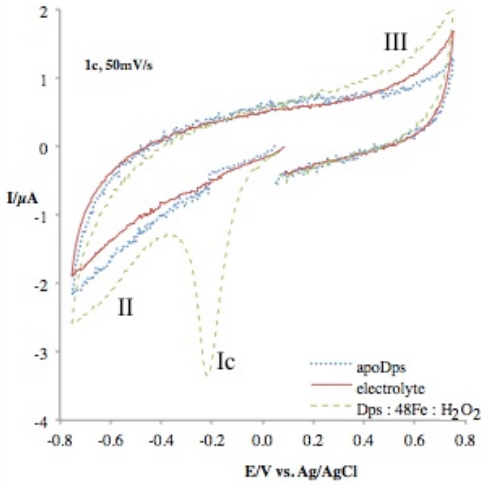

Figure 4.18– Voltammograms from cycle 1 of apoDps (dashed light blue line), supporting electrolyte (red line), direct assay Dps : 48 Fe : 48x15 H_2O_2 (dashed green line) and at 50 mV/s from -0.75 to 0.75 V, moving from E_{OCP} in the reductive direction.

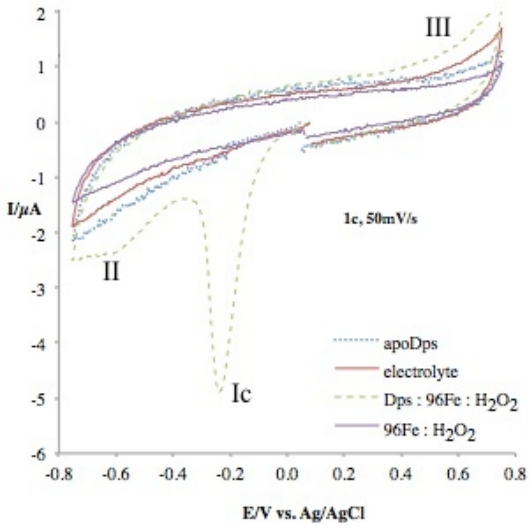

Figure 4.19 – Voltammograms from cycle 2 of apoDps (dashed blue line), supporting electrolyte (red line), direct assay Dps : 96Fe : 96x15 H_2O_2 (dashed green line) and 96Fe : 96x15 H_2O_2 (purple line) at 50 mV/s from -0.75 to 0.75 V, moving from E_{OCP} in the reductive direction.

In the assays with both substrates and without Dps, the electrochemical behavior is different, since oxygen reduction was detected and possibly catalyzed or co-participated with Fe. However, comparing this with the Dps assay, the protein's electrocatalytic ability was higher when both co-substrates are present. In the Dps+H_2O_2 assay, there is no catalytic effect given the absence of iron – the observed catalysis is due to the Fe incorporation inside the ferroxidase centers. Increasing the number of assays should increase reproducibility. The difference relative to other assays only with H_2O_2 without iron-incubated Dps and where the presence of O_2 is observed can be due to H_2O_2 having enough time to dismutate and imply the presence of O_2, which would then be reduced inside the electrochemical system.

Evolution of the Dps cathodic current peak in solution assays is proportional in 6; 12; 24 and 36 Fe : Dps ratios up to 48 Fe at about -0.22 V. The comparative graph on Figure 4.20 below shows all direct assays at the first scan (50 mV/s):

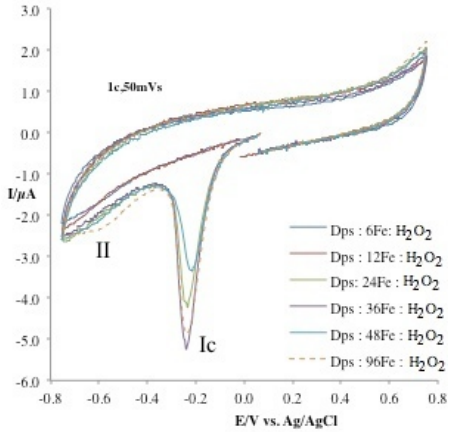

Figure 4.20 – Voltammograms from cycle 1 at 50 mV/s, comparing direct assays Dps: 6; 12; 24; 36; 48 and 96Fe; excess proportional H_2O_2 addition, from -0.75 to 0.75 V, moving from E_{OCP} in the reductive direction.

Observing Figure 4.20 above, the first scan rate of all direct assays can indicate that only Fe (III) is present and reduced to Fe(II) (peak I_c) at approximately -0.22 V. Therefore, it is possible that iron enters the ferroxidase centers and, consequently, into the dodecamer cavity where it forms oxides through reactions 1.5-1.7 presented on Chapter I; it is then suggested that the electrochemical response should only be due to iron presence and its incorporation reactions. Since all solution scans start at E_{OCP} and are performed in the cathodic direction, any iron reduction observed initially will have originated on iron oxidation (Fe(II) / Fe(III)) on Dps before any potential was applying, during incubation.

However, iron-incubated Dps assays with 6 and 12 Fe and proportional H_2O_2 show no significant variation, probably due to partial filling of the ferroxidase centers blocking contact between iron and the electrode due to iron interacting with Dps amino acids. Since the system is under diffusive control, that added iron is lower than the number of centers and that the reaction begins immediately upon H_2O_2 addition at low speed, the amount of detected Fe(II) can be under the detection limit and therefore does not appear in the cyclic voltammogram in substoichiometric ratios.

Addition of suprastoichiometric amounts of iron to Dps in the direct assays originated a proportional increase of 24 and 36 Fe : Dps ratios, decreasing in the 48 Fe ratio and increasing again in the 96 Fe ratio. The reduction peak for Fe(III) / Fe(II) was formed at approximately 0.22 V (peak I_c).
Also of note in the above figure is the consistent increase of cathodic current at approximately -0.5 V; its shape relative to the remaining voltammogram indicates that it should not originate from insufficient deaeration. This current increase should be due to oxygen formation through H_2O_2 addition and subsequent reduction, since it is absent from the above control assays. It can also be suggested that oxygen production seems to be directly proportional to the increase in iron ion availability to Dps.

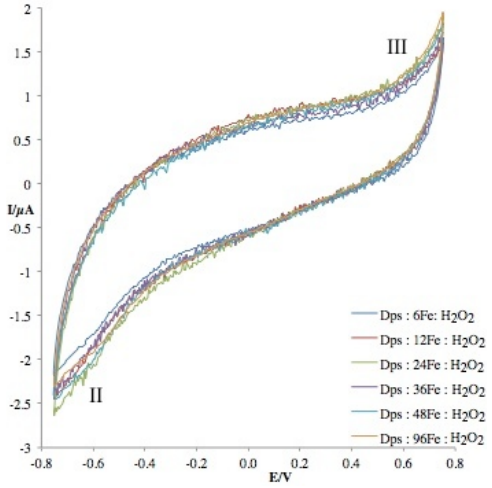

Figure 4.21 - Voltammograms from cycle 2 at 50 mV/s, comparing direct assays Dps: 6;12;24;36;48 and 96Fe; excess proportional H_2O_2 addition, from -0.75 to 0.75 V, moving from E_{OCP} in the reductive direction.

The following scans registered a cathodic current decrease as opposed to the first scans at 50 mV/s above on Figure 4.21; at the last scan performed in the direct assays, no peak is observed at that potential, rather a "shoulder" approximately at -0.6 V that may be connected to hydrogen peroxide oxidation or core formation, given that, as Fe enters the Dps cavity after filling the ferroxidase centers, its electrochemical behavior and consequently its potential will change, given the formation of iron oxides inside the Dps cavity.

Comparison voltammograms are shown below on Figure 4.22 with Dps : 24Fe : H_2O_2, first and second scans at 50 mV/s and respective control assays containing iron.

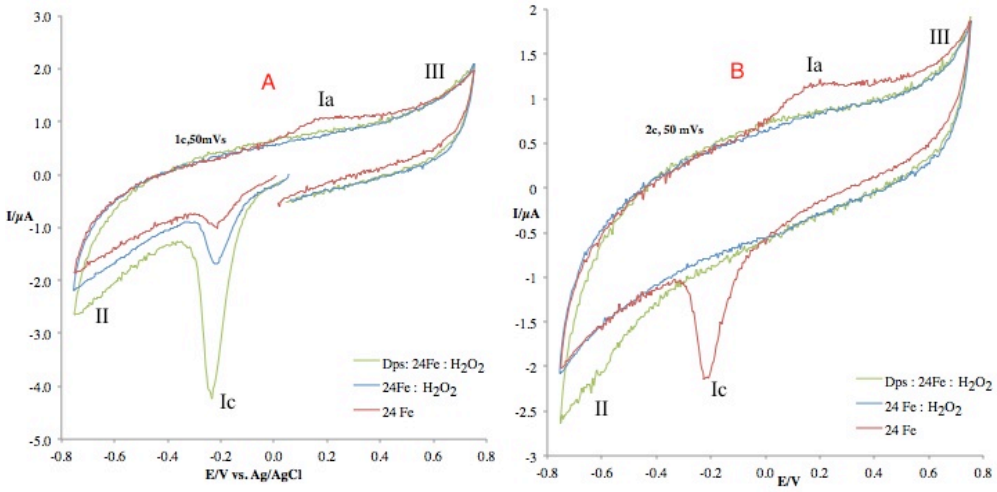

Figure 4.22 – Voltammograms from cycle 1 (A) and 2 (B) at 50 mV/s comparing direct Dps : 24 Fe : H_2O_2 and respective control assays containing iron, from -0.75 o 0.75 V, moving from E_{OCP} in the reductive direction.

Observing Figure 4.22 above, the electrochemical evolution from the first to the second potential scans on Dps containing both co-substrates shows that the Fe(III) / Fe(II) reduction peak at approximately -0.2 V is only detected on the first scan, disappearing from the second scan. Comparing assays containing Dps with control assays shows that Fe characteristic peaks continue on assays only containing iron. However, assays containing both co-substrates show a smaller Fe(III) / Fe(II) reduction peak than in assays containing Dps, disappearing on the second potential scan, which might be due to irreversible interaction between Fe(III) and H_2O_2.

A comparison graph is presented below on Figure 4.23 to understand the relationship between Fe : Dps ratios on the last assay scan (cycle 2 at 20 mV/s) and resulting peak currents, when present, on all solution assays.

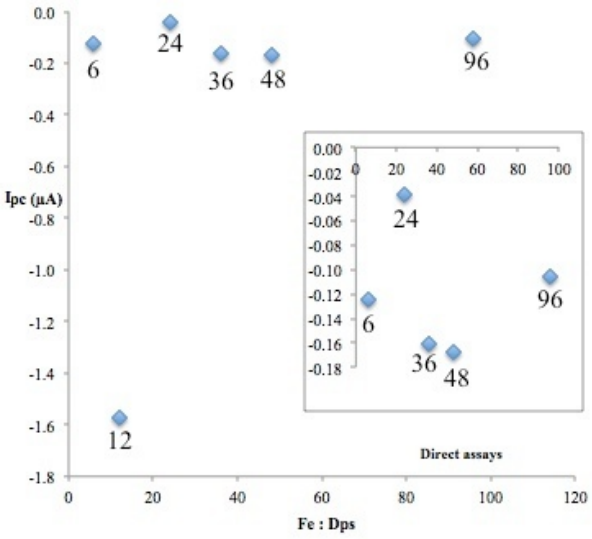

Figure 4.23 – Direct assay cathodic peak current intensity variation at approximately -0.2 V with increasing Fe : Dps ratios, from cycle 2 at 20 mV/s.

Figure 4.23 above suggests no relationship between current intensity and Fe : Dps ratios on Dps direct assays. Fe (III) / Fe (II) reduction occurs independently of Fe ratio above 24 Fe and inclusive. Current intensity on substoichiometric iron ratio assays may not be seen due to technique sensitivity.

Phased assays:

Comparing with the direct assays, phased assays were monitorized by cyclic voltammetry in 2 phases: in the 1st phase only iron-incubated Dps is present in the ratios specified below, after which H_2O_2 was added proportionally with 15x excess. A protocol schematization is presented back in Figure 4.10. This assay variation can allow for observation of the individual influence of both Dps co-substrates on its mechanism, possibly showing whether iron incorporation and core formation are dependent upon H_2O_2 addition and which ratios cause Dps electrochemical behavior alteration. Figure 4.25 below shows the comparison between the last scan at all iron ratios tested.

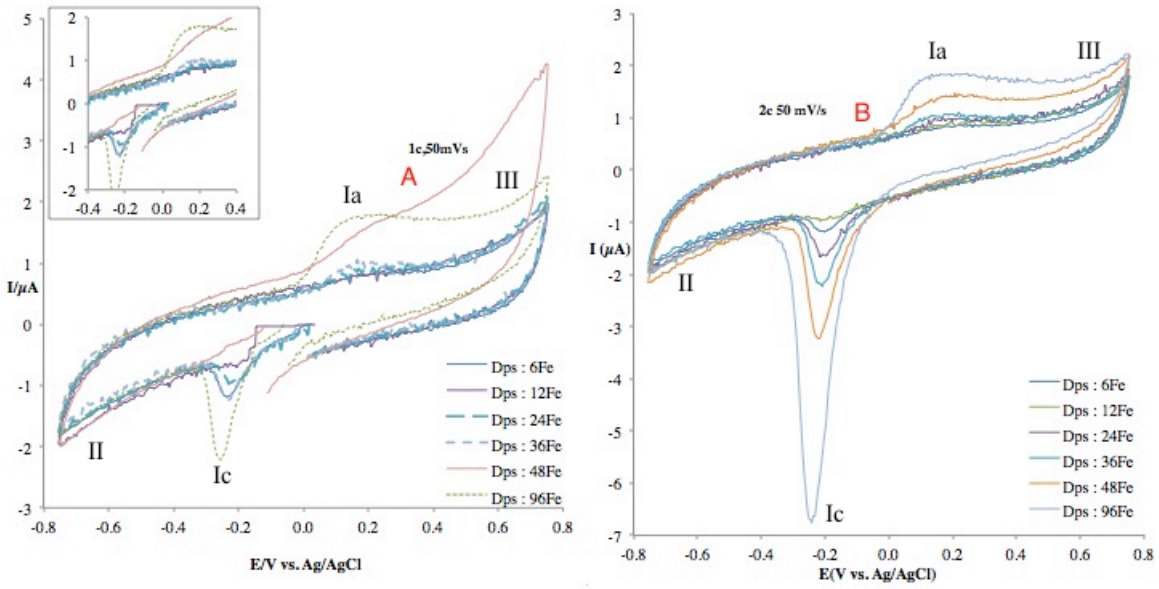

Figure 4.24 – Voltammograms from cycles 1 (A) and 2 (B) at 50 mV/s, comparing phased assays Dps: 6; 12; 24; 36; 48 and 96 Fe from -0.75 to 0.75 V, moving from E_{OCP} in the reductive direction.

The electrochemical behaviour of Dps on cycle 2 at 50 mV/s and subsequent scans at 100 and 20 mV/s is similar. An example of the electrochemical behaviour at 20 mV/s is shown below on Figure 4.25:

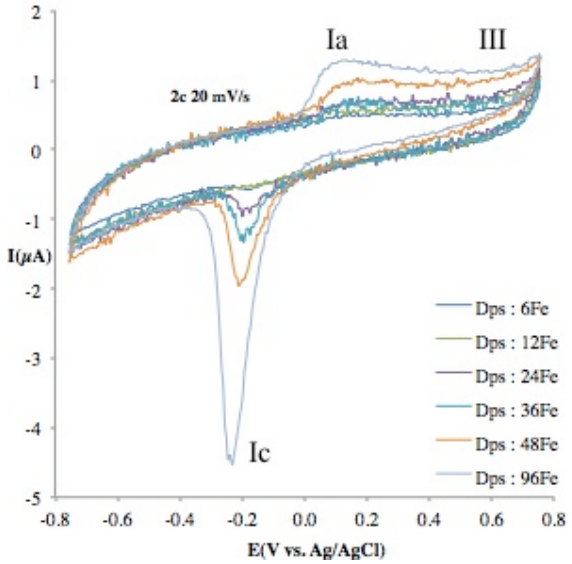

Figure 4.25 – Voltammograms from cycle 2 at 20 mV/s, comparing phased assays Dps: 6; 12; 24; 36; 48 and 96 Fe from -0.75 to 0.75 V, moving from E_{OCP} in the reductive direction.

Observing Figure 4.25 above, with increasing Fe:Dps ratios, a cathodic peak can be observed at approximately -0.2 V, increasing with each successive Fe : Dps ratio. The respective anodic peak can also be observed at approximately 0.12 V. Although Dps is always iron-incubated for 30 minutes, iron can hypothetically be free and in contact with the electrode surface, or already incorporated inside the protein. However, control assays show that iron must be incorporated, since the same amount of iron in solution does not show spontaneous passage from Fe(II) to Fe(III) on 1st cycle

assay the same corresponding reduction peak potential. This indicates that the iron incorporation process in Dps may occur in the absence of its physiological oxidant, H_2O_2.

Also of note is the Dps : 48 Fe assay on Figure 4.24 A, where a significant anodic current is observed (wave III). In the 48Fe : Dps assay, there is an electrochemical behavior change in Dps containing both co-substrates, since the waveform and current intensity is remarkably different from the other assays. One such behavior alteration may be due to core formation in the form of iron oxides at the Dps cavity; however, further assays must be performed to investigate this hypothesis.

Figure 4.26 below further indicates that cathodic peak current intensity in Dps increases linearly at -0.2 V on phased assays in the absence of H_2O_2.

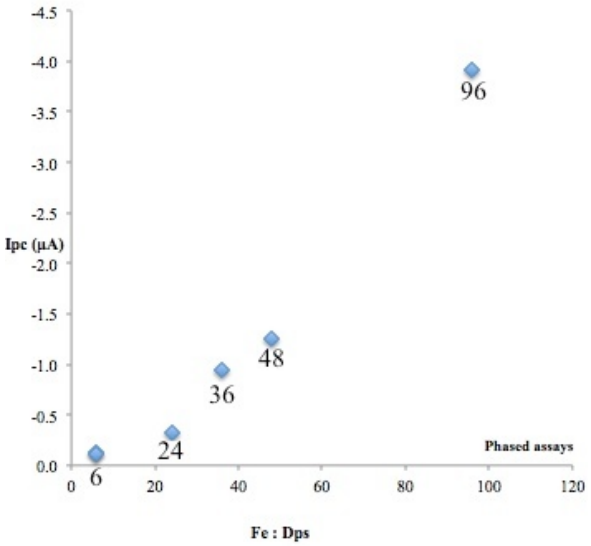

Figure 4.26 – Phased assay cathodic peak current intensity variation at approximately -0.2 V with increasing Fe : Dps ratios, from cycle 2 at 20 mV/s.

On the other hand, evolution of anodic peak current intensity on Figure 4.27 below shows a similar linear pattern to that of cathodic peak intensity in the same assay until 48 Fe, at which it hits a plateau. Anodic current peak intensities are lower than cathodic peak intensities, which can be related to Fe(III) electrochemical stabilization as oxides or hydroxides.

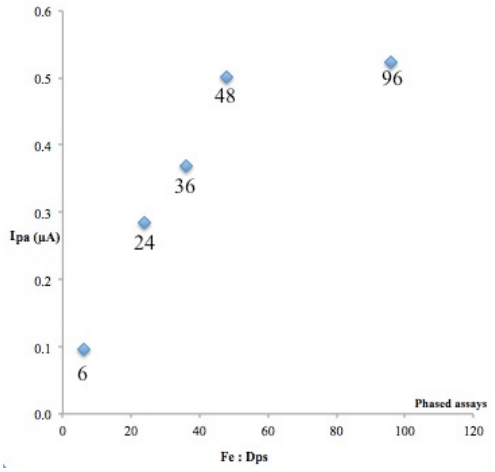

Figure 4.27 – Phased assay anodic peak current intensity variation at approximately 0.12 V with increasing Fe : Dps ratios, from cycle 2 at 20 mV/s.

After the initial scans containing only iron-incubated Dps, an excess of H_2O_2 15x the iron ratio was added to the reaction mixture. Figure 4.28 below shows the first assay scans at 50 mV/s.

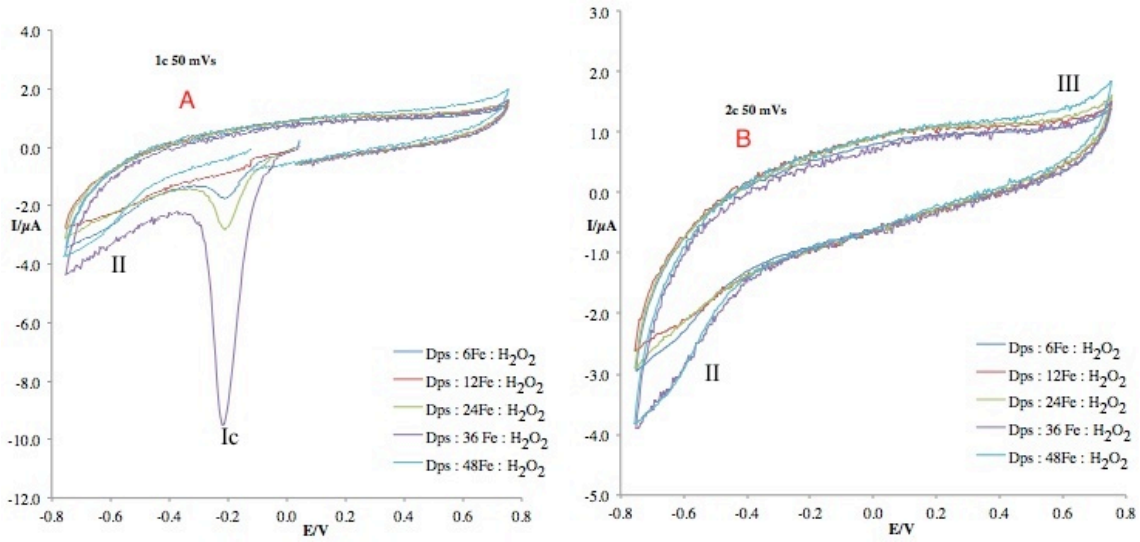

Figure 4.28 – Voltammograms from cycle 1 (A) and 2 (B) at 50 mV/s, comparing Dps phased assays (Dps: 6; 12; 24; 36 and 48 Fe : excess proportional H_2O_2 addition) from -0.75 to 0.75 V, moving from E_{OCP} in the reductive direction. Assay 6' (Dps : 96Fe) is not shown due to conductivity loss.

Comparing phased assays in the presence and absence of H_2O_2 (Figures 4.24 and 4.28 above), the iron reduction current peak indexed to iron is lower from 6 to 96 iron ratios when only iron-incubated Dps is present. Beyond that, the appearance of a new cathodic wave II at -0.6 V is probably due to oxygen reduction.

On the first scan rate in the presence of hydrogen peroxide, the cathodic peak (peak I_c) is probably resulting form Fe(III) / Fe(II) reduction. The scan was performed in the reductive direction, so no current before Fe is detected inside Dps. Little oxidative current is observed at the expected potential (peak I_a), indicating that Fe can possibly enter the Dps cavity and remain there, not using the exit channels. It can be speculated that this situation can also occur at high Fe : Dps ratios, closer to the top capacity of 500Fe per Dps molecule, to maintain iron homeostasis. Iron incorporation is limited by the slower ferroxidation reaction in Dps, which promotes iron entry and prevents iron oxidation detection at the electrode surface.

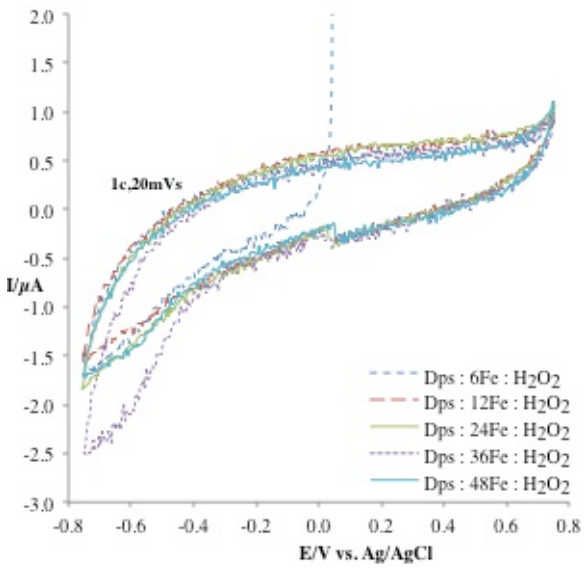

Figure 4.29 – Voltammograms from cycle 1 at 20 mV/s, comparing Dps phased assays (Dps: 6;12;24;36;and 48Fe : excess proportional H_2O_2 addition) from -0.75 to 0.75 V, moving from E_{OCP} in the reductive direction. Assay 6' (Dps : 96Fe : 96x15 H_2O_2) is not shown due to conductivity loss.

At the last potential scan at low rate above on Figure 4.29 above, as the Fe : Dps ratio increases, the cathodic current increases as well at -0.6 V up to 36Fe : Dps, possibly indicating oxygen reduction and/or core formation.

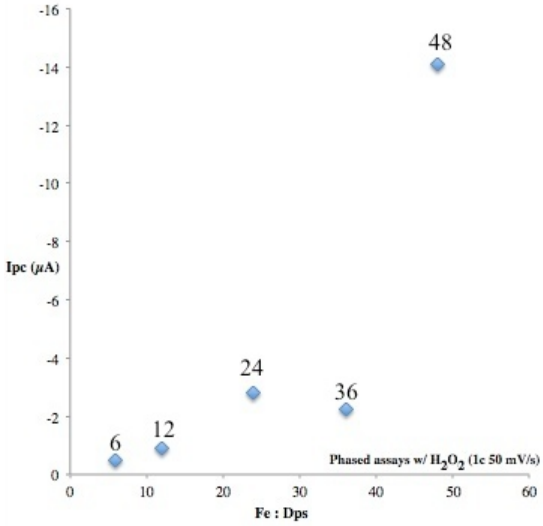

Figure 4.30 – Phased assay cathodic peak current intensity variation at approximately -0.22 V with varying Fe : Dps ratios in the presence of H_2O_2, from cycle 2 at 20 mV/s.

Figure 4.30 above shows the evolution of peak current intensity with successive iron ratios. A gradual increase is visible in the comparison graph except on the 36Fe : Dps ratio.

Comparing control assays in high amounts of substrate with Dps assays on Figure 4.31 below show that, in the absence of protein, assays containing only iron have a reversible redox pair which shows no variation between cycles 1 and 2 of each scan rate performed, a markedly different electrochemical behavior than iron in presence of Dps as has been shown above on several occasions.

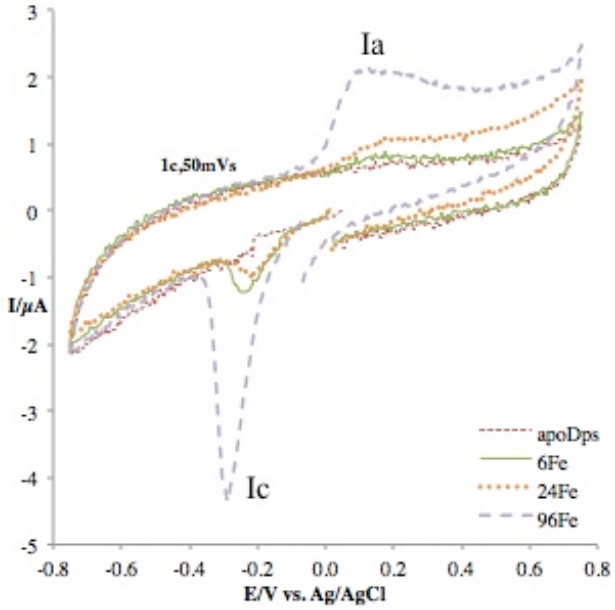

Figure 4.31 – Voltammograms from cycle 2 of apoDps (dashed red line), 6Fe (green line), 24 Fe (dashed orange line) and 96Fe (dashed light purple line) at 50 mV/s from -0.75 to 0.75 V, moving from E_{OCP} in the reductive direction.

Comparing Figure 4.31 with Figure 4.25 above, while the cathodic peak current at -0.2 V is remarkably similar, showing that Fe(III) / Fe(II) process is observed in both assays, meaning there is a spontaneous Fe(III) / Fe(II) reduction occurring on a percentage of iron present on control assay. However, the cathodic peaks on the first scan on assays containing Dps are remarkably higher, which suggests that in the presence of Dps, interaction between Dps and Fe(II) promotes its passage to Fe(III). Also, anodic peak current is higher on assays only containing iron, which can indicate that the amount of oxidized iron in contact with the electrode surface in the presence of Dps is lower.

Comparing phased assays only containing iron-incubated Dps, with control assays containing only supporting electrolyte and Fe, it is verified that in the first scan, at 50 mV/s, exclusive presence of iron in the electrochemical cell corresponds to a redox pair with increasingly higher current and potential separation in proportion to increasing iron ratios. In the presence of Dps, free iron detected by the electrode is 2 times lower for the same potential scan, indicating that part of the iron is already inside the protein, presumably inside the ferroxidase centers given that no core formation is detected.

Comparison between phased vs. direct Dps solution assays

A comparison between direct and phased assay was performed for all assays; however, Figure 4.32 below presents the most significant results - between assays containing 36Fe : Dps.

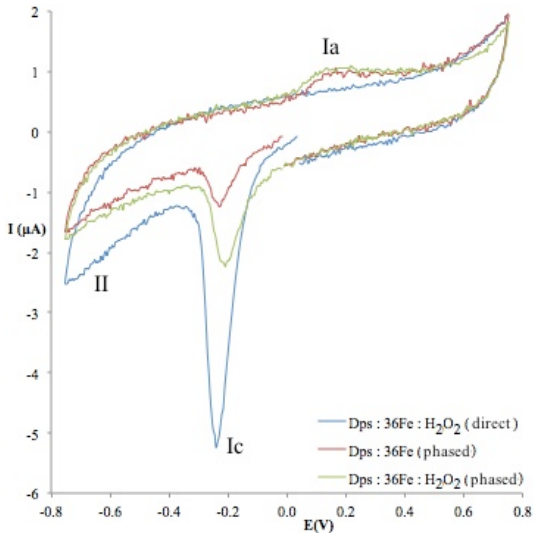

Figure 4.32 – Voltammograms from cycle 1 of Dps : 36 Fe : 36x15 H_2O_2 (direct assay, blue line), Dps : 36 Fe (red line), Dps : 36 Fe : 36x15 H_2O_2 (phased assay, green line) at 50 mV/s from -0.75 to 0.75 V, moving from E_{OCP} in the reductive direction.

On Figure 4.32 above, the direct assay (green line) shows a redox pair in the first scan with a reductive peak approximately 3x the size of the oxidation current intensity of the phased assay (green line), indicative of iron interaction with Dps. This current peak diminishes with the number of scans.

On the other hand, in the phased assay, electrochemical behavior differences between assays in the presence and absence of H_2O_2 (respectively, blue and green lines above on Figure 4.28). Hydrogen peroxide addition to the mixture represented in red, with a well defined redox pair at -0.25 V and 0.1 V) shifts the cathodic peak for more positive potentials. Predictably, hydrogen peroxide addition also increases cathodic current at the Fe(III) / Fe(II) reduction peak – a reduction increase detected at the electrode surface indicates that iron entry in Dps increases in the presence of H_2O_2, which had already been suggested above. However, a comparison between these initial scans shows unequivocally the presence of the iron redox pair, whose peak currents are extremely dissimilar in the absence of H_2O_2. Therefore, it can be suggested that iron entry in Dps happens in the absence of hydrogen peroxide as has been reported in literature[18,23] as a mark of increasing Dps catalytic behavior, not denying the potentiation effect of H_2O_2 to the iron incorporation in Dps, as can be seen comparing both phased scans (red and green lines).

The last highlight is the presence of different amounts of cathodic current generalized from -0.4 V to -0.75 V, especially at -0.5 V, the potential at which oxygen is reduced to water. It is observed that oxygen production is indicative of a reaction between Dps and H_2O_2 much larger in the direct assays, indicated by the higher current intensity. On the other hand, it would be expected that the phased assay in the presence of H_2O_2 had a discernible current difference in relation to an assay without hydrogen peroxide; however, lower O_2 production from the reaction between Dps and H_2O_2 can be connected to the limiting Fe amount in solution, since hydrogen peroxide is in excess as has been previously explained.

Prolonged electrochemical behavior monitorization: Dps phased multicycle assays

After all initial scans at 50; 100 and 20 mV/s were finished, 10 scans were performed at 20 mV/s to monitorize the effect of prolonged scanning iron-incubated Dps.

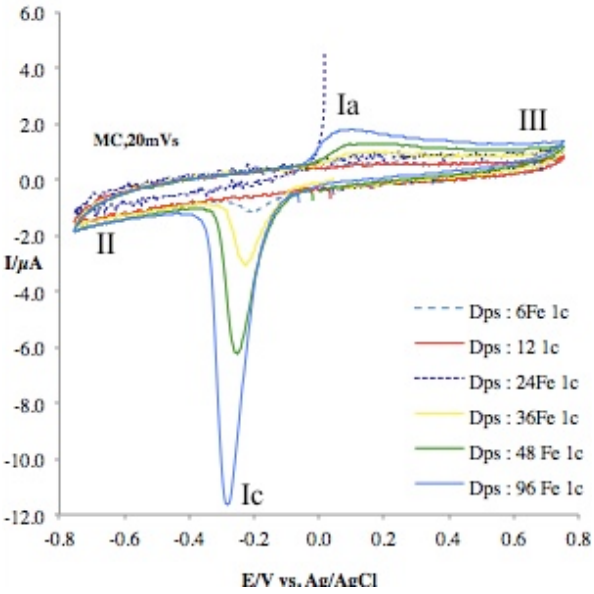

Figure 4.33 – Voltammograms from cycle 1 of Dps multicycle phased assays (Dps: 6; 12; 24; 36; 48; 96 Fe) at 20 mV/s from -0.75 to 0.75 V, moving from E_{OCP} in the reductive direction.

Comparing all 1st multicycle scans in increasing Fe : Dps ratios on Figure 4.33 above, an increase of cathodic current intensity is observed and moving progressively to more negative potentials from -0.22 V to -0.27 V, which can correspond to Fe(III) / Fe(II) reduction. Current increases at extreme potentials shown in waves II and III increase slightly with increasing Fe : Dps ratios, which may indicate oxide production and reduction at the bare electrode.

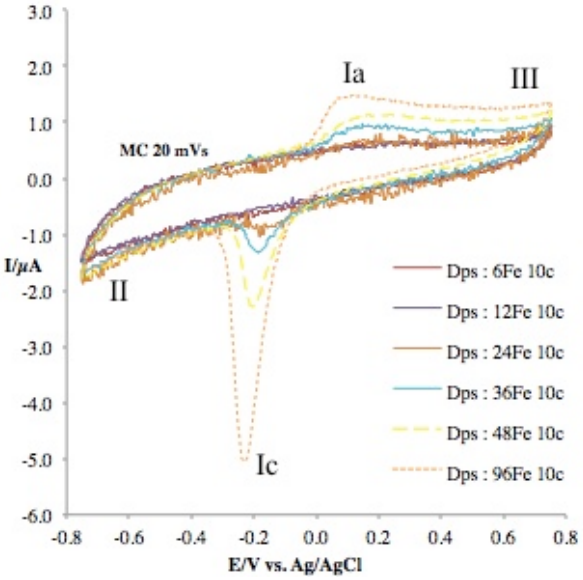

Figure 4.34 – Voltammograms from cycle 10 of Dps multicycle phased assays (Dps: 6; 12; 24; 36; 48; 96 Fe) at 20 mV/s from -0.75 to 0.75 V, moving from E_{OCP} in the reductive direction.

In the last multicycle scans with increasing Fe : Dps ratios on Figure 4.34 above, the same phenomenon is observed albeit with lower current intensity at peak I_c although current intensity at peak I_a is similar to the first scans. Therefore, it is suggested that iron enters the ferroxidase centers where it is reduced to Fe(II) entering the cavity (core). Therefore, the generalized increase on anodic current observed should correspond to iron still outside of the Dps core (in suprastoichiometric conditions) and is oxidized to be reduced in the following scan, until the maximum amount Dps can withstand. At the end of the 10th scan, there is still Fe available for reduction and its amount in solution is proportional to the Fe ratio added to Dps for incubation, as would be expected.

The cathodic and anodic peaks in the first and last multicycle phased assays were plotted in a Fe : Dps ratio vs. current intensity graph, to observe the relationship of current with the increasing Fe : Dps ratio. The following Figures 4.35 to 4.37 were obtained:

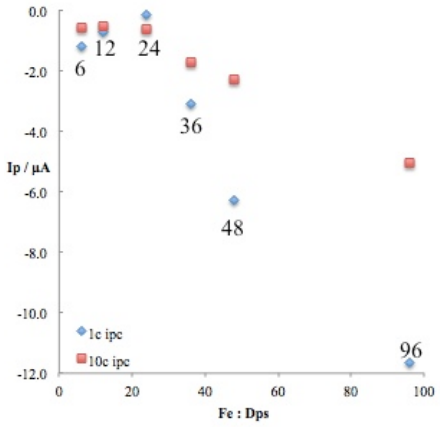

Figure 4.35 – Comparison graph between cathodic peak current intensity of cycles 1 and 10 at 20 mV/s of increasing Fe : Dps ratios (6 to 96) in multicycle phased assays.

Figure 4.35 above shows cathodic peak current intensity at approximately -0.2 V decreases between 6 and 24 Fe : Dps in cycles 1 and 10 and increases again until 96 Fe : Dps; however, at 6 and 12 iron ratios, current intensity may be difficult to detect since these results are not reproducible, while Figure 4.36 below shows a similar behavior: anodic peak current intensity at approximately 0.1 V decreases until 12 Fe : Dps (cycle 1) and 24 Fe : Dps (cycle 10) and increases again until 96 Fe : Dps.

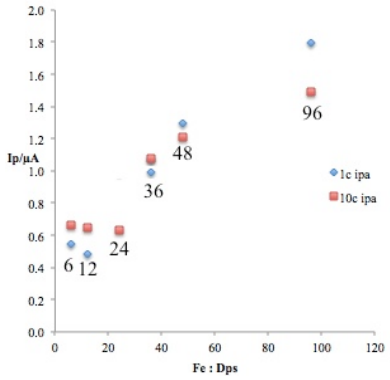

Figure 4.36 – Comparison graph between anodic peak current intensity of cycles 1 and 10 at 20 mV/s of increasing Fe : Dps ratios (6 to 96) in multicycle phased assays.

Given the disparity between the absolute current values, a current intensity subtraction comparison is shown below on Figure 4.37. The subtraction was made between the first and last multicycle assays, showing peak evolution for a prolonged period of time. As has been described above, anodic peak current intensity subtraction is almost constant in all Fe : Dps ratios; cathodic peak current intensity subtraction, on the other hand, increases linearly with successive iron ratios. Electrochemical evolution from multicycles 1 to 10 show decreasing cathodic current intensity which may indicate stabilization of the oxidized species due to oxide formation.

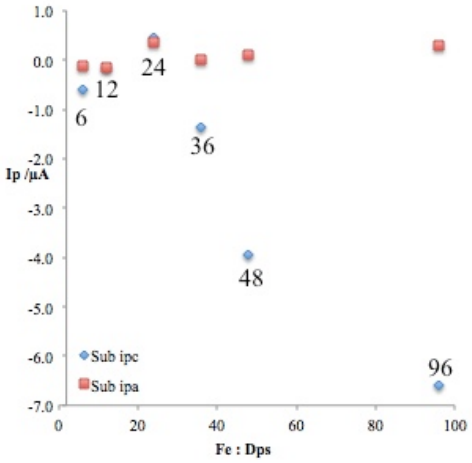

Figure 4.37 – Comparison graph between current subtractions of both cathodic and anodic peak currents of cycles 1 and 10 at 20 mV/s of increasing Fe : Dps ratios (6 to 96) in multicycle phased assays.

Table 4.III below encompasses all redox peak data from direct and phased Dps assays under diffusive control transport system.

Table 4.III – Redox peak potentials and currents for the anodic and cathodic peaks in the Dps assays and controls done in solution.

Control	Mixture	*v* (mV/s)	E_{pc} (V)	E_{pa} (V)	RE	i_{pc} (μA)	i_{pa} (μA)	WE
Diffusion	Dps;6Fe	10	-0.165	0.157	Ag/AgCl peek	$-1.29E^{-01}$	$9.56E^{-02}$	Glassy carbon
	add H_2O_2		-0.531	-		$-1.66E^{-01}$	-	
	Dps;12Fe	20	-	-		-	-	
	add H_2O_2		-0.140	-		$-4.20E^{-01}$		
	Dps;24Fe	20	-0.201	0.151		$-3.26E^{-01}$	$2.85E^{-01}$	
	add H_2O_2		-0.564	-		$-8.70E^{-02}$	-	
	Dps;36Fe	20	-0.195	0.172		$-9.50E^{-01}$	$3.69E^{-01}$	
	add H_2O_2		-0.614	-		$-2.27E^{-01}$	-	
	Dps;48Fe	20	-0.199	0.138		$-1.25E^{+00}$	$5.02E^{-01}$	
	add H_2O_2		-0.613	-		$-2.34E^{-01}$	-	
	Dps;96Fe	20	-0.232	0.100		$-3.91E^{+00}$	$5.24E^{-01}$	
	add H_2O_2		-	-			-	
	Dps:6Fe:6x15 H_2O_2	10	-0.017	-		$-1.25E^{-01}$	-	
	Dps:12Fe:12x15 H_2O_2	20	-0.688	-0.167		$-1.57E^{+00}$	$8.25E^{-02}$	
	Dps:24Fe:24x15 H_2O_2	20	-0.077	-		$-3.82E^{-02}$	-	
			-0.639	-		$-1.03E^{-01}$	-	
	Dps:36Fe:36x15 H_2O_2	20	-0.011	-		$-1.61E^{-01}$	-	
			-0.577	-		$-1.27E^{-01}$	-	
	Dps:48Fe:48x15 H_2O_2	20	-0.551	-		$-1.67E^{-01}$	-	
	Dps:96Fe:96x15 H_2O_2	20	-0.502	-		$-1.05E^{-01}$	-	
	Dps	20	-	-		-	-	
	Dps:6x15 H_2O_2	20	-	-		-	-	
	6Fe:6x15 H_2O_2	20	-0.190	0.088		$-9.91E^{-02}$	$1.26E^{-01}$	
	24Fe:24x15 H_2O_2	20	-0.203	0.281		$-8.01E^{-02}$	$7.26E^{-02}$	
	96Fe;96x15 H_2O_2	20	-	-		-	-	
	6Fe	20	-0.147	0.165		$-1.04E^{-01}$	$1.48E^{-01}$	
	24Fe	20	-0.199	0.162		$-6.97E^{-01}$	$2.85E^{-01}$	
	96Fe	20	-0.224	0.088		$-3.94E^{+00}$	$8.59E^{-01}$	
	$6H_2O_2$	20	0.490	-		$-6.50E^{-02}$	-	
	$24H_2O_2$	20	-0.015	0.195		$-8.86E^{-02}$	$8.53E^{-02}$	
	$96H_2O_2$	20	-0.27	0.080		$-3.91E^{+00}$	$7.07E^{-01}$	
	electrolyte	20	0.077	-		$-5.13E^{-02}$	-	

IV.2 Monitoring oxygen production in the Dps electrochemical system: assays on the Clark electrode (Chronoamperometry)

Clark electrodes measure oxygen production at a platinum WE through reaction

$$O_2 + 4e^- + 2H_2O \rightarrow 4OH^- \quad (\mathbf{4.1})$$

and are formed by a reaction chamber separated from the WE and CE (soaked in saturated KCl) from a Teflon® membrane and a cellulose spacer that increase WE selectivity and lessen electrode poisoning. The membrane is permeable to molecular oxygen and promotes the selective interaction with the electrode, where it is reduced. The applied potential allows for linearity between the observed current and oxygen production in a diffusive system. Both membrane and spacer were replaced in each assay to increase electrode lifetime avoid protein coat formation.

For the purposes of this work, it was intended to check oxygen production from Dps inside the gloved box chamber, within the Clark electrode chamber, in which the presence of oxygen gas would have originated only from Dps reactions after the addition of both co-substrates (Fe and H_2O_2). Chronoamperometry assays were performed at -0.7 V, at which it is established a linear relationship between observed current and oxygen concentration at a diffusive system. Current differences thus represent oxygen production from Dps. Control assays were performed only with deaerated supporting electrolyte or hydrogen peroxide, ensuring that oxygen present in both reagents does not influence oxygen concentration in Dps assays by excess.

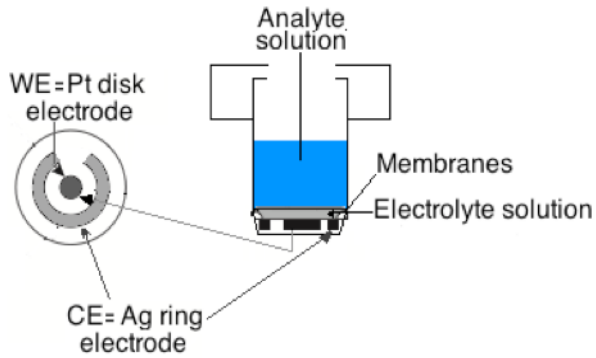

Figure 4.38 – Schematization of a Clark electrode with a built-in cell, used in the chronoamperometric assays. An Ag/AgCl peek RE was added to this system, as well as a guide needle to insert the protein incubated with several Fe ratios and the oxidant molecule (O_2-saturated buffer or H_2O_2) (adapted from [91]).

Calibration curves were made through sequential addition of O_2-saturated supporting electrolyte to test the Clark electrode before Dps assays. Figure 4.39 shows results from the calibration curve.

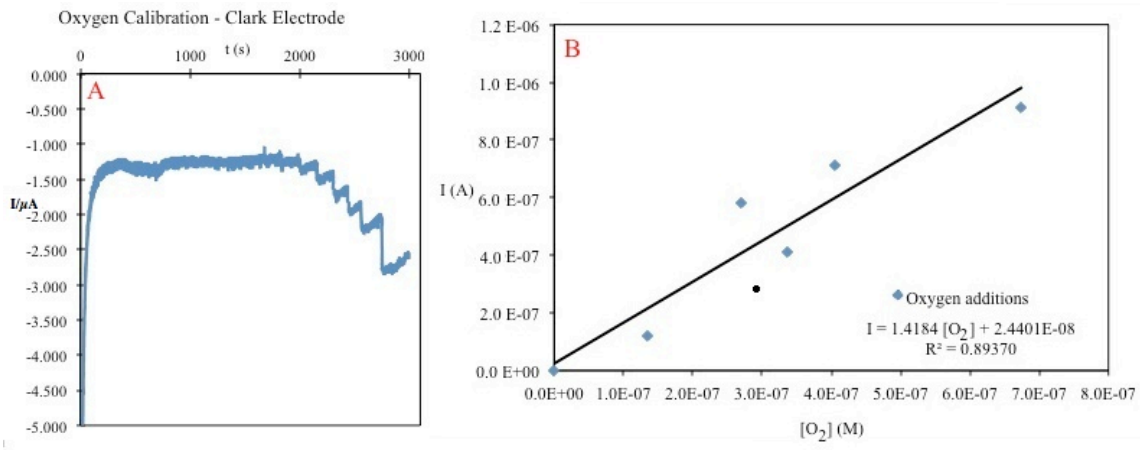

Figure 4.39 – **A** – Oxygen calibration chronoamperogram, using a Clark electrode as WE (polarized at -0.7 V *vs.* SCE RE) with 0.7 s interval between current measurements; **B** – Oxygen calibration curve showing current increase after O_2 additions

Knowing oxygen solubility in water ($2.71E^{-4}$ mol/dm^3)[92] it was possible to design a calibration curve and calculate oxygen consumption at the Clark electrode in the Dps assays interpolating the results in the calibration curve. Dps was incubated for 30 minutes with 12Fe per protein molecule before addition to the electrochemical cell containing supporting electrolyte. After the current stabilized, H_2O_2 was added in 12x15 excess and the current intensity variation was recorded as shown in Figure 4.40 A and B below. A control assay was performed through addition of the same H_2O_2 amount to supporting electrolyte and is shown on Figure 4.41.

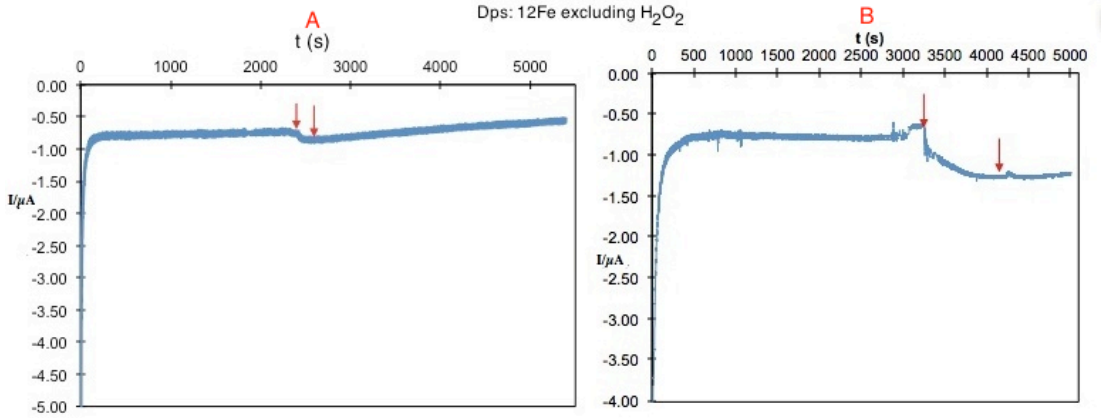

Figure 4.40 – A and B: Chronoamperometric duplicate assays of Dps:12Fe. The left arrow in both graphs shows current intensity variation upon hydrogen peroxide addition; the right arrow indicates current stabilization. using a Clark electrode as WE (polarized at -0.7 V *vs.* SCE) with 0.7 s interval between current measurements.

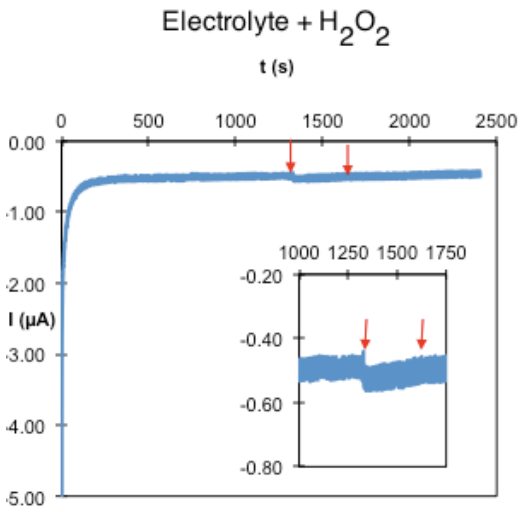

Figure 4.41 – Chronoamperometric control assay of electrolyte (200 mM MOPS pH 7.1 / 200 mM NaCl). H_2O_2 was added in the first arrow and current variation was followed until stabilization shown by the second arrow.

Oxygen formation was detected through consumption at the Clark electrode, on both Dps : 12Fe assays. The current variation in control conditions was subtracted on the Dps assays and normalized to mol O_2/mol Dps. Obtained values for both assays were, respectively, 8.64 and 1.14 mol O_2/mol Dps. This limited set of results show nonetheless that O_2 production due to Dps activity can be detected at the Clark electrode. During the assay timeframe, gaseous oxygen production was low in relation to the amount of H_2O_2 added to the reaction chamber, which suggests that most oxygen produced either has low $t_{1/2}$ or remains inside the Dps as Fe(III) oxides.

IV.3 Dps-DNA interaction assays (square wave voltammetry and cyclic voltammetry)

Dps-DNA interaction was followed, firstly, with ssDNA through cyclic voltammetry (50 and 10 mV/s) and then square wave voltammetry on a gold electrode. Thiolated ssDNA was adsorbed at the WE for 20 h, washed and deaerated for 20 minutes before starting the assay. Control assays were performed substituting ssDNA for 5 µL MilliQ water. The first electrochemical technique used for these assays was cyclic voltammetry, whose results are shown below on Figure 4.42:

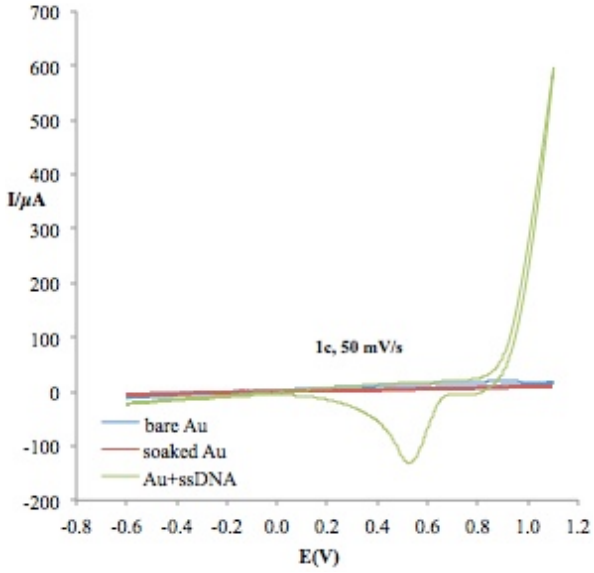

Figure 4.42 – Cyclic voltammograms from cycle 1 using a bare Au working electrode with electrolyte (blue line), WE soaked in H_2O MilliQ for 20 h (red line) and ssDNA (green line) incubated on the WE for 20 h , from -0.6 to 1.1 V in the oxidative direction at 50 mV/s (platinum counter electrode and SCE reference electrode).

As is concluded through observing the figure above, this electrochemical technique is not suitable for this system since it may have caused irreversible DNA oxidation through destruction of the adsorbed layer. The gold surface appears to be mostly unoccupied with the intended molecule in the ssDNA assay (green line), observed in the high current intensity shown at 0.8 V and higher potentials.

Given these results, square wave voltammetry was then applied and is presented below on Figure 4.43 below.

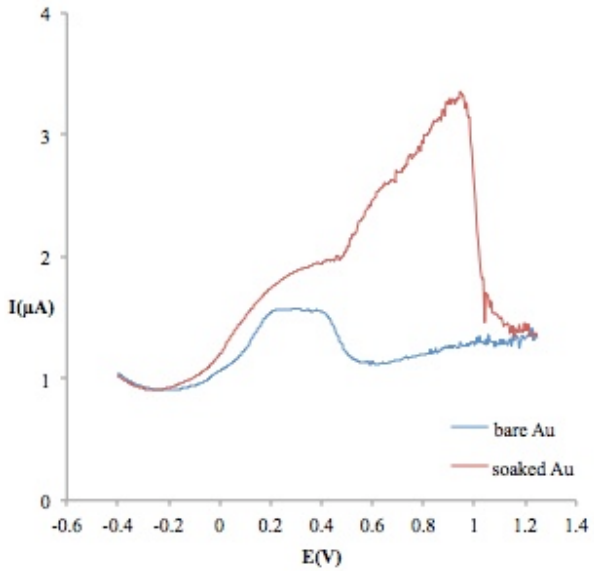

Figure 4.43 – Square wave voltammograms from the bare (blue line) and WE soaked in H_2O MilliQ for 20 h (red line), moving in the oxidative direction from -0.4 to 1.3 V at 0.01995 V amplitude, 0.0051 V step potential and 8 Hz frequency.

Through square wave voltammetry, current intensity is much lower in the control assays even at high potentials, indicating that the amount of gold oxides are lower at the electrode surface. However, soaking the Au electrode in water markedly influences the electrode behavior in relation to the bare assay, suggesting that different electrochemical processes occur only through water incubation, such as oxide formation over time in a bare electrode. These processes are also present at the ssDNA assay below on Figure 4.44, albeit in a generalized higher current intensity given the presence of an electroactive species.

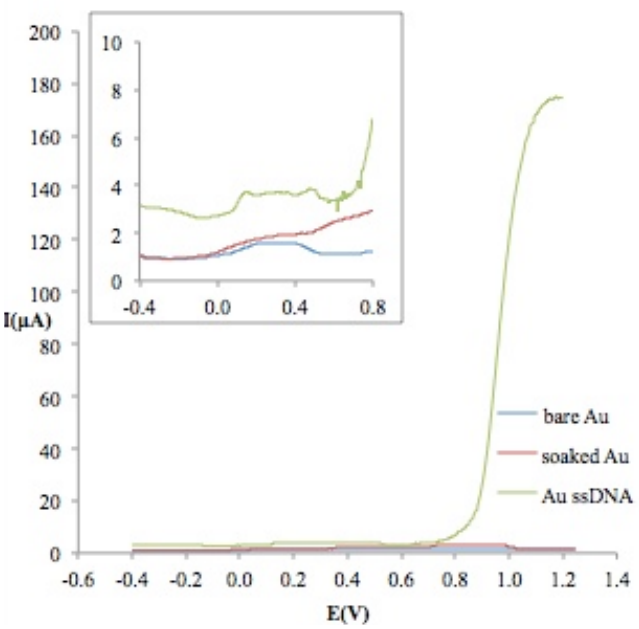

Figure 4.44 – Square wave voltammograms from the bare and WE soaked in H_2O MilliQ and ssDNA incubated for 20 h on the Au WE, moving in the oxidative direction from -0.4 to 1.25 V at 0.01995 V amplitude, 0.0051 V step potential and 8 Hz frequency

Electrochemical assays with 5' thiolated-ssDNA were made after a 20 h incubation period on the WE, monitoring electrochemical behaviour between each successive addition of Dps and/or its co-substrates. Addition of thiolated ssDNA partially blocks the electrode surface as it was expected. At high potentials, current intensity at high potentials is lower in the presence of Dps with both co-substrates sequentially added which may indicate nucleic acid protection by the protein; however, this effect does not occur with apoDps. Two processes may have occurred here: irreversible DNA oxidation that provokes the disappearance of electrochemical wave or, alternatively, Dps protection of DNA. To verify the correct hypothesis, independent assays in the presence and absence of Dps, without successive addition to work around the electrochemical oxidation issue.

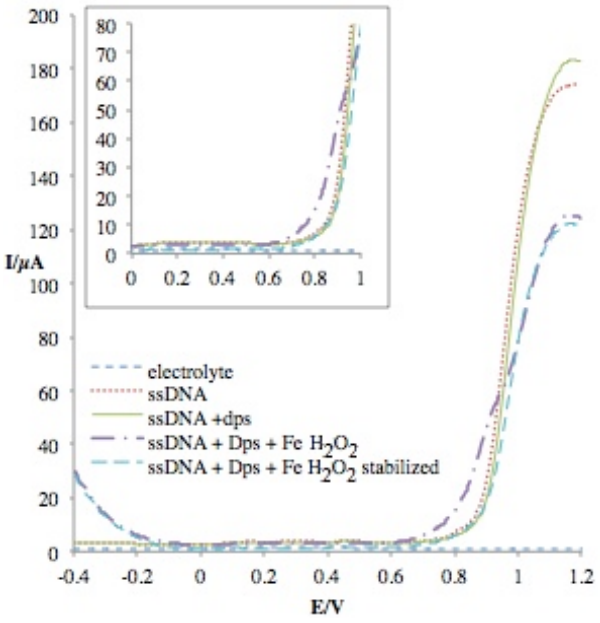

Figure 4.45 – Square wave voltammograms from ssDNA assays and sequential addition of Dps, Fe and H_2O_2 at the Au WE. ssDNA + dps + Fe + H_2O_2 assays (purple and light blue lines) were performed, respectively, immediately and after H_2O_2 addition stabilization moving in the oxidative direction from -0.4 to 1.2 V at 0.01995 V amplitude, 0.0051 V step potential and 8 Hz frequency.

Assays with dsDNA were made through incubation of ssDNA (5'-thiolated forward sequence) for 20 h and hybridization with reverse sequence for 2 h. Assays in the presence and absence of Dps were made through sequential addition of co-substrates, monitoring the electrochemical behavior between each addition. Figure 4.46 below shows the influence of apoDps on dsDNA.

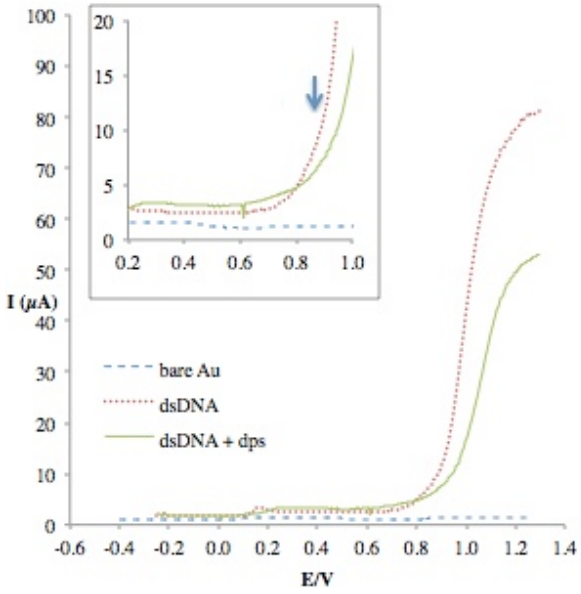

Figure 4.46 – Square wave voltammograms from the dsDNA and Dps influence at the Au WE, moving in the oxidative direction from -0.4 to 1.25 V at 0.01995 V amplitude, 0.0051 V step potential and 8 Hz frequency.

After H_2O_2 addition, square wave voltammograms are repeated until the electrochemical wave is stabilized. Figure 4.46 above shows that dsDNA has an anodic current at 1.2 V that is characteristic of surface immobilization.

In addition, a small anodic shoulder is detected at approximately 0.9 V, in the absence of Dps and a smaller one at 0.7 V with Dps, which might indicate DNA base oxidation. However, upon Dps addition the waveform changes considerably, showing lower current intensity at high potentials. These changes indicate an alteration of the electrochemical system at the gold surface. This data concur with the observation that dsDNA protection by Dps is not dependent upon substrate incorporation, since anodic current has diminished upon protein addition, consequently lowering DNA stress at the electrode. However, addition of co-substrates has the opposite effect on dsDNA as it had on ssDNA as can be seen on Figure 4.47 below, lowering protection, which can be observed through high current intensity on high potentials with possible guanine oxidation at approximately 0.9 V shown on free dsDNA and upon H_2O_2 addition (dashed red and blue lines below). The protocol for this assay was repeated several times but this process proved not to be reproducible since DNA hybridization at the electrode was inefficient.

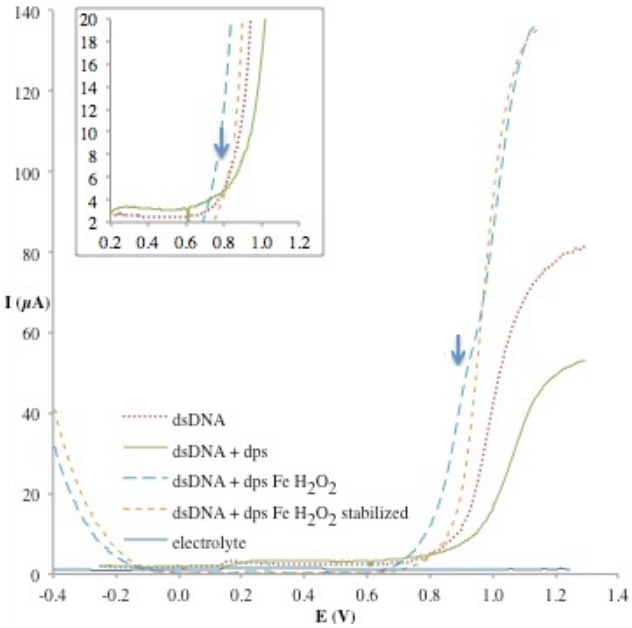

Figure 4.47 – Square wave voltammograms from dsDNA assay with sequential addition of Dps, Fe and H_2O_2 at the Au WE, moving in the oxidative direction from -0.4 to 1.3 V at 0.01995 V amplitude, 0.0051 V step potential and 8 Hz frequency.

Next assays were made immobilizing propanethiol after ssDNA immobilization and before hybridization, monitoring the electrochemical behavior upon Dps and co-substrate addition. Results on Figure 4.47 above show differences on anodic peak widths and intensities around 1.1 V. In the presence of Dps and iron, the anodic peak width is smaller, not showing the anodic shoulder at 0.9 V, which may indicate Dps protection (purple line below on Figure 4.48).

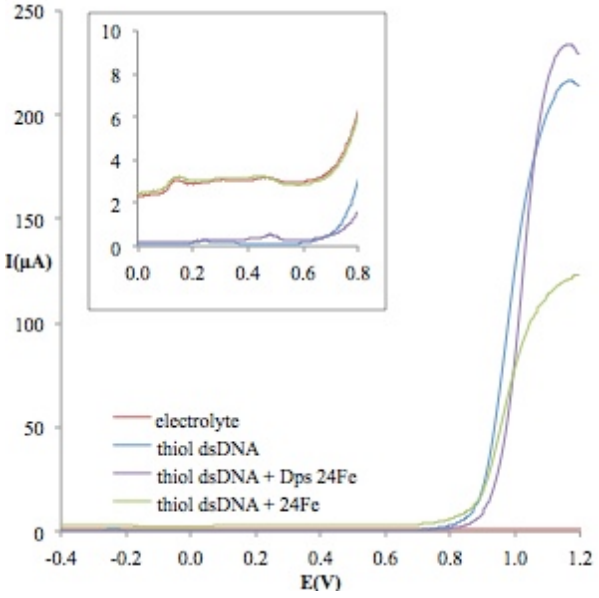

Figure 4.48 – Square wave voltammograms from dsDNA assays with propanethiol added before hybridization showing influence of Dps and iron at the Au WE, moving in the oxidative direction from -0.4 to 1.2 V at 0.01995 V amplitude, 0.0051 V step potential and 8 Hz frequency.

Upon peroxide addition and stabilization, the electrochemical behavior changes again as is shown below on Figure 4.49:

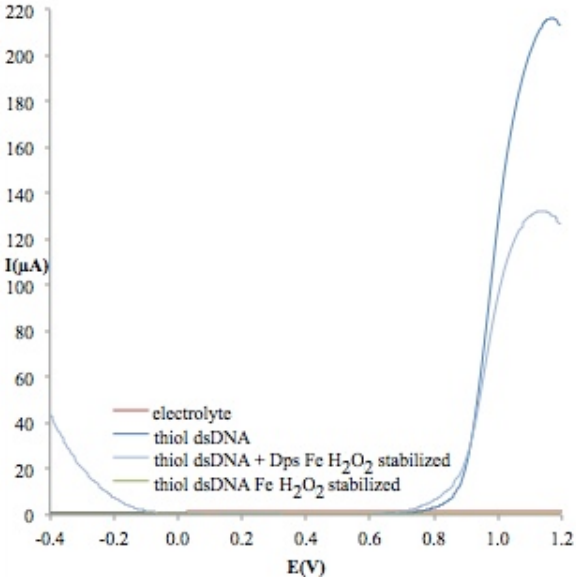

Figure 4.49 – Square wave voltammograms from dsDNA assays with propanethiol added before hybridization upon sequential addition of Dps, Fe and H_2O_2 at the Au WE, moving in the oxidative direction from -0.4 to 1.2 V at 0.01995 V amplitude, 0.0051 V step potential and 8 Hz frequency.

On Figure 4.49 above, anodic current intensity in the presence of Dps, iron and hydrogen peroxide starts to develop at approximately 0.7 V, unlike assays only containing dsDNA with propanethiol addition before hybridization, at which the current intensity only develops at 0.8 V. Therefore, it can be concluded that, at the assay experimental conditions, there is no DNA protection by Dps in the presence of H_2O_2.

Other changes can be expected, such as oxide interference at low potentials, resulting from H_2O_2 dismutation. Conclusions for this system are fallible due to lack of assay reproducibility

DNA-Dps electrochemical interaction assays were also attempted with non-complementary dsDNA, through addition of thiolated-ssDNA and a second non-complementary ssDNA strand, following the same protocol above, not shown due to lack of reproducibility.

In conclusion, following electrochemical behaviour of Dps in presence of several forms of DNA could not be properly followed due to system instability and hybridization inefficiency. Both hybridization and electrochemical assay protocol need optimization.

IV.4 Dps: non-electrochemical approaches - Spectroscopy

IV.4.1 Dps quantification

After completing the Dps purification protocol, spectrophotometric quantification was performed before attempting the remaining experimental work with a 1:50 pure Dps dilution from 250 to 800 nm to verify and exclude most contaminants. Appropriate control spectres were also performed sequentially with MilliQ water and Dps buffer before the assay. Total protein has a maximum absorbance at 280 nm (aromatic amino acids), the wavelength used for application of the Lambert-Beer Law (Abs = εbc).

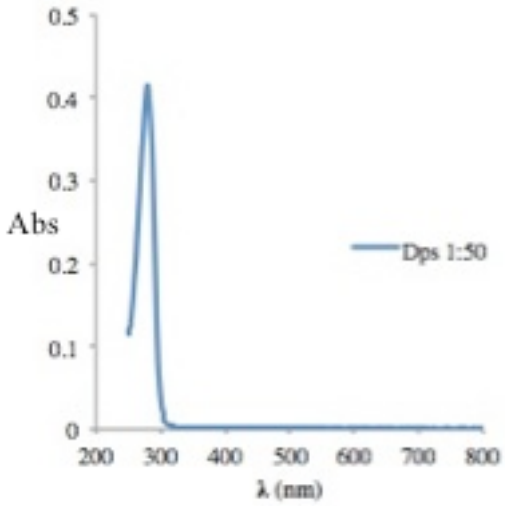

Figure 4.50 – Pure diluted Dps UV-Visible spectrum results (250-800 nm absorbance interval).

Knowing dodecameric Dps molar absorptivity ($2.9x10^5$ M^{-1} cm^{-1})[93], Dps concentration can be calculated precisely and is shown below:

Table 4.IV – Pure Dps absorbance and concentration.

Sample	$Abs_{280\ nm}$	Corrected [Dps] (µM)
Pure Dps	0.414	71.40

IV.4.2 Dps activity at 310 nm

Pure Dps activity is distinct than in presence of both co-substrates at 310 nm, on which a characteristic shoulder shows that Dps stores iron oxides in its ferroxidase centers. Dps incorporation activity was thus assessed spectrophotometrically through sequential addition of 500 µL newly purified Dps, 120 Fe per protein molecule and 5x excess H_2O_2 in supporting electrolyte (200 mM MOPS pH 7.1 / 200 mM NaCl). As Figure 4.51 shows, Dps is active and can store iron in its ferroxidase centres if iron and hydrogen peroxide are sequentially added - interestingly, its storage capacity increases greatly within the first minute of H_2O_2 addition and stabilizes within approximately 2 minutes of hydrogen peroxide addition.

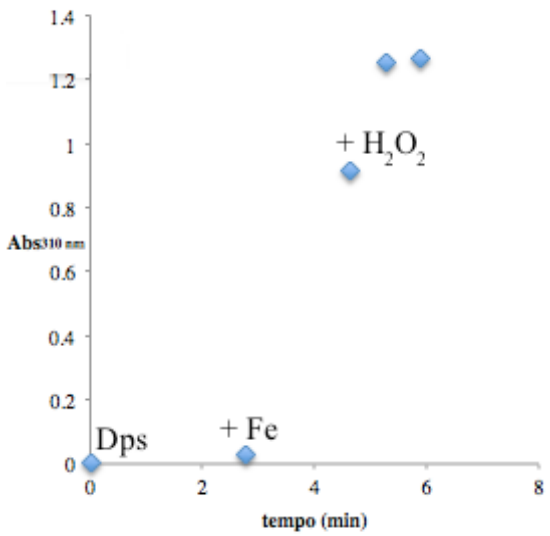

Figure 4.51 – Dps absorbance results for Dps activity *vs.* time assay.

Table 4.V – Dps activity assay absorbance results for apo and iron-incubated forms of Dps at 310 nm.

Assay	**$Abs_{310\ nm}$ (Au)**	**time at $Abs_{310\ nm}$(min)**
Dps	2.000E-3	0.000
+ Fe	2.8E-2	2.767
+ H_2O_2	9.140E-1	4.650
~ 60 sec	1.251	5.280
~ 120 sec	1.263	5.880

As can be seen above in Fig 4.51, Dps activity increases marginally upon iron addition; only after H_2O_2 addition does Dps physiological activity increase in a time-dependent manner until a plateau is reached. This is in accordance with previous knowledge[36,38,43,67,89].

Chapter V – Conclusion

In this work, Dps was overexpressed in *E. coli* without interfering contamination from catalase or other proteins, obtaining 2 different diluted fractions (F1 and F2). In electrochemical assays, the purest Dps fraction (F1) was used.

Dps was studied through electrochemical and spectroscopic techniques to better understand its cellular action mechanism. Through electrochemical study, it was possible to obtain direct electron transfer results without resorting to promoters. It was possible to observe the Dps iron incorporation mechanism: after successfully incorporating iron, it was observed that hydrogen peroxide may have been converted to oxygen and subsequently reduced as a result of potential application.

It was possible to monitor Dps electrochemical behavior in the presence of iron and peroxide with two types of electrodes (graphite and glassy carbon) upon successive iron ratio additions, comparing to apoDps. Particularly, iron incorporation was successfully followed under diffusive control system with the glassy carbon working electrode.
The incorporation reaction occurs in aerobic and anaerobic environment, although its monitorization is simplified and more easily detected in anaerobic environment. In the absence of oxygen, it is possible to follow oxygen formation and release due to Dps catalytic mechanism in the presence of both co-substrates (Fe and H_2O_2).

Electrochemical results obtained through peak current intensity analyses are unexpected in the light of current mechanistic theories of iron incorporation and ferroxidation in Dps and are thus worthy of more in-depth studies.

Chronoamperometry assays were performed in a modified Clark electrode allowing the quantification of oxygen produced after Dps electrocatalysis in iron-incubated Dps. Oxygen production detection ranged from 1 to 8 mol O_2 per mol Dps.
Dps-DNA interaction studies were performed using cyclic voltammetry and square wave voltammetry to detect changes in DNA stability in the presence Dps and its co-substrates. Iron and H_2O_2 were also independently added to DNA to study its influence on DNA electrochemical behavior. Although these assays were irreproducible, there seems to be a small protection of DNA by Dps relatively to electrochemical oxidation of DNA.

VI. Future perspectives

In the present work, the most successful set-up was anaerobic cyclic voltammetry at the glassy carbon electrode under diffusive control. However, all the techniques used throughout this work can potentially be optimized to achieve more reproducible results. Some suggestions will be displayed below:

- Increase assay reproducibility through system optimization and performance of more successful electrochemical assays in the same experimental conditions to confirm previous conclusions;

- System minimization through use of small commercial graphite or glassy carbon electrode adequate for system minimization, which would allow for less protein and reagent waste, increase assay preparation speed and productivity;

- Working electrode modification to increase Dps interaction with the electrode. Namely, increase the positive charge of the electrode surface through promoter monolayers (e.g., neomycin sulphate, ditiobis(N-succinimydyl propionate (DTSP) on gold working electrodes) so that Dps can adsorb to the electrode surface and be stable through electrochemistry scans;

- Nucleic acid adsorption to different electrodes (e.g., graphite[94],) for interaction assays with Dps.

- increase assay reproducibility and achieve optimization of electrochemical Dps-DNA interaction, through square wave voltammetry;
- study length effect of the dsDNA strand on interaction with Dps;
- optimization of DNA immobilization comparing varied DNA sequences with polynucleotides poly-A and poly-G
- assays with electrochemically active intercalator to monitor DNA integrity in the presence of Dps and its co-substrates;
- surface analysis techniques such as Atomic Force Microscopy to monitor structural changes on Dps upon iron incorporation.

Bibliography

(1) Harrison PM *et al*., *BBA*, 1275 (1996), 161-203.
(2) Andrews, SC *et al*., *FEMS Microbiology Rev*. 27 (2003), 215-237.
(3) Chiancone, E. *et al.*, *Biometals* 17 (2004), 197-202.
(4) Williams, RJP, *FEBS Lett.* 140(1), (1982), 3-10.
(5) Vanýsek, P., *Electrochemical Series*, in *Handbook of Chemistry and Physics: 88th Edition* (Chemical Rubber Company) (2007), pgs. 8-20--8-29.
(6) Lewin, A *et al.*, *Dalton Trans.* (2005), 3597-3610.
(7) Imlay, JA, *Ann. Rev. of Microbiol.* 57 (2003), 395-418.
(8) Rush, JD *et al.*, *FEBS Lett.*, 138 (1990), 33-36.
(9) Miller, RA *et al.*, *Clin. Microbiol. Rev.*, 10 (1) (1997), 1-18.
(10) González-Flecha, B *et al.*,270 (23) (1995), 13681-13687.
(11) Park, S *et al.*, *PNAS*, 102(26) (2005), 9317-9322.
(12) Imlay, JA *et al.*, *J. Bacteriol.*, 166 (1986), 519-527.
(13) Imlay, JA *et al.*, *Science*, 240 (1988), 640-642.
(14) Kehrer, JP, *Toxicology*, 149 (2000), 43-50.
(15) Czapski, G., *Isr. J. Chem.*, 24 (1984), 29-32.
(16) Liu, XF *et al.*, *Acc. Chem. Res.,* 38 (2005), 167-175.
(17) Chasteen, ND *et al.*, *J. Struct. Biol.*, 126 (1999), 182-194.
(18) Ilari A *et al.*, *Nat. Struct. Biol.* 7(1) (2000), 38-43.
(19) Uchida, M *et al.*, *BBA*, 1800 (2010), 834-845.
(20) Haikarainen, T *et al.*, *Cell. Mol. Life Sci.*, 67 (2010), 341-351.
(21) Frienkel-Krispin, D *et al.*, *EMBO J.*, 20(5) (2001), 1184-1191.
(22) Almirón, M *et al.*, *Genes Dev.*, 6 (1992), 2646-1654.
(23) Castruita, M *et al. Appl. Environ. Microbiol*. 72(4) (2006), 2918-2924.
(24) Peña, MMO *et al.*, *J. Biol. Chem.*, 270 (1995), 22478-22482.
(25) Wiedenheft, B *et al.*, *PNAS*, 102(30) (2005), 10551-10556.
(26) Reindel, S *et al.*, *BioMetals,* 19 (2005), 387-397.
(27) Nair, S *et al.*, *J. Bacteriol.*, 186(13) (2004), 4192-4198.
(28) Azam, TA *et al.*, *J. Biol. Chem.* 274 (46) (1999), 33105-33113.
(29) Azam, TA *et al.*, *J. Bacteriol.* 181(20) (1999), 6361-6370.
(30) Ishikawa, T *et al.*, *J. Bacteriol.*, 185(3) (2003), 1010-1017.
(31) Bellapadrona, G *et al*., *Free Rad. Biol. Med.*, 48 (2010), 292-297.
(32) Kauko, A *et al.*, *J. Mol. Biol.* 364 (2006), 97-109.
(33) Romão, CV *et al.*, *J. Biol. Inorg. Chem.*, 11 (2006), 891-902.
(34) Saumaa, S *et al.*, *J. Bacteriol.* 189(15) (2007), 5504-5514.
(35) Pacello, F *et al.*, BBA, 1780 (2008), 226-232.
(36) Franceschini, S *et al.*, *FEBS J.* 273 (2006), 4913-4928.
(37) Ueshima, J *et al.*, *Infect. Immun.* 71(3) (2003), 1170-1178.
(38) Bozzi, M et al., *J. Biol. Chem.*, 272(2) (1997), 3259-3265.
(39) Nicodème, M *et al.*, (2004), *Curr. Microbiol.*, 48 (2004), 51-56.
(40) Ren, B *et al.*, *J. Mol. Biol.*, 329 (2003*)*, 467-477.
(41) Papinutto, E *et al.*, *J. Biol. Chem.*, 277(17) (2002), 15093-15098.
(42) Gupta, S *et al.*, *J. Biol. Chem.*, 278(7) (2003), 5235-5241.
(43) Ceci, P *et al.*, *J. Biol. Chem.*, 278(22) (2003), 20319-20326.
(44) Tonello, F *et al.*, *Mol. Microbiol.*, 34(2) (1999), 238-246.
(45) Su, M *et al.*, *Biochem.* 44 (2005), 5572-5578.
(46) Jeong, KC *et al.*, *BMC Microbiol.*,8 (2008), 181-193.
(47) Thieme, D *et al.*, *Microbiol. Res.*, 165 (2010), 108-115.
(48) Havukainen, H *et al.*, *Protein Sci.*, 17 (2008), 1513-1521.
(49) Li, H *et al., J. Prot. Res.*, 7 (2008), 4040-4049.
(50) Piao, H *et al.*, *Neurochem. Res.*, 36 (2011), 58-66.
(51) Yu, MJ *et al.*, *J. Basic Microbiol.* 49 (2009), S79-S86.
(52) Brent, TJ *et al.*, *J. Bacteriol.*, ,178(3) (1996), 808-816.

(53) Chimera 1.5.3 for MacOSX 10.6, Computer Program downloaded at http://www.cgl.ucsf.edu/chimera; Petersen, EF *et al.*, *J. Comput. Chem.*, 25(13) (2004), 1605-1612
(54) Swiss Pdb Viewer, Computer Program downloaded at www.expasy.org/spdbv; Guex, N, Peitsch, M.C., *Electrophoresis* 18 (1997), 2714-2723
(55) Chiancone, E *et al.*, *BBA*, 1800 (2010), 798-805.
(56) Roy S *et al.*, *J. Mol. Biol.* 370 (2007), 752–767.
(57) Grant, RA *et al.*, Nat. Struct. Biol., 5 (1998), 294-303.
(58) Macara, IG *et al.*, *Biochem. J.*, 126 (1972), 151-162.
(59) Diaz, PI *et al.*, *J. Bacteriol.*, 188(7) (2006), 2454-2462.
(60) Altuvia, S *et al.*, *Mol. Microbiol.*, 13 (1994), 265-272.
(61) Åslund, F *et al.*, *PNAS USA Biochemistry*, 96 (1999), 6161-6165.
(62) Martinez, A *et al.*, Kolter R, *J. Bacteriol.,* 179(16) (1997), 5188-5194.
(63) Stephani, K *et al.*, *Mol. Microbiol.*, 49(6) (2003), 1605-1614.
(64) Wolf, SG *et al.*,*Nature* 400 (1999), 83-85.
(65) Ohniwa, RL *et al.*, *EMBO J.*, 25(23) (2006), 5591-5602.
(66) Azam, TA *et al.*, *Genes to Cells,* 5 (2000), 613-626.
(67) Zhao, GH *et al.*, *J. Biol. Chem.,* 277(31) (2002), 27689-27696.
(68) Vasuki Ranjani, C *et al.*, *Int. J. Biol. Macromol.*, 43 (2008), 333-338.
(69) Yamamoto, Y *et al.*, *J. Bacteriol.*, 184 (2002), 2931-2939.
(70) Nunoshiba, T *et al.*, *J. Biol. Chem.*, 274(49) (1999*)*, 34832-34827.
(71) Velayudhan, J *et al.*, *Mol.Microbiol.*, 63(5) (2007), 1495-1507.
(72) Lodish, H. *et al.*, *Molecular Cell Biology*, 5th Edition, W.H. Freeman and Company, NY.
(73) de-los-santos Álvarez, P. *et al.*, *Electroanalysis* 18(15) (2004), 1193-1204.
(74) Lindahl, T, *Nature*, 362 (1993), 709-715.
(75) Lindahl, T *et al.*, *Biochem.* ,11(19) (1972), 3610-3618.
(76) Frenkiel-Krispin, D *et al.*, *Mol. Microbiol.*, 51(2) (2004), 395-405.
(77) Theil, EC, *Biometals*, 20 (2007), 513-521.
(78) Ceci, P *et al.*, *Nuc. Ac. Res.*, 32(19) (2004), 5935-5944.
(79) Bhattacharyya G *et al.*, *J. Biol. Chem.,* 282 (16) (2007), 11921-11930.
(80) Bard, AJ, Faulkner, LR, *Electrochemical methods – Fundamentals and Applications*, (Elizabeth Swain, ed.), John Wiley & Sons, Inc. (2001).
(81) Monk, P., *Fundamentals of electroanalytical chemistry* (David J. Ando, ed.), John Wiley & Sons, Ltd. (2001).
(82) Gossner, Jr., D.K., Cyclic voltammetry. Simulation and Analysis of Reaction Mechanisms, Wiley-VCH (1994).
(83) Patnaik, P., Dean's Analytical Chemistry Handbook, McGraw-Hill (2004).
(84) *Handbook of Electrochemistry*, (2007) (Cynthia Zoski, ed.), Elsevier.
(85) Steel, AB *et al.*, Biophys. J. 79(2) (2000), 975-981
(86) Sowerby, SJ *et al.*, *PNAS*, 98(3) (2001), 820-822.
(87) Márcia Guilherme, *Estudos mecanísticos e estruturais da oxidação de ferro por ferritinas rápidas*, Tese de Doutoramento (2009), FCT-UNL, PT.
(88) Ana Moura, *Estudos electroquímicos sobre a proteína Dps de* Ps. nautica *617*, Relatório de Projecto de Biotecnologia (2009), FCT-UNL, PT.
(89) Joana Cristóvão, *Estudo do mecanismo de proteínas protectoras de DNA por métodos electroquímicos*, Relatório de Projecto de Bioquímica (2010), FCT-UNL, PT.
(90) Tânia Cardoso, *Mecanismos de desintoxicação celular e protecção de DNA – Caracterização de um mutante da Dps de* Pseudomonas nautica *por espectroscopia de UV-Vis e electroquímica*, Relatório de Projecto de Química Aplicada (2011), FCT-UNL, PT
(91) Harvey, D, *Modern Analytical Chemistry*, McGraw Hill International Edition, (2000), pp. 520.
(92) Truesdale, GA, Downing, AL, *Nature* 173 (1954), 1236.
(93) ExPAsy online Protein Parameter program (SIB Swiss Institute of Bioinformatics) accessed on http://web.expasy.org/protparam/; Gasteiger, E, *et al.*, *Nucleic Acids Res.*, 31 (2003), 3784-3788
(94) Wu, LL *et al.*, *Electrochim. Acta* 45 (2000), 2923-2927.

Appendices

A - Culture medium utilized for Dps overexpression in *E.coli*

A.1 LB (Lysogeny Broth)

Table A.1– Composition for 1 L LB culture medium.

Bactotryptone	10 g
Yeast extract	5.0 g
NaCl	10 g

To prepare solid LB culture medium for Petri dishes, add 20 g of agar per liter, make up to the desired volume and autoclave at 120ºC for 20 minutes.

A.2 Antibiotic – Ampicillin

The Dps overexpression vector (pET-21c(+)) has an ampicillin resistance gene in its sequence. Therefore, 100 µg/mL ampicillin was added to all culture mediums, allowing for the selection of the transformed bacteria and avoiding the occurrence of contamination,

A 100 mg/mL stock solution of ampicillin was prepared through flame filtration and stored in 1 mL aliquots at -20ºC. 2 g ampicillin were weighed and diluted in 20 mL deionized water.

B – General protocols for biochemical methods used in Dps purification

B.1 Cell disintegration

Cell disintegration was accomplished through two consecutive steps:

- 3 liquid nitrogen freezing/thawing cycles
- utilization of a *French Pressure Cell Press* (*Thermo Electric Corporation*) with a 30 mL chamber at 16,000 Psi. Cellular extracts were collected in an iced collector, avoiding sample overheating during disintegration. Cell rupture was accomplished through 4 successive passages in the Cell Press for each sample.

Before initiating cell disintegration, DNase was added to the cell suspension, aiming to hydrolyze DNA released during disintegration.

Sample viscosity was controlled after disintegration by ressuspending the cell extract after low speed centrifugation in 1-2mL 10 mM Tris-HCl pH 7.6.

B.2 Denaturing polyacrylamide gel electrophoresis

Denaturing polyacrylamide gel electrophoresis (SDS-PAGE) was used to observe the total protein content of the cell culture, as well as evaluate the purity level of the successive protein fractions matching the purification steps and in the determination of protein molecular weight. This technique was applied with reference to both Laemmli[1] and Hames & Rickwood[2] works.

In the present work, 12.5% acrylamide in SDS-PAGE gels was performed for 1h30 and variable voltage (80-120 V). Gel polymerization was performed according to Biorad Protocol[3]. Necessary solutions and respective amounts are presented in tables B.I and B.II. Samples were prepared for SDS-PAGE with sample buffer containing ß-mercaptoethanol. On one occasion, 4-12% prepared gradient acrylamide gels for 35 minutes at 200 V were used with accompanying buffers.

To lower viscosity of earlier cell sample, a 45-minute water bath was maintained at 70-80ºC before gel application; if viscosity wasn't an issue, samples were exposed to a 5-minute boiling water bath before gel application.

The molecular weight markers used in SDS-PAGE electrophoresis were LMW for low molecular weight samples (*nzytech*) and SeeBlue Prestained Protein Marker (*Invitrogen*). Their electrophoretic profile is presented in Figure B.1.

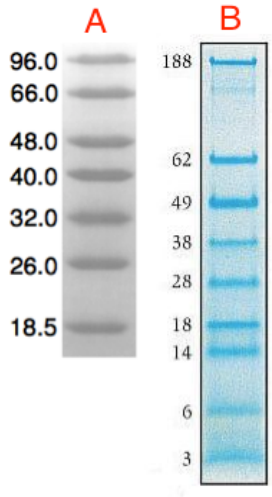

Figure B.1 – **A**: Molecular weight marker (*LMW – SDS-PAGE Marker*) from *nzytech*, applied in a polyacrylamide gel (12.5% acrylamide) in denaturing conditions. Known molecular weight (kDa) of each protein at the left of each band; **B**: Molecular weight marker (*SeeBlue Prestained*) from *Invitrogen*, applied in a 10-20% Tricine Gel. Known molecular weight (kDa) of each protein is at the left of each band.

SDS-PAGE gels were stained with *Brilliant Blue Coomassie R-250* staining solution and destained with destaining solution, presented in table B.I. After destaining, gels were photographed.

Table B.I Stock solutions used for SDS-PAGE

Solutions	Reagents	Amount	Notes
Running gel buffer (Solution I)	Tris Base 2.5 M Concentrated HCl H_2O	30.3 g pH 8.8 make up to 100 mL	pH 8.8-9.0
Stacking gel buffer (Solution II)	Tris Base 0.5 M Concentrated HCl H_2O	6.06 g pH 6.8 make up to 100 mL	pH 6.6-6.8
Acrylamide/Bisacrylamide (Solution III)	Acrylamide (*Biorad*) Bisacrylamide (*Biorad*) H_2O	30 g 0.8 g make up to 100 mL	-
10% SDS	SDS H_2O	10 g make up to 100 mL	-
10% PSA	PSA H_2O	0.02 g make up to 200 µL	Single use
Electrophoresis buffer Tris-Glycine 10x	Tris Base 0.25 M Glycine 1.92 M (*nzytech*) 0.1 % SDS H_2O	30.3 g 144.1 g 10 g make up to 1 L	pH 8.3 Dilute 1:10 before use
Sample buffer	Solution II 10% SDS ß-mercaptoethanol (*Sigma Aldrich*) Glycerol (*Sigma Aldrich*) Bromophenol blue (*Riedel*) H_2O	5 mL 8 mL 1 mL 2 mL 4 mg make up to 20 mL	-
Coomassie R-250 Brilliant Blue staining solution	Coomassie R-250 Glacial acetic acid (*Sigma Aldrich*) Methanol (*Sigma Aldrich*) H_2O	1 g 15 mL 90 mL make up to 200 mL	-
Destaining solution	Glacial acetic acid (*Sigma Aldrich*) Methanol(*Sigma Aldrich*) H_2O	75 mL 450 mL make up to 1 L	-

Table B.II Solutions used for manufacturing 1 SDS-PAGE 12.5 acrylamide gel.

Solution	Stacking gel (5% acrylamide) (mL)	Running gel (12.5% acrylamide) (mL)
Solution I	-	0.750
Solution II	0.450	-
Solution III	0.300	2.08
10% SDS (nzytech)	$1.80E^{-2}$	$5.00E^{-2}$
dH_2O	1.02	2.00
10% PSA (Biorad)	$1.35E^{-2}$	$3.80E^{-2}$
TEMED (Sigma-Aldrich)	$2.00E^{-3}$	$2.50E^{-3}$

B.3 Transformation protocol of competent E. coli BL21 (DE3) cells

For the transformation of Dps, an adapted protocol[4] from the manufacturer (*nzytech*) was used and succinctly described below.

Competent cells are thawed in ice and gently mixed. 2µL plasmid DNA is added to 100 µL BL21 competent cells, mixing the tube through gentle tapping. Incubate cells on ice for 30 minutes. Heat shock cells at 42ºC for 40 seconds in a water bath without mixing. Transfer immediately to ice and incubate for 2 minutes. Add 900 µL room temperature LB culture medium. Incubate for 1h at 37ºC at 225 rpm. Spread 100-200 µL transformed cells in LB-agar plates containing 100µg/mL ampicillin. To concentrate cells, centrifuge 1000µL cell culture for 1 minute at 5000 rpm, removing 800 µL supernatant and spread cells after resuspending the remaining medium. Incubate overnight at 37ºC.

C – Methods and protocols used in extraction, purification and Dps electrochemical and spectroscopic assays

C.1 DEAE Sepharose Fast Flow (FF) Column

DEAE Sepharose FF column (160 mL) was equilibrated in 20% ethanol and was properly treated before use as is described below. All reactants have been filtered through a 0.4 µm pore.

The column was washed (using ”System wash method” program from AKTA) with MilliQ water with 3 column volumes at 2 mL/min until ethanol had been removed. This step is essential to avoid buffer ion precipitation. Before protein injection, the column was treated through sequential addition of 2 M NaCl for 10 minutes at 3 mL/min (elution of previous protein contaminants), 1 M NaOH for 30 minutes at 5 mL/min (elution of previous bacterial contaminants), and enough MilliQ water to lower conductivity. After sample injection, 3 successive linear gradients were applied (0-30%, 30-70% and 70-100% buffer B) at 4 mL/min collecting all fractions After use, the column is washed with buffer A to lower conductivity, then with 3 column volumes MilliQ water and 1 column volume of ethanol and kept at 4ºC.

C.2 Q Resource Column

Q Resource column (6 mL) was equilibrated in 20% ethanol and was properly treated before use as is described below. All reactants have been filtered through a 0.4 µm pore filter.

The column was washed through *System Wash Method* program from AKTA) with MilliQ water for 3 column volumes until its conductivity reached 180 µS (characteristic of MilliQ water), to avoid buffer ion precipitation. 100% buffer A is then added to the column until stabilization at the Autozero. After sample injection, a linear 150 mL buffer B gradient was applied at 4 mL/min, collecting all fractions. After use, the column is washed with buffer A to lower conductivity, then with 3 column volumes MilliQ water and 1 column volume of ethanol and kept at 4ºC.

C.3 Dps concentration

Dps fractions were concentrated in a Vivacell® 70 with 30kDa MWCO (molecular weight cut-off) (*Sartorius*) with 93% solute recovery. Dodecamer Dps molecular weight is ~200 kDa; therefore the protein is efficiently concentrated until a desired volume is obtained to dialyze and stock or inject in a ionic exchange chromatography column. The concentration equipment was also used for buffer exchange from the purification buffer (10 mM Tris-HCl pH 7.6) to the assay buffer (200 mM MOPS pH 7.1 / 200 mM NaCl).

C.4 Iron quantification

Iron quantification was achieved by performing successive addition of 10% hydroxylamine hydrochloride, and 0.3% phenanthroline, using standard iron solution as control. Hydroxylamine reduces all iron to Fe(II), which then forms a orange-red ion complex with phenanthroline; the complex formation was then monitorized through absorbance measurements at 510 nm following a previously obtained protocol[5,6].

$$2Fe^{3+} + NH_2OH + 2OH^- \rightarrow 2Fe^{2+} + N_2 + 4H_2O \quad \textbf{(C.1)}$$

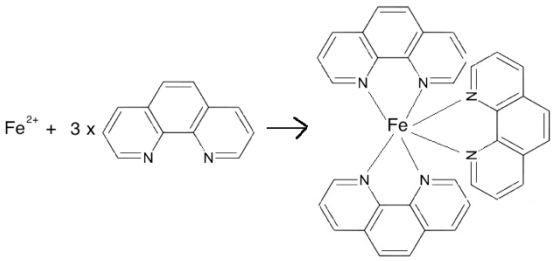

(C.2)

The parent $FeCl_2$ solution was used for the samples. After obtaining the absorbance measurements at 510 nm, the true iron concentration was calculated using Lambert-Beer's Law,

$$Abs = \varepsilon bc \quad \textbf{(C.3)},$$

in which ε stands for absorptivity constant, determined through a calibration curve, shown below:

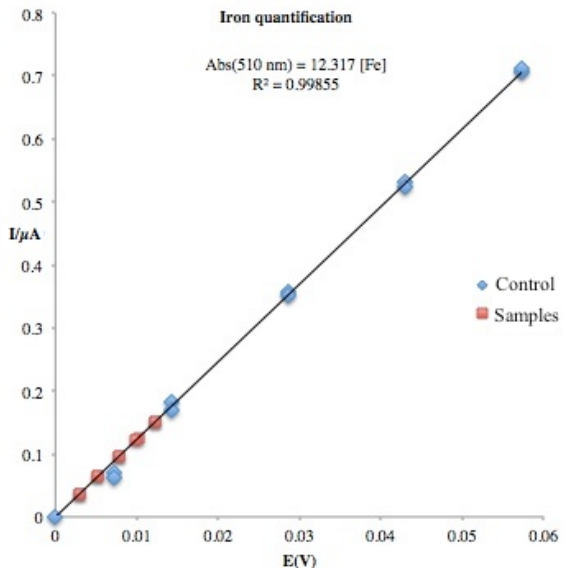

Figure C.1 - Iron quantification calibration curve and sample intrapolation, through the phenanthroline method.

Table C.I – Rectified control results used to calculate the calibration curve. Corrections were made averaging the absorbance of zero iron.

$Abs_{510\ nm}$	[Fe] (mM)
-0.0005	0
0.0005	0
0.0705	7.162E-03
0.0635	7.162E-03
0.1835	1.432E-02
0.1695	1.432E-02
0.3565	2.865E-02
0.3515	2.865E-02
0.5305	4.297E-02
0.5235	4.297E-02
0.7075	5.730E-02
0.7115	5.730E-02

After obtaining the sample quantification, the average iron concentration of all samples were calculated, coming to 10.5 ± 0.8 mM, which represents a 5% deviation from the initially assumed iron concentration (10 mM) on all the assays performed afterwards.

Table C.II – Differences between supposed iron ratios and experimental ratios in all stoichiometries used in the electrochemical assays

	Supposed ratio ([Fe]=10 mM)	Experimental ratio ([Fe]=10.5 mM)	Absolute error	Relative error
sub-stoichiometric	6	6.3	0.3	5
	12	12.6	0.6	5
stoichiometric	24	25.2	1.2	5
supra-stoichiometric	48	50.5	2.5	5
	96	101.0	5.0	5
	120	126.2	6.2	5

C.5 Hydrogen peroxide quantification

Hydrogen peroxide (H_2O_2) solutions exposed to air and temperature vatiation suffer dismutation/decomposition over time, as is presented in equation D4 below:

$$2H_2O_2 \rightarrow 2H_2O + O_2 \quad \textbf{(D.4)}$$

Thus, as exact measurements are needed for this work, H_2O_2 quantification was achieved through absorbance measurements of several diluted H_2O_2 samples from a 30% parent solution (*Sigma*) at 230 nm and using the calculated ε_{230}=72.4 M^{-1} cm^{-1}. The real parent H_2O_2 concentration throughout the several quantification assays was calculated to be 18.5 M, and was then diluted as needed[7].

C.6 Glassy carbon electrode test

After completing the first set of electrochemical assays under non-diffusive control, a new working electrode was introduced to the system and thus was properly tested before use. For this test, an extremely well defined redox pair was chosen for maximum precision.

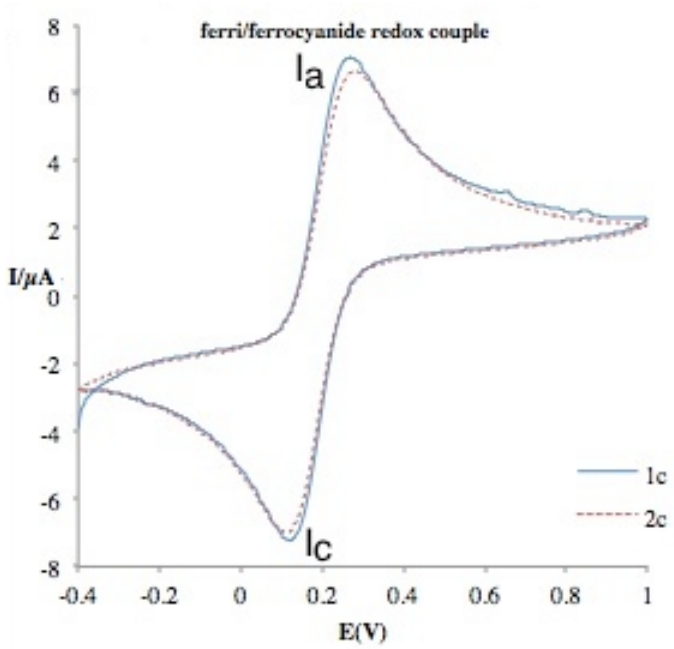

Figure C.2 – Voltammogram for glassy carbon electrode test, using a 10 µM ferri/ferrocyanide solution in 0.1 M HCl between -0.4 to 1 V interval potential (*vs.* SCE) at 50 mV/s.

The standard reduction potential of the ferri/ferrocyanide redox pair, is 0.56 V *vs.* SHE[8], which corresponds to 0.316 V *vs.* SCE and indicates that the electrode is active and ready to be manipulated and used in electrochemical assays.

C.7 Clark oxygen consumption calibration table

Table C.III – Oxygen consumption at the Clark electrode for calibration.

Adição	$[O_2]$ / µM	| I |/µA
0	0.00E+00	0
1	2.71E-01	0.58
2	4.05E-01	0.71
3	6.74E-01	0.91
4	1.35E-01	0.12
5	6.74E-02	0
6	3.36E-01	0.41

C.8 Formal reduction potentials of important electrochemical species

The reduction potential table below shows the concentration unit ratio between the reduced and oxidized forms of a redox pair at 298 K, atmospheric pressure (gaseous) or unit activity (solid, liquid or aqueous), wherever applicable. Variations to the values above are to be expected with pH, solvent and buffer in any given electrochemical system

Table C.IV– Formal reduction potentials of electrochemical species studied in this work.

Half-reaction	$E^{0'}$ (V *vs.* SHE)	Reference
$Fe^{2+} + 2e^- \leftrightarrow Fe\ (s)$	-0.440	9
$Fe^{3+} + 3e^- \leftrightarrow Fe\ (s)$	-0.037	10
$[Fe(CN)_6]^{3-} + e^- \leftrightarrow [Fe(CN)_6]^{4-}$	0.560	10
$O_2\ (g) + 2H_2O + 4e^- \leftrightarrow 4OH^-\ (aq)$	0.400	9
$O_2\ (g) + 2H^+ + 2e^- \leftrightarrow H_2O_2\ (aq)$	0.700	10
$Fe^{3+} + e^- \leftrightarrow Fe^{2+}$	0.770	10
$O_2\ (g) + 4H^+ + 4e^- \leftrightarrow 2H_2O$	1.23	9

C.9 DNA quantification at 260 nm

DNA hybridization protocol was repeated inside an eppendorf flask for spectrophotometric UV/Vis quantification. 5 µL thiolated ssDNA (forward DNA sequence) was diluted in 600 µL and hybridized with 5 µL complementary DNA; spectres were taken before, immediately and 2 h after hybridization. ss- and dsDNA maximum absorbance occurs at 260 nm; consequently, spectres from 200 to 400 nm were performed to test for contaminants and hybridization efficiency. Methylene blue, a DNA intercalator was also added to the mixture and tested individually.

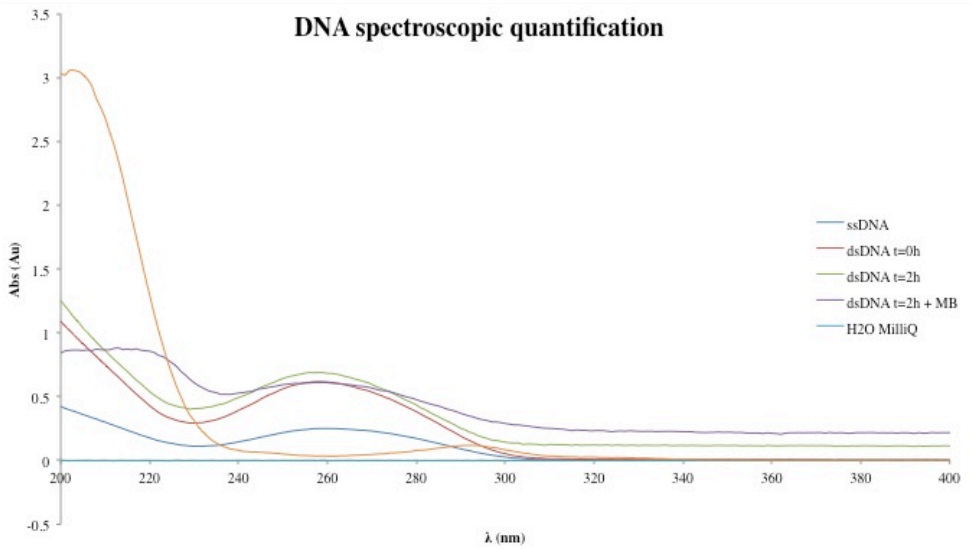

Figure C.3 – DNA spectroscopic quantification direct spectrum results for all samples between 200 and 400 nm.

Table C.V – DNA spectroscopic quantification absorbance results for ssDNA, dsDNA before and after incubation and all controls used in this experiment.

Assay	**$Abs_{260\ nm}$**
H_2O MilliQ	0
Methylene blue (MB)	0.035
ssDNA	0.251
dsDNA t=0h	0.615
dsDNA t=2h	0.753
dsDNA t=2h + MB	0.610

As expected from literature, dsDNA has higher $Abs_{260\ nm}$ than ssDNA immediately after hybridization and after its completion.

D – Alternative purification series results

In accordance to the earlier explanation, below are the results for the first Dps purification series, which achieved greater purification grade and yield, following the same protocol.

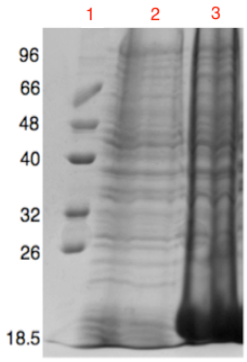

Figure D.1 - – SDS-PAGE (12.5% acrylamide) assessing coding gene sequence overexpression of Dps in *E. coli*. Lanes: **1.** Molecular Weight Marker (LMW-SDS Marker, *nzytech*); **2.** Total protein content before induction; **3**. Total protein content after induction with 0.5 mM IPTG.

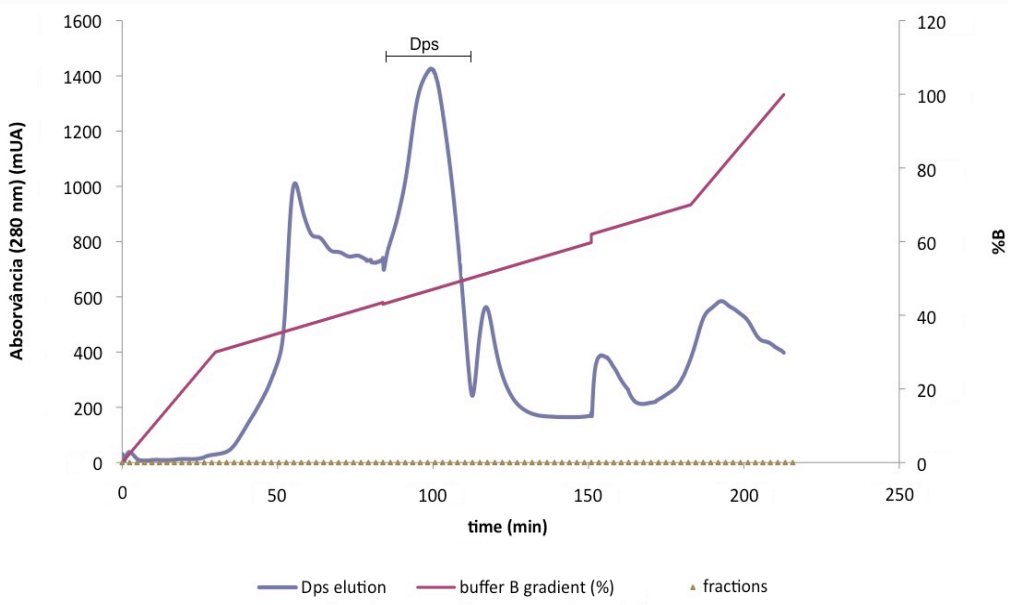

Figure D.2 – Elution profile of *DEAE Sepharose Fast Flow* chromatographic column (2.6 x 30 cm) used in Dps purification. After equilibrating the column in buffer A (10 mM Tris-HCl pH 7.6), a discontinuous linear 5mL/min gradient of buffer B (10 mM Tris-HCl pH 7.6/ 500 mM NaCl) was applied. Fraction I Dps (purest) was collected from 218 to 248 mM NaCl (43.6-49.6% buffer B gradient), while Fraction II Dps was collected from 205.5-217.5 and 251-260 mM NaCl (41.1-43.5 and 50.2-52 % gradient).

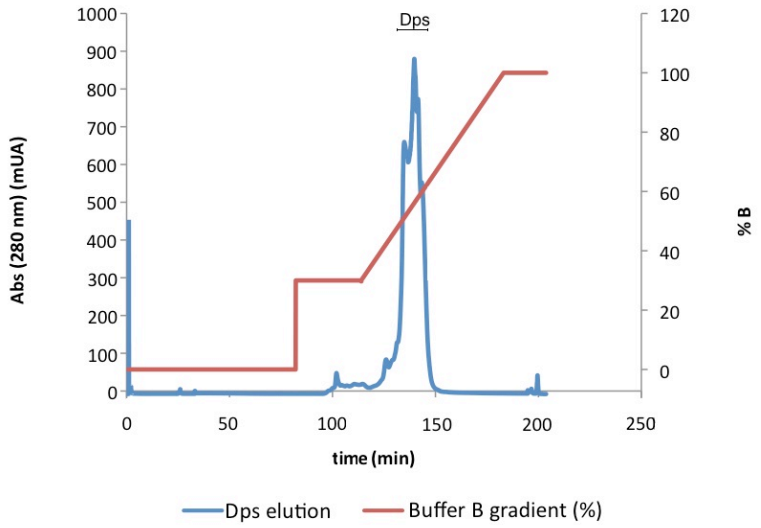

Figure D.3 – Elution profile of *Q-Resource* chromatographic column (6 mL capacity, *GE Healthcare*) used as a second purification step of Dps. After equilibrating with buffer A (10 mM Tris-HCl pH 7.6), a linear gradient (both continuous and discontinuous, with several applied flows) of buffer B (10 mM Tris-HCl pH 7.6 / 500 mM NaCl) was applied. Pure Dps was collected from 218 to 260 mM NaCl (44-52% buffer B gradient).

Figure D.4 below presents the main purification steps of Dps:

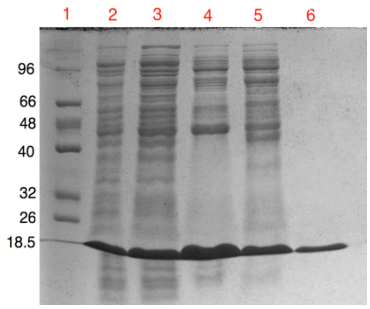

Figure D.4 – SDS-PAGE (12.5 % acrylamide) presenting Dps purification steps. Lanes: **1.** Molecular Weight Marker (*LMW-SDS Marker*, *nzytech*); **2.** Dps after ultracentrifugation; **3.** Dps after dialysis; **4**.-**5.** Dps after ionic exchange chromatography using *DEAE Sepharose Fast Flow* resin (respectively the purest and second purest Dps fractions); **6.**Pure Dps in 10 mM Tris-HCl pH 7.6.

E – Instrumentation

E.1 Weighing

The digital scales used were "Acculab" and CP224S (*Sartorius*).

E.2 pH Electrode

A "pH Meter, Basic 20" electrode (*Crison*) was used during this work.

E.3 Simultaneous agitation and incubation

2 orbital incubator shakers were used, "Max 4000" (*Barnstead/Lab Line*) and "Ovan".

E.4 Centrifugation

The *E. coli* cell culture from which Dps was isolated was collected after centrifugation in a *Sigma 3-18K* (*Sartorius*) centrifuge using *Swinging Bucket 11180* rotor. For all other low speed centrifugations, the *Sigma 1-14* (*Sartorius*) centrifuge. Ultracentrifugations were performed on the "Optima LE-80K" ultracentrifuge (*Beckman Coulter*), using the 70TI rotor at 40 000 rpm and 4º C.

E.5 Autoclaving

A "Labo Autoclave" (*Sanyo*) autoclaving chamber was used during this work.

E.6 Spectrophotometer

An "Evolution 300 UV-VIS" (*Thermo Scientific*) spectrophotometer was used.

E.7 Electrophoresis and Camera

Biorad material was used (including *Mini Protein (R) Tetra System* tray and accompanying material) and an "Electrophoresis Power Supply – 301" (*GE)* voltage source. To photograph SDS-PAGE gels, a *Gel Logic 100 Imaging System* photographic machine (*Kodak*) was used.

E.8 French Press

A French Pressure Cell Press (*Thermo Electric Corporation)* was used during this work.

E.9 Material used in Ionic Exchange chromatography

For the first ionic exchange chromatography step in Dps purification, a XK26/40 column (2.6x40 cm, *GE Healthcare*) was used after pre-packaging with DEAE Sepharose Fast Flow resin (*GE Healthcare*) to 30 cm column height.

For the second ionic exchange chromatography step in Dps purification, a Q Resource column (1 mL, *GE Healthcare*) was used after pre-packaging with Source 15 Q resin (*GE Healthcare*).

For data processing of both steps, an "ÄKTA prime plus" system (*GE Healthcare*) was used. For column refrigeration, a "WK 2200" chiller (*Lauda*) was used.

E.10 Concentration through ultrafiltration

A VivaCell® 70, 30 kDa MWCO (*Sartorius*) cell was used.

E.11 Potentiostat

A µAutolab Type III potentiostat (*Autolab*) was used for the electrochemical assays.

E.12 Gloved chamber

An *UniLab* gloved chamber (*MBraun*) with two entry antechambers was used in the anaerobic electrochemical assays.

E.13 Chronoamperometry assay materials

A Clark electrode (*Hansatech Limited*) was used with rice cellulose spacer (*Miquel Y Costas & Miquel SA*), *Teflon*® membrane (*Hansatech Limited*) and 3.5 kDa cutoff *Spectra Pro* dialysis membrane (*Spectrum UM Lapse*).

F – Sequence alignment data

F.1 Interspecies Dps sequence alignment

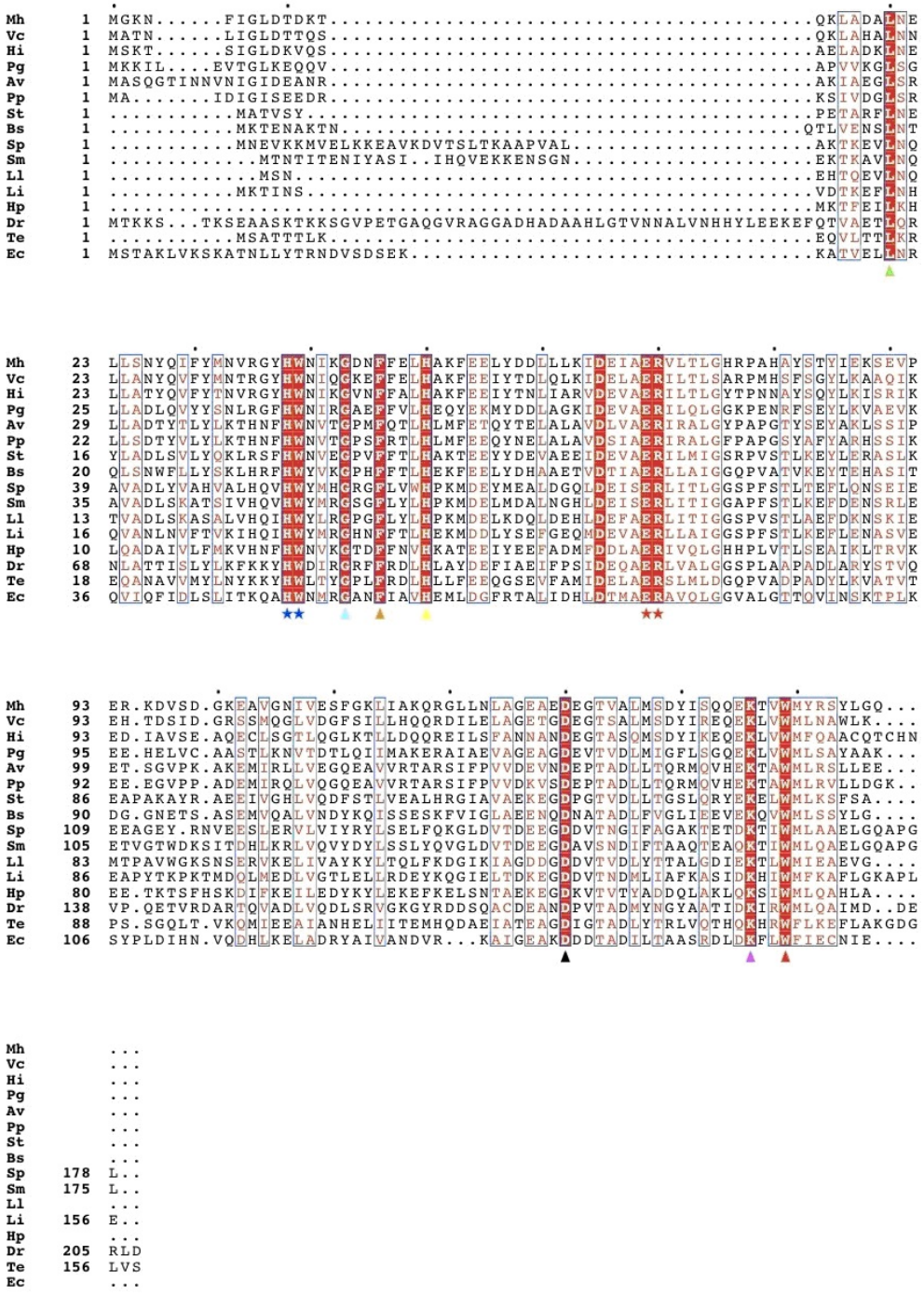

Figure F.1 – Dps sequence alignment data. Mh (*Pseudomonas nautica aka Marinobacter hydrocarbonoclasticus*), Vc (*Vibrio cholerae TMA 21*), Hi (*Haemophilus influenzae F3031*), Pg (*Porphyromonas gingivalis*), Av (*Anabaena variabilis ATCC 29413*), Pp (*Pseudomonas putida GB-1*), St (*Spirochaeta thermophila DSM 6192*), Bs (*Bacillus subtilis*), Sp (*Streptococcus pneumoniae TIGR4*), Sm (*Streptococcus mutans UA159*), Ll (*Lactococcus lactis Il1403*), Li (*Listeria innocua*), Hp (*Helicobacter pylori*), Dr (*Deinococcus radiodurans R1*), Te (*Thermosynechococcus elongatus BP-1*), Ec (*Escherichia coli*) [11].

F.2 Organism under study

The Dps protein used for this study originated from an oil-degrading obligate marine Proteobacteria, *Pseudomonas nautica 617*. The representative strain for the species, *Pseudomonas nautica sp.*, has been reclassified as *Marinobacter hydrocarbonoclasticus*[12,13]. It is an extremely halotolerant chemoorganotroph gram-negative rod, growing in media containing 0.08-0.3 M NaCl, denitrificant but not capable of fermentation[14].

It was chosen to use Dps from this organism due to its availability at considerably low cost and sequence proximity to other Dps-containing bacteria, as is shown on Figure F.2 below:

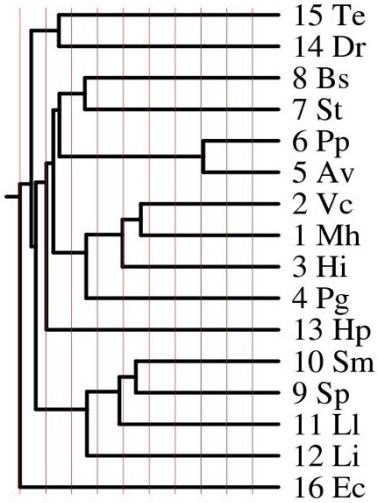

Figure F.2 – Alignment tree data for Dps from bacterial organisms, including: 1. Mh (*Marinobacter hydrocarbonoclausticus aka Pseudomonas nautica 617*); 2. Vc (*Vibrio cholerae TMA 21*), 3. Hi (*Haemophilus influenzae F3031*), 4. Pg (*Porphyromonas gingivalis*), 5. Av (*Anabaena variabilis ATCC 29413*), 6. Pp (*Pseudomonas putida GB-1*), 7. St (*Spirochaeta thermophila DSM 6192*), 8. Bs (*Bacillus subtilis*), 9. Sp (*Streptococcus pneumoniae TIGR4*), 10. Sm (*Streptococcus mutans UA159*), 11. Ll (*Lactococcus lactis Il1403*), 12. Li (*Listeria innocua*), 13. Hp (*Helicobacter pylori*), 14. Dr (*Deinococcus radiodurans R1*), 15. Te (*Thermosynechococcus elongatus BP-1*), 16. Ec (*Escherichia coli*) [17] .

G– DNA sequence data

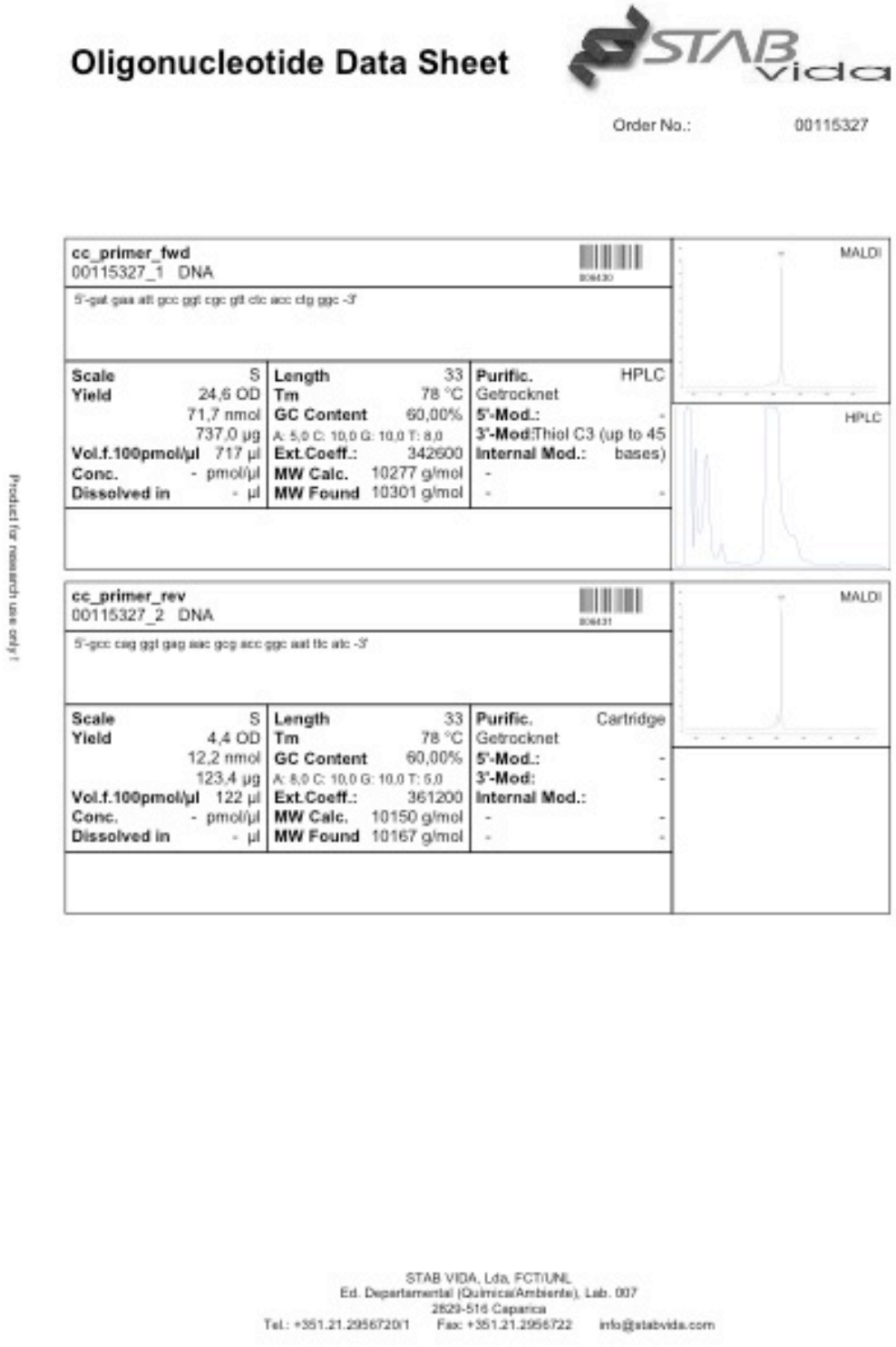

Oligonucleotide Data Sheet

STAB vida

Order No.: 00115327

cc_primer_fwd
00115327_1 DNA

5'-gat gaa att gcc ggt cgc gtt ctc acc ctg ggc -3'

MALDI

Scale	S	**Length**	33	**Purific.**	HPLC
Yield	24,6 OD	**Tm**	78 °C	Getrocknet	
	71,7 nmol	**GC Content**	60,00%	**5'-Mod.:**	-
	737,0 µg	A: 5,0 C: 10,0 G: 10,0 T: 8,0		**3'-Mod:**	Thiol C3 (up to 45
Vol.f.100pmol/µl	717 µl	**Ext.Coeff.:**	342600	**Internal Mod.:**	bases)
Conc.	- pmol/µl	**MW Calc.**	10277 g/mol	-	
Dissolved in	- µl	**MW Found**	10301 g/mol	-	-

HPLC

cc_primer_rev
00115327_2 DNA

5'-gcc cag ggt gag aac gcg acc ggc aat ttc atc -3'

MALDI

Scale	S	**Length**	33	**Purific.**	Cartridge
Yield	4,4 OD	**Tm**	78 °C	Getrocknet	
	12,2 nmol	**GC Content**	60,00%	**5'-Mod.:**	-
	123,4 µg	A: 8,0 C: 10,0 G: 10,0 T: 5,0		**3'-Mod:**	-
Vol.f.100pmol/µl	122 µl	**Ext.Coeff.:**	361200	**Internal Mod.:**	
Conc.	- pmol/µl	**MW Calc.**	10150 g/mol	-	-
Dissolved in	- µl	**MW Found**	10167 g/mol	-	-

Product for research use only !

STAB VIDA, Lda, FCT/UNL
Ed. Departamental (Química/Ambiente), Lab. 007
2829-516 Caparica
Tel.: +351.21.2956720/1 Fax: +351.21.2956722 info@stabvida.com

Figure G.1 – Forward and reverse primer DNA sequence and purification state as ordered from StabVida.

H – Other important electrochemical assays

Adsorption assays

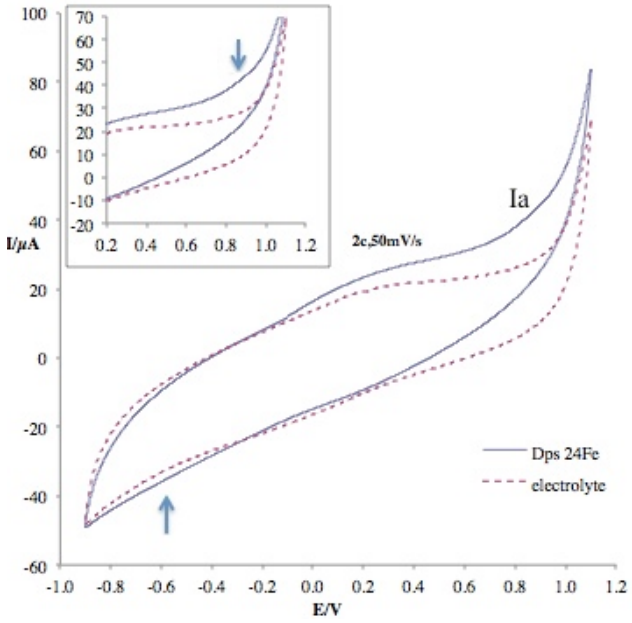

Figure H.1 – Voltammograms from cycle 2 of Dps with 24 Fe ratio added at the time of adsorption (dashed red line) and electrolyte (continuous blue line) from -0.9 to 1.1 V (Dps) and from -1 to 1.2 V (electrolyte) at 50 mV/s.

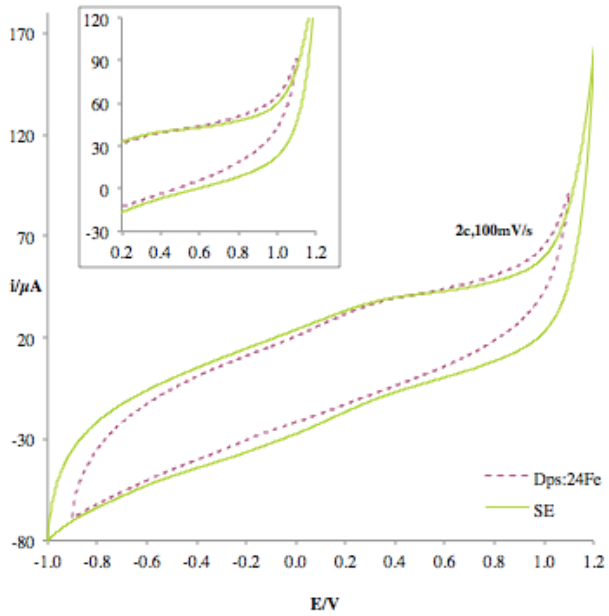

Figure H.2 – Voltammograms from cycle 2 of Dps with 24 Fe ratio added at the time of adsorption (dashed red line) and electrolyte (continuous green line) from -0.9 to 1.1 V (Dps) and from -1 to 1.2 V (electrolyte) at 100 mV/s.

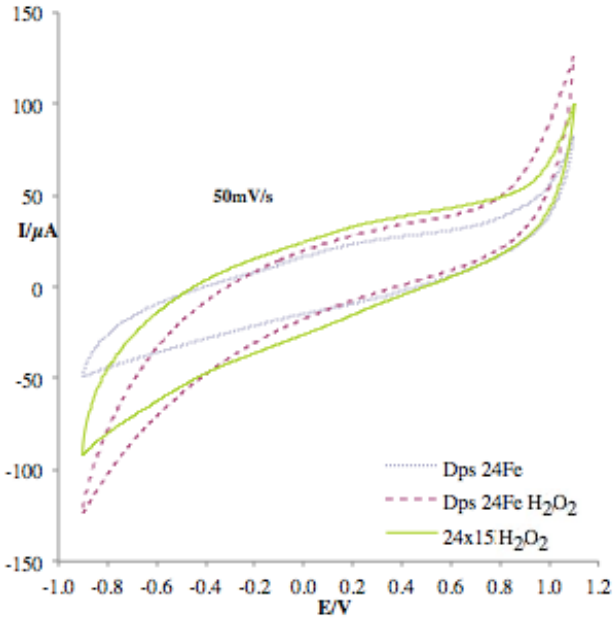

Figure H.3 – Voltammograms from cycle 2 of Dps with 24 Fe added at the time of adsorption in the absence (thin blue dashed line) and the presence (red dashed line) of H_2O_2 *versus* control with electrolyte and hydrogen peroxide (continuous green line) at 50 mV/s.

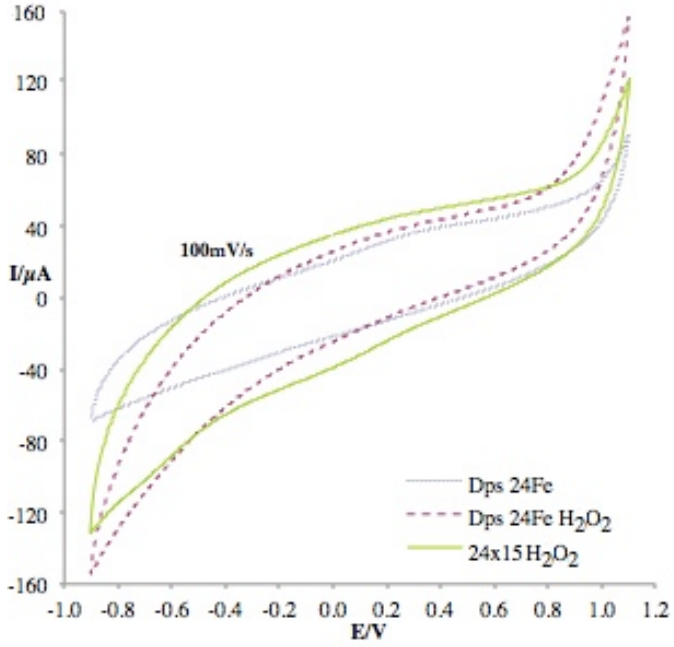

Figure H.4 – Voltammograms from cycle 2 of Dps with 24 Fe added at the time of adsorption in the absence (thin blue dashed line) and the presence (red dashed line) of H_2O_2 *versus* control with electrolyte and hydrogen peroxide (continuous green line) at 100 mV/s.

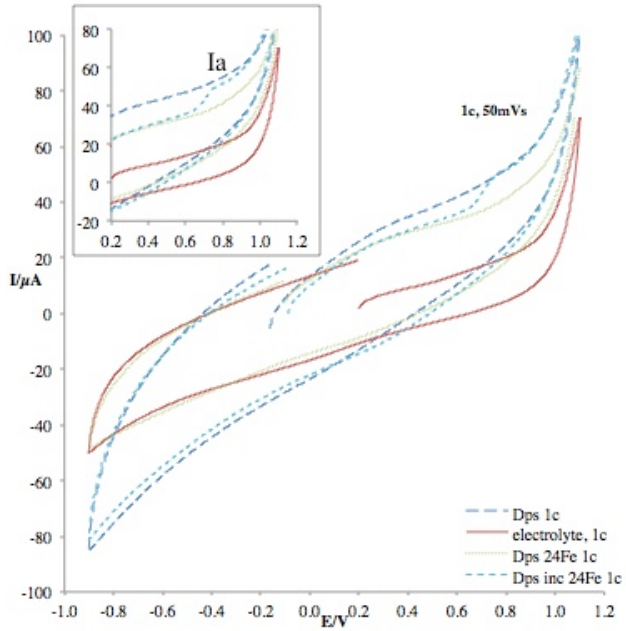

Figure H.5 – Voltammograms from cycle 1 of apoDps (dashed blue line), electrolyte (continuous red line), Dps with 24 Fe added at the time of adsorption (dashed green line) and Dps incubated with 24 Fe (light blue dashed line) at 50 mV/s from -0.9 to 1.1 V, moving from E_{OCP} in the oxidative direction.

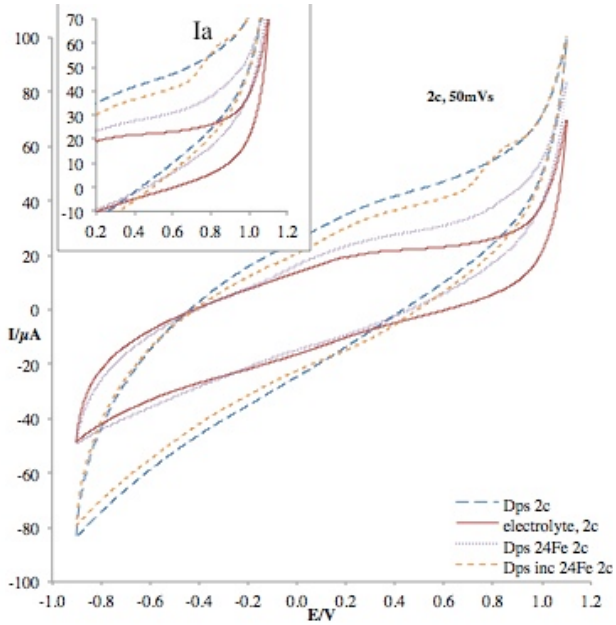

Figure H.6 – Voltammograms from cycle 2 of apoDps (dashed blue line), electrolyte (continuous red line), Dps with 24 Fe added at the time of adsorption (purple dashed line) and Dps incubated with 24 Fe (orange dashed line) at 50 mV/s from -0.9 to 1.1 V, moving from E_{OCP} in the oxidative direction.

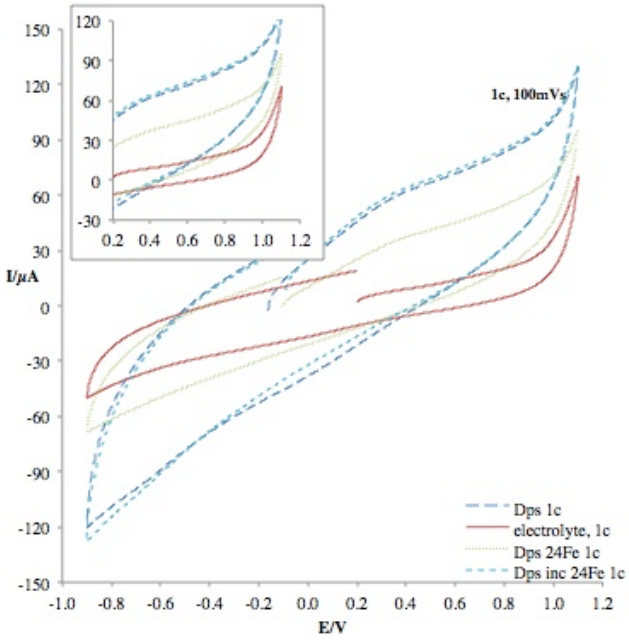

Figure H.7 – Voltammograms from cycle 1 of apoDps (dashed blue line), electrolyte (continuous red line), Dps with 24 Fe added at the time of adsorption (dashed green line) and Dps incubated with 24 Fe (light blue dashed line) at 100 mV/s from -0.9 to 1.1 V, moving from E_{OCP} in the oxidative direction.

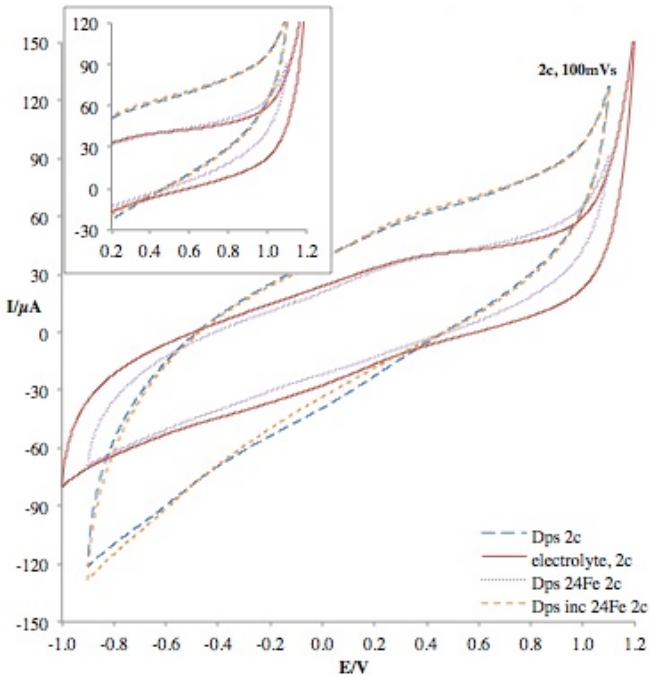

Figure H.8 – Voltammograms from cycle 2 of apoDps (dashed blue line), electrolyte (continuous red line), Dps with 24 Fe added at the time of adsorption (dashed purple line) and Dps incubated with 24 Fe (orange dashed line) at 100 mV/s from -0.9 to 1.1 V (electrolyte from -1 to 1.2 V), moving from E_{OCP} in the oxidative direction.

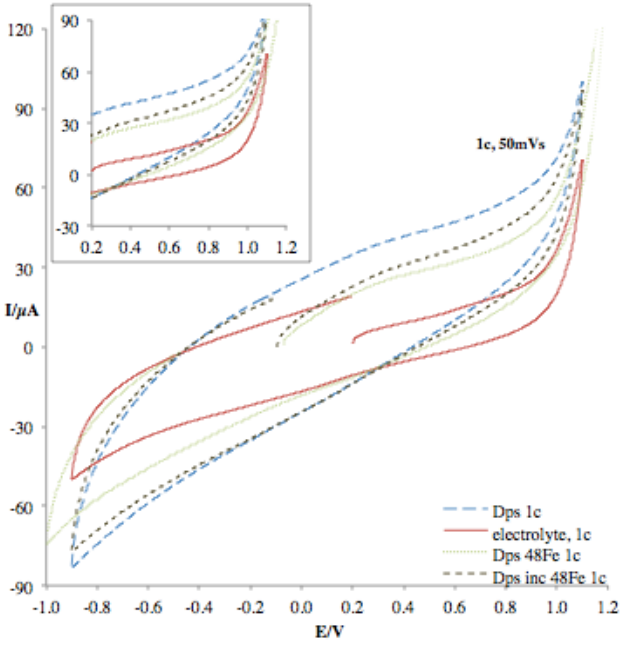

Figure H.9 – Voltammograms from cycle 1 of apoDps (dashed blue line), electrolyte (continuous red line), Dps with 24 Fe added at the time of adsorption (dashed green line) and Dps incubated with 48 Fe (light blue dashed line) at 50 mV/s from -0.9 to 1.1 V, moving from E_{OCP} in the oxidative direction.

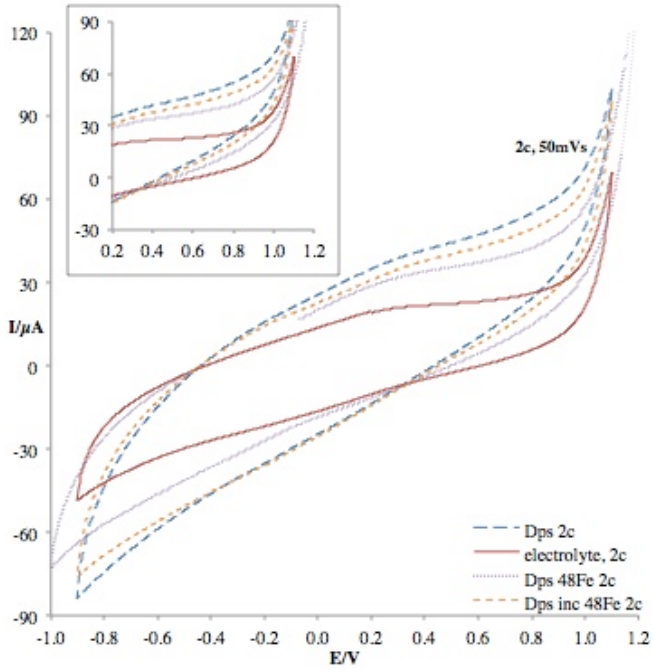

Figure H.10 – Voltammograms from cycle 2 of apoDps (dashed blue line), electrolyte (continuous red line), Dps with 24 Fe added at the time of adsorption (dashed purple line) and Dps incubated with 48 Fe (orange dashed line) at 50 mV/s from -0.9 to 1.1 V, moving from E_{OCP} in the oxidative direction.

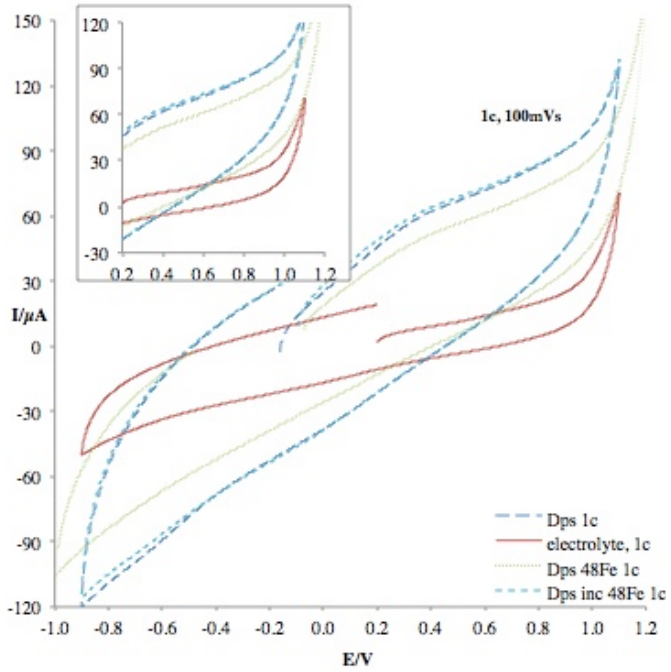

Figure H.11 – Voltammograms from cycle 1 of apoDps (dashed blue line), electrolyte (continuous red line), Dps with 24 Fe added at the time of adsorption (dashed green line) and Dps incubated with 48 Fe (light blue dashed line) at 100 mV/s from -0.9 to 1.1 V, moving from E_{OCP} in the oxidative direction.

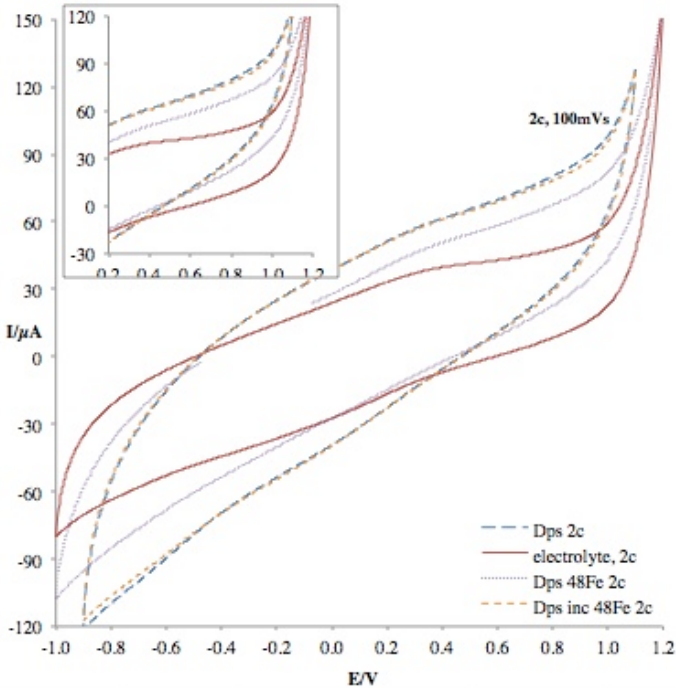

Figure H.12 – Voltammograms from cycle 2 of apoDps (dashed blue line), electrolyte (continuous red line), Dps with 24 Fe added at the time of adsorption (dashed purple line) and Dps incubated with 24 Fe (orange dashed line) at 100 mV/s from -0.9 to 1.1 V, moving from E_{OCP} in the oxidative direction.

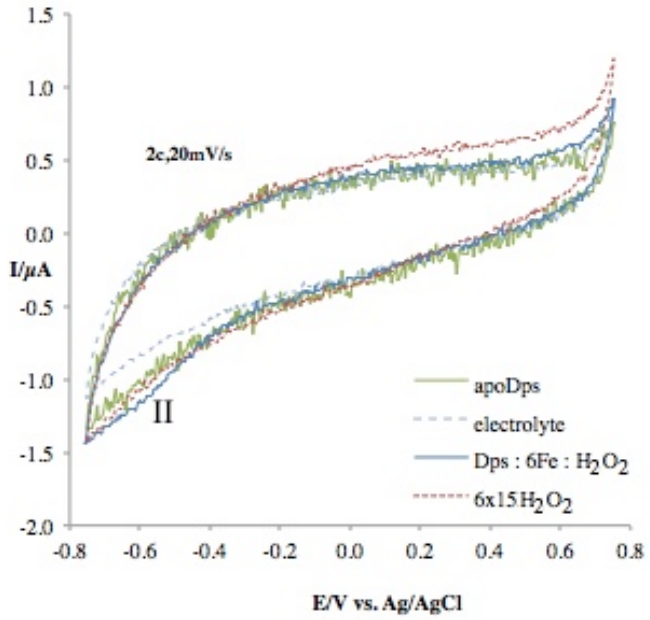

Figure H.13 – Voltammograms from cycle 2 of apoDps (green line), supporting electrolyte (dashed light blue line), Dps : 6Fe : 6x15 H_2O_2 (blue line) and 6x15 H_2O_2 (dashed red line) at 20 mV/s from -0.75 to 0.75 V, moving from E_{OCP} in the reductive direction.

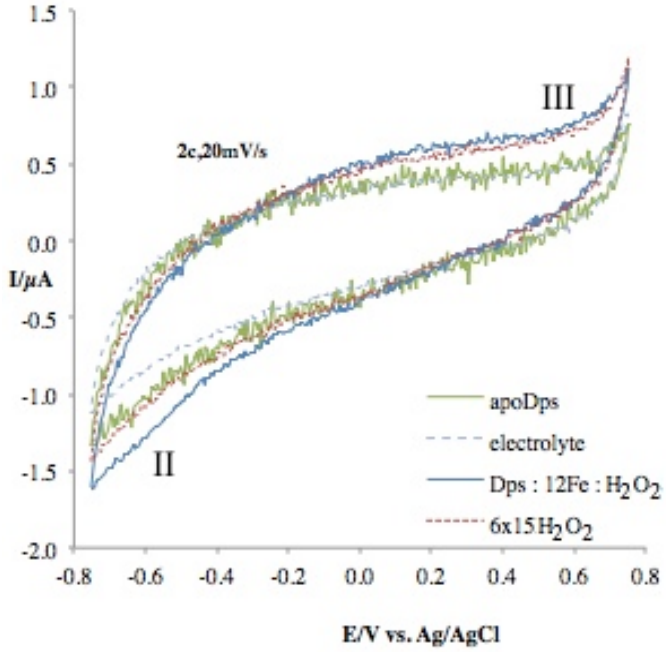

Figure H.14 – Voltammograms from cycle 2 of apoDps (green line), supporting electrolyte (dashed light blue line), Dps : 12Fe : 12x15 H_2O_2 (blue line) and 6x15 H_2O_2 (dashed red line) at 20 mV/s from -0.75 to 0.75 V, moving from E_{OCP} in the reductive direction.

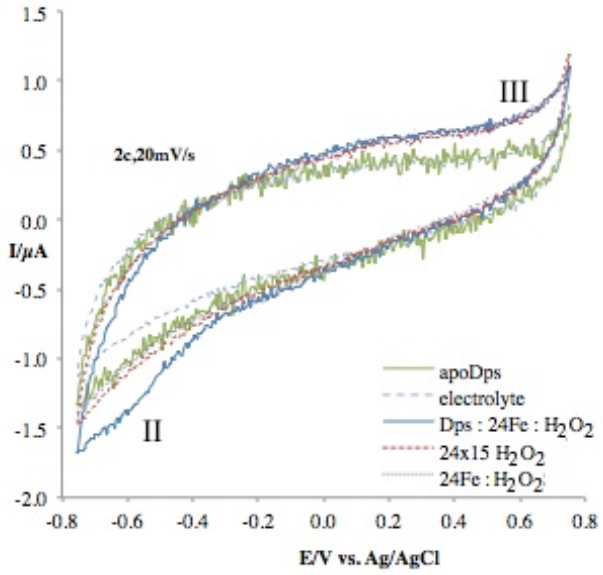

Figure H.15 – Voltammograms from cycle 2 of apoDps (green line), supporting electrolyte (dashed light blue line), Dps : 24Fe : 24x15 H_2O_2 (blue line), 24x15 H_2O_2 (dashed red line) and 24 Fe : 24x15 H_2O_2 (dashed purple line) at 20 mV/s from -0.75 to 0.75 V, moving from E_{OCP} in the reductive direction.

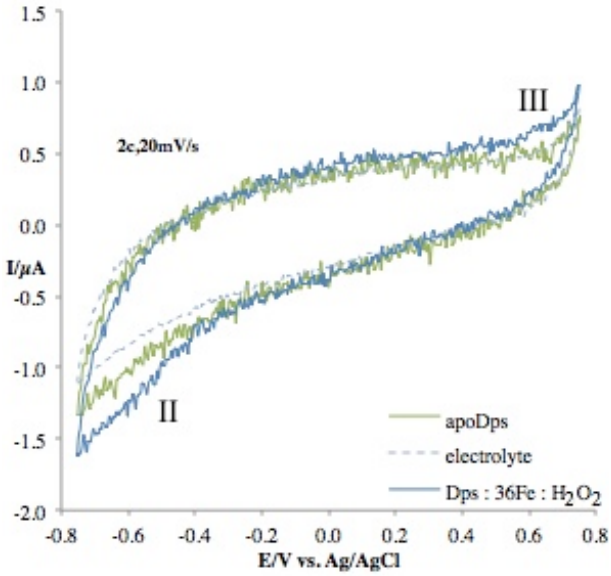

Figure H.16 – Voltammograms from cycle 2 of apoDps (green line), supporting electrolyte (dashed light blue line) and Dps : 36Fe : 36x15 H_2O_2 (blue line) at 20 mV/s from -0.75 to 0.75 V, moving from E_{OCP} in the reductive direction.

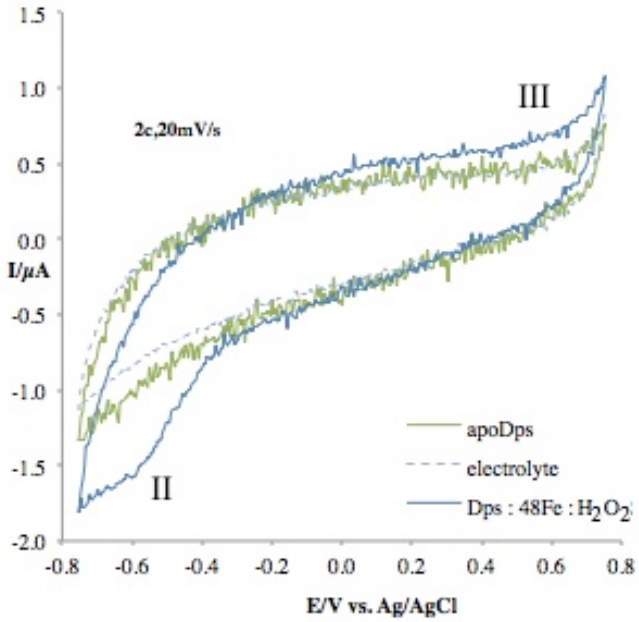

Figure H.17 – Voltammograms from cycle 2 of apoDps (green line), supporting electrolyte (dashed light blue line), and Dps : 48Fe : 48x15 H_2O_2 (blue line) at 20 mV/s from -0.75 to 0.75 V, moving from E_{OCP} in the reductive direction.

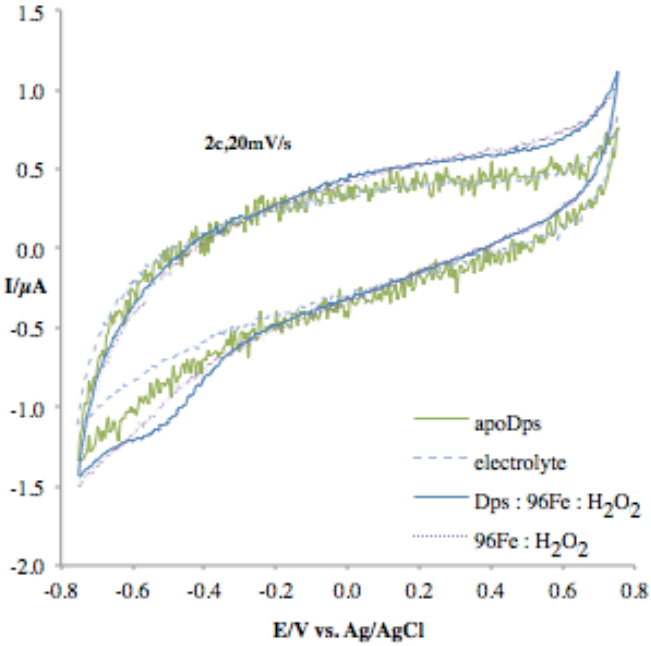

Figure H.18 – Voltammograms from cycle 2 of apoDps (green line), supporting electrolyte (dashed light blue line), Dps : 96Fe : 96x15 H_2O_2 (blue line), 96x15 H_2O_2 (dashed red line) and 96 Fe : 96x15 H_2O_2 (dashed blue line)at 20 mV/s from -0.75 to 0.75 V, moving from E_{OCP} in the reductive direction.

Appendix References

(1) Laemmli, UK. *Nature*, 227 (1970), 680-685.
(2) Hanes, BD *et al.*, *Gel Electrophoresis of proteins – a practical approach*, IRL Press. (1994).
(3) Mini Protean ® 3 Cell Instruction Manual (*Biorad*), accessed at www.bio-rad.com in October 2010.
(4) Transformation protocol (*nzytech*), accessed at www.nzytech.com/site/ in October 2010.
(5) Experiment 9: Determination of Iron with 1,10-Phenanthroline accessed on http://www.chem.utk.edu/~chem319/Experiments/exp10.pdf.
(6) Maloney, KM, Quiazon, EM, Indralingam, R, *J. Chem. Educ*., 85 (2008), 399.
(7) Maehly, A, Chance, B, *Methods. Biochem. Anal.*, 1 (1954), 357-424.
(8) Bard, AJ, Faulkner, LR, *Electrochemical methods – Fundamentals and Applications*, (Elizabeth Swain, ed.), John Wiley & Sons, Inc. (2001).
(9) Atkins, P., *Physical Chemistry*, 6th Edition, W.H. Freeman and Company, NY (1997).
(10) Vanýsek, P., *Electrochemical Series*, in *Handbook of Chemistry and Physics: 88th Edition* (*Chemical Rubber Company*) (2007), pgs. 8-20--8-29.
(11) http://espript.ibcp.fr/ESPript/ESPript/ – Easy Sequencing in Postscript (Espript 2.2) visited on February 2011.
(12) Gauthier, MJ *et al.*, *Int. J. of Syst. Bacteriol.*, 42(4) (1992), 568-576.
(13) Spröer, C *et al.*, *Int. J. of Syst. Bacteriol*. 48 (1998), 1445-1448.
(14) Yakimov, MM *et al.*, *Curr. Opin. Biotechnol.*, 18 (3) (2007), 257-266.
(15) http://mordred.bioc.cam.ac.uk/~jiye/evoltrace/evoltrace.html - Phylogenetic Analysis Alignment in Evolutionary Trace Server (Trace Suite II, Cambridge Department of Biochemistry) visited on February 2011.